COMPUTATIONAL MODELING OF DYNAMIC PHASE CHANGE MATERIALS IN THERMAL ENERGY STORAGE FOR CONCENTRATED SOLAR POWER

BY

JESSICA NICHOLSON

THESIS

Submitted in partial fulfillment of the requirements
for the degree of Master of Science in Mechanical Engineering
in the Graduate College of the
University of Illinois Urbana-Champaign, 2025

Urbana, Illinois

Adviser:

Professor Nenad Miljkovic

ABSTRACT

Energy demand is rapidly growing on a global scale. Population growth, electrification, and the advent of artificial intelligence and other high-power computing functions are among the biggest drivers of this increasing demand. The design and implementation of reliable, modernized power systems such as modular, networked microgrids is essential to meet this growing demand. Thermal energy resources such as parabolic trough concentrated solar power (CSP) are commonly used in microgrids to support thermal power demands, but CSP power production is intermittent. Implementing thermal energy storage to modulate the power output of thermal energy systems can manage intermittence. Power system planning, however, involves uncertainty around the quantitative impact that power resource investments such as concentrated solar power (CSP) and thermal energy storage will have on the reliability and resilience of a microgrid. Conventional latent thermal energy storage technologies have shortcomings, such as migration of the melting front over time. This introduces additional conductive resistance during the charge cycle that negatively impacts heat flux into the energy storage phase change material (PCM). A new conceptual technology called dynamic phase change materials (dynPCMs) have been developed to address this shortcoming by applying mass or piston-based pressure to the solid state of the energy storage PCM to keep close contact between the heated boundary and the solid portion of the PCM as it melts. This technology theoretically improves the performance of thermal energy storage. This study introduces a computational model that calculates metrics for the expected performance of parabolic trough Concentrated Solar Power (CSP) systems with conventional latent thermal energy storage versus dynPCM thermal energy storage. The model includes a control system to modulate the CSP system's power output and match a power

demand profile as closely as possible. This study shows that, while latent thermal energy storage enables the example CSP system to achieve a power availability of 68.6%, dynPCM thermal energy storage enables the CSP system to achieve a higher power availability than latent thermal energy storage—as high as 79.5%. The study also involves a parametric analysis of the factors which influence the power availability of the system. This model is built for incorporation into a larger computational model which we term Analysis of Microgrid Performance, Reliability, and Resilience (AMPeRRe) to evaluate the performance impacts of incorporating CSP systems and thermal energy storage in larger microgrids. The stand-alone model and AMPeRRe will produce actionable analytics for decision-makers to inform their investment decisions around implementing CSP and thermal energy storage in varied applications. The results shown here can enable a better understanding of thermal energy storage-coupled intermittent energy resources that can meet the energy security needs of a growing world.

ACKNOWLEDGMENTS

I would like to extend my sincere appreciation to my advisor, Nenad Miljkovic, for his exceptional guidance, support, and encouragement throughout the course of this project. I am also greatly thankful to Vivek Garimella, who provided valuable feedback and a critical technical perspective that consistently strengthened the rigor and clarity of this work.

Special thanks to my colleagues and friends at the Construction Engineering Research Laboratory (CERL) – Thomas Bozada, Camryn Anderson, Matthew Gross, and Natalie O'Leary – who have helped broaden the reach of my thesis work and incorporate it into an advanced digital modeling toolbox.

I am profoundly grateful to my family for their incredible love, patience, and belief in me, which has made this journey not only possible but meaningful.

Finally, I would like to acknowledge the CERL for funding my adjacent work and providing me with the opportunity to pursue my masters' degree.

TABLE OF CONTENTS

CHAPTER 1: INTRODUCTION

Rapidly growing energy demand has created a critical need to expand energy infrastructure that supports various industries and residential communities. Several power resources have been developed that can serve as solutions to this growing energy demand, which are integrated into power systems from small-scale microgrids to large-scale utilities. Power systems must be designed with power resources and distribution tailored to the application, the location, and the conditions that the power system will be under. Conventional resources such as generators, nuclear, and coal-driven power plants may be incorporated as well as renewable resources such as solar, wind, and geothermal to address the power demand problem. Intermittent renewable power resources, such as PV solar and concentrated solar power (CSP), are dependent on the changing availability of natural resources. This presents a challenge when these intermittent resources are stand-alone, as their power output cannot be matched to power demand from the customer. In utility-connected systems, photovoltaic (PV) solar and CSP systems often create a phenomenon called the duck curve. Solar power production offsets power demand on the utility. When solar production peaks during the day, the demand on the utility experiences a sharp decline that creates challenges for utility power management and negatively impacts power stability. To address this and the challenge of intermittence, energy storage is often integrated with solar power systems to modulate their power output by capturing surplus energy and discharging energy during periods of shortage.

Multiple types of energy storage exist that can be chosen to support these systems depending on the resources that need support and the power system application. Lithium-ion battery energy storage is the most common due to advantages such as its high energy density and

a long life cycle. Lithium is becoming scarcer, however, and large-scale lithium-ion batteries can be expensive. Other forms of electrochemical energy storage such as sodium-ion and solid-state batteries present opportunities to overcome this. Solid-state sodium-ion batteries do not achieve energy density as high as lithium-ion batteries, but they have abundant sources of raw materials and high safety (Si, 2025). These batteries can be used in fixed power systems given no significant size constraints. Kinetic energy storage such as flywheel energy storage systems can be incorporated as well. Flywheels are valued for their rapid response, high power output, and frequency regulation (Iwayemi, 2025). They generally require more maintenance, however, due to mechanical components. Each of these energy storage systems often support intermittent power resources, but are primarily used for non-thermal power systems.

Thermal energy storage systems are commonly used in heat-based energy technologies that convert captured thermal energy to electricity, such as CSP, geothermal, and nuclear. While thermal energy storage systems are not yet as efficient as battery energy storage, they are optimal in renewable thermal energy technologies to negate the need for additional energy conversion between thermal and electric (Sharma, A Comprehensive Review of Sensible Heat Thermal Energy Storage for High Temperature Applications, 2025). The efficiency of a thermal energy storage system depends on the thermal conductivity of the materials involved, so selecting a material with high thermal conductivity is essential to achieving a thermal energy storage efficiency comparable to that of electrochemical energy storage such as lithium-ion. Melt front propagation can also reduce the efficiency of latent thermal energy storage systems as time progresses during a charge cycle. A well-designed thermal energy storage system can overcome efficiency challenges, and certain materials can create a low-cost system with a high life cycle. These thermal energy storage systems can capture excess heat energy and discharge to

supplement produced heat energy. Given the right control system, thermal energy storage systems can modulate the power output of the power resources they support.

1.1: PARABOLIC TROUGH CONCENTRATED SOLAR POWER (CSP)

Parabolic trough concentrated solar power (CSP) systems use thermal-to-electric power conversion to provide power to customers. CSP systems are sized differently for different applications. Some are utility-scale, while other single-dish (5-25 kW per dish) and parabolic trough systems are smaller scale to be incorporated in microgrids (Moya, 2012). These systems consist of parabolic trough reflectors that concentrate solar radiation onto a receiver, which heats a working fluid within the receiver. Figure 1 visualizes a cross-section of this aperture (Oshilalu, 2015).

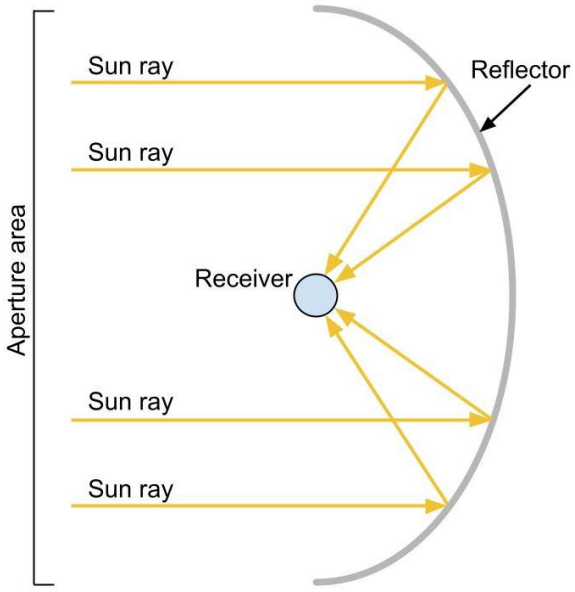

Figure 1: Parabolic Trough Aperture and Receiver

The working fluid in the receiver travels to thermal energy storage or to a heat exchanger. Thermal energy storage within CSP systems can be sensible, which uses liquid or solid materials

to store thermal energy without changing phase, or latent, which uses materials that change phase when storing or releasing thermal energy (Gasa, 2022). In the heat exchanger, the working fluid creates a heated boundary that transfers thermal energy to a second material – usually water – to create steam. The steam powers a turbine with a steam generator to bring power to customers (Sivalingam, 2024). The simplified operation of a CSP system can be described by the following stages. Figure 2 visualizes each of these stages using a diagram of a parabolic trough CSP system with thermal energy storage.

1. A working fluid passes through the receiver, and the parabolic trough reflector concentrates solar energy onto the receiver to heat the working fluid.
2. The working fluid, at its highest temperature, flows to a junction where some fluid is routed to the thermal energy storage (TES) system and some to the heat exchanger.
3. Thermal energy storage charges from the working fluid or discharges thermal energy into the working fluid, depending on current state and power demand.
4. The working fluid reconverges into the same channel and travels to the heat exchanger.
5. The working fluid moves through the exchanger and acts as a heated boundary to produce steam.
6. The steam travels to a turbine connected to a Stirling engine or Brayton Cycle engine to produce power.
7. Some power is routed to external battery energy storage when the CSP power output is in surplus of the power demand.
8. Power from the CSP system is routed to fulfill the power demand, paired with power from the external battery when the CSP system's power output is insufficient.

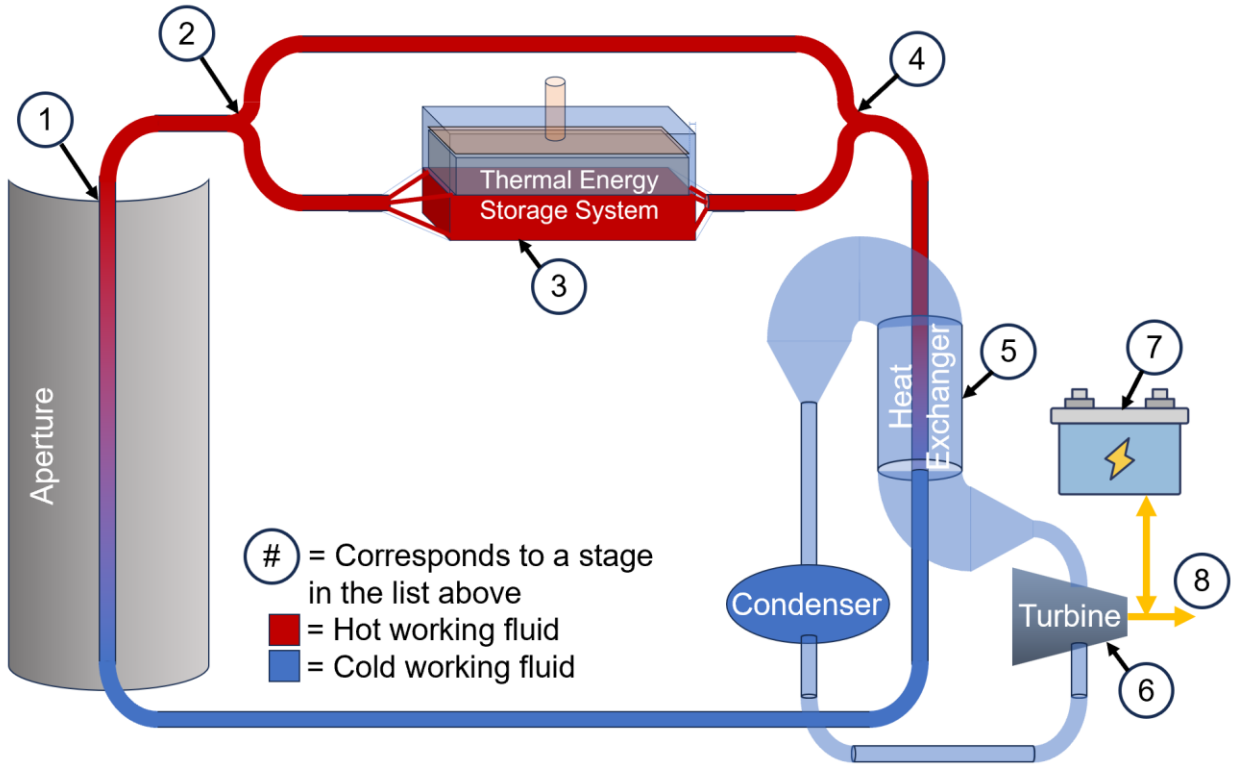

Figure 2: Stages of Operation of a CSP System with Thermal Energy Storage

The energy transitions that occur within this system are:

Solar irradiation → Thermal energy → Stored thermal energy → Kinetic energy → Electricity.

The power output of a parabolic trough CSP system is dependent on the concentrated solar power collected in the receiver and the dynamics of any thermal energy storage included in the system. The rate of solar power collection in the receiver is dependent on the size of the receiver relative to the size of the parabolic trough mirrors. The working fluid material, the size of the thermal energy storage system, the material used for thermal energy storage, and the area of the heat transfer surface each have an impact on power output as well. Under specific conditions, the flow of the working fluid through the thermal energy storage system can be modulated to make the CSP system power output align with the power demand.

1.2: THERMAL ENERGY STORAGE IN CSP SYSTEMS

Sensible thermal energy storage refers to the storage of thermal energy in a material that does not change phase. Latent thermal energy storage refers to the storage of thermal energy in a material that changes phase during its operation (Gasa, 2022). These materials have a melting point that the temperature inside the thermal storage tank is expected to surpass, allowing for the storage of thermal energy in a different (most commonly liquid) phase. A latent material's specific heat, density, and thermal conductivity are dependent on phase. The material's transition to liquid phase can achieve a more effective charge cycle to support parabolic trough CSP systems and other thermal-based energy resources.

For certain parabolic trough CSP systems, the objective of incorporating thermal energy storage is to modulate the system's power output to match an expected power demand profile as closely as possible. This can maximize the power availability of a stand-alone CSP system. Both sensible and latent thermal energy storage can be used to achieve this regulation. Alternatively, given sufficient external battery energy storage, the objective may be to maximize the power output of the CSP system. This can be achieved by maximizing the efficiency of the thermal energy storage charge cycle through maximizing heat flux into the PCM. Several innovations in thermal energy storage technologies aim to achieve this objective and address PCM challenges, such as optimizing the geometry of thermal energy storage systems to maximize the area of heat transfer and selecting PCMs for evaluated thermal energy storage systems that maximize energy density and charge state efficiency. One example of geometry optimization is a set of inner tubes within shell-and-tube thermal energy storage systems that have been designed with fins to

maximize heat transfer area between the working fluid and the PCM (Kirincic, 2024). Another method to address PCM challenges and maximize heat flux is to design a thermal energy storage system that allows for close contact melting. This refers to a system with sufficient channels for the melted material to travel away from the heated boundary so that gravity keeps the solid-phase material in close contact with the heated boundary. The best PCMs selected for thermal energy storage are commonly those with high specific heat capacity, thermal conductivity, and a melting point conducive to maximizing latent heat transfer, such as paraffin wax, salt hydrates, and molten salts (Mehta P. e., 2025).

Geometry design, close contact melting, and material selection can improve the efficiency of the charge cycle to increase the overall power output of the CSP system, but this study explores a newer conceptual method to maximize the efficiency of latent thermal energy storage and the power output of the CSP system it supports. A new concept has been introduced in which a dynamic mechanism applies pressure to an energy storage system's solid-state phase change material (DynPCM) during the charge cycle (Fu, 2022). The portion of the solid material against the boundary melts during this charge cycle, and the liquid is displaced as the dynamic pressure keeps the solid edge on the boundary. DynPCMs theoretically minimize the liquid boundary layer between the heated surface and the solid-state PCM in the storage tank to lower conductive thermal resistance, increase the heat flux into the PCM, and capture more energy. Equation 1 calculates the heat flux into thermal energy storage during its charge phase for which DynPCM pressure is applied to the solid state PCM (Fu, 2022). The charge phase occurs when the working fluid temperature exceeds the temperature of the PCM. When the temperature of the PCM exceeds that of the working fluid, the energy storage system is in the discharge phase, and the heat flux formula reverts to the conventional heat transfer model (Equation 2).

Equation 1: Heat Flux into PCM - DynPCM

$$q" = 1.24\left(k_l * (T_{ss} - T_m)\right)^{\frac{3}{4}} * \left(\frac{\rho_s\left(L + (T_m - T_i)c_{p,s}\right)P}{W^2\mu_l}\right)^{\frac{1}{4}} \quad (1)$$

Equation 2: Total Heat Transfer Rate and Heat Flux into PCM – Non-DynPCM

$$\dot{Q} = \dot{m}c_p(T_{hot,in}[t] - T_{hot,out}[t]) \quad (2a)$$

$$q" = \frac{\dot{Q}}{A} \quad (2b)$$

The thickness of the liquid layer between the solid-state PCM and the heated boundary directly impacts the heat flux into the PCM and the efficiency of the charge cycle. Equation 3 determines the thickness of this liquid layer(Fu, 2022) using the principles of Stefan adhesion, or squeeze flow. The higher the pressure applied to the solid-state PCM, the smaller the liquid layer thickness and the higher the efficiency of the charge cycle.

Equation 3: Liquid Layer Thickness – Square Heat Transfer Surface

$$\delta = \sqrt[3]{\frac{0.42W^2\mu_l q''}{P(\rho_s L + (T_m - T_i)\rho_s c_{p,s})}} \quad (3)$$

Equation 4 calculates the melting speed of the PCM(Fu, 2022), which depends on the heat flux into the system and PCM thermophysical properties. Calculating the melting speed is important to determine the proportion of solid-state material remaining and liquid-state material present in a time-based model. The PCM is a finite material, so this informs when the PCM's solid-state is fully depleted. When the solid-state material is fully depleted and only the liquid state remains, any further heat transfer into the PCM becomes sensible.

Equation 4: Melting Speed

$$u = \frac{q''}{\rho_s L + (T_m - T_i)\rho_s c_{p,s}} \quad (4)$$

The higher the pressure applied to the solid-state material in a DynPCM thermal energy storage system, the higher the melting speed and the lower the liquid boundary layer thickness. This theoretically results in higher heat flux and power production of the CSP system under the same input conditions and system parameters.

The impact of incorporating DynPCMs in thermal energy storage systems for real scenarios has not yet been studied. This work has developed and applied a computational model to evaluate the expected outcomes of DynPCM incorporation. The model also quantifies the comparative expected outcomes of incorporating different types of sensible, latent, and DynPCM-supported thermal energy storage in parabolic trough CSP systems. Thermal energy storage systems are frequently applied to other energy technologies as well (aside from concentrated solar power), so this calculation process can expand in scope. Calculated outcomes will factor into the optimization capabilities of an existing digital analysis tool termed Analysis of Microgrid Performance, Reliability, and Resilience (AMPeRRe) to find the system configurations needed to minimize losses associated with applying thermal energy storage to energy technologies.

CHAPTER 2: COMPUTATIONAL MODEL PARAMETERS

The computational model presented in this paper calculates the power output and power availability of parabolic trough concentrated solar power systems that incorporate thermal energy storage. Incorporating dynamic phase change materials (dynPCMs) in thermal energy storage can maximize heat flux into the storage system to make the charge cycle more efficient compared to storage systems with conventional phase change materials (PCMs) (Fu, 2022). This model shows that, when implemented properly, dynPCMs in thermal energy storage within Concentrated Solar Power (CSP) systems can improve the power availability of CSP technologies. This model assumes that the thermal energy storage discharges thermal energy to the working fluid during low solar irradiance for which the power output of the system would be insufficient for the power demand. High solar irradiance causes thermal energy storage to experience a charge cycle due to high working fluid temperatures, which would cause power output in surplus of the power demand if some energy is not transferred to the thermal energy storage system. This is possible by modulating the proportion of the working fluid flow through two channels, one with the thermal energy storage system and one without. When the fluid in the two channels reconverges, the temperature of the fluids combines, and the working fluid reaches a heat exchanger to transfer its energy to steam. This flow modulation achieves a reconverged working fluid temperature that enables the solar CSP system's power output to match power demand at every timestep as closely as possible. The mathematical model of this system is developed into a program for which it can be easily repeated for different parameters. This allows for quick, direct modeling and comparison between different systems in terms of

performance and power availability. Analysis results from this model can aid the power system planning process by informing investments into thermal energy storage and CSP systems.

A set of data and parameter inputs must be provided to run the calculation model for a CSP system with thermal energy storage. These inputs include time-domain datasets with regular intervals over a specified time period (typically an annual period). These datasets are the power demand (load) profile of the site that will depend on the CSP system, as well as historical natural resource datasets such as direct normal solar irradiance (DNI) and ambient temperature. The thermal energy storage PCM and working fluid in the CSP system must be specified along with system parameter inputs summarized in Table 1. The mass flow rate can be provided as a direct input or calculated by the model based on the time taken for the working fluid to travel from the input to the output of the receiver.

This study includes analysis results for an example case of a CSP system with thermal energy storage. The analysis results correspond to each stage of the calculation process. The inputs used for this example case are for a parabolic trough solar CSP system with a latent heat transfer thermal energy storage system. The working fluid in this CSP system is sodium nitrate, and the PCM in the thermal energy storage is lithium fluoride salt. Sodium nitrate is a molten salt mixture that has excellent thermal stability and heat storage capacity. It can withstand high temperatures, which is necessary to capture enough energy in a CSP system (Bozorg, 2023). Lithium fluoride salt has a high melting point, which is important for a thermal energy storage PCM that is expected to cycle between a high range of temperatures due to charge and discharge cycles. This PCM's melting point of 848 C is ideal to maximize the number of phase changes that occur in the example scenario. The more phase changes that occur, the more the thermal energy storage benefits from latent heat transfer. Lithium fluoride also has good thermophysical

properties such as specific heat, thermal conductivity, viscosity, and density that we assume to remain constant between its solid and liquid phases (Sharopov, 2025).

Table 1: Inputs for the Example Case

Parabolic Trough and Receiver			
Heat transfer surface k [kW/(m^2·K)]	0.32	Mass flow rate [kg/s]	0.15
Specific heat working fluid [kJ/(kg·K)]	0.1318	Cleanliness losses due to soiling	0.86
Density of working fluid [kg/m^3]	2.17	Optical efficiency	0.6
Length of receiver tube [m]	40	Incident angle modifier	1
Radius of receiver tube [m]	0.0125	Thermal efficiency	0.73
Width of parabolic trough aperture [m]	7.5		
Heat Exchanger			
Inner radius – working fluid [m]	0.4	Specific heat of water [J/(kg·K)]	4.184
Outer radius – water / steam [m]	0.5	Specific heat of steam [J/(kg·K)]	1.996
Heat exchanger length [m]	10	Density of water [kg/m^3]	1000
h for working fluid [W/(m^2·K)]	1640	Density of steam [kg/m^3]	0.598
h for steam [W/(m^2·K)]	100	Transfer surface k [kW/(m^2·K)]	10
Thermal Energy Storage System			
PCM melting point [C]	848	PCM Initial Temperature [C]	250
PCM solid density [kg/m^3]	1700	Heat transfer surface height [m]	1
PCM liquid density [kg/m^3]	1700	Heat transfer surface length [m]	4
PCM solid specific heat [kJ/(kg·K)]	2.428	Heat transfer surface width [m]	2
PCM liquid specific heat [kJ/(kg·K)]	2.428	Transfer surface thickness [m]	0.05
h for solid PCM [kW/(m^2·K)]	2.1	Transfer surface k [kW/(m^2·K)]	10
h for liquid PCM [kW/(m^2·K)]	19	Latent heat of fusion [kJ/kg]	1.041
Other			
Turbine efficiency	0.7	External battery capacity [kWh]	10
Initial PCM temperature [C]	250	Battery max charge rate [kW]	2.5

User inputs include time-based datasets such as the power demand profile, direct normal solar irradiance, and ambient temperature. Figures 3 through 5 show the dataset inputs used for this example case. In each following figure, the first time-based plot shows the series across the full period. The second plot zooms in on the x-axis to show a section of the series and allow for a clearer view of detailed trends. Figure 3 visualizes this zoomed x-axis, and each subsequent figure shows the same.

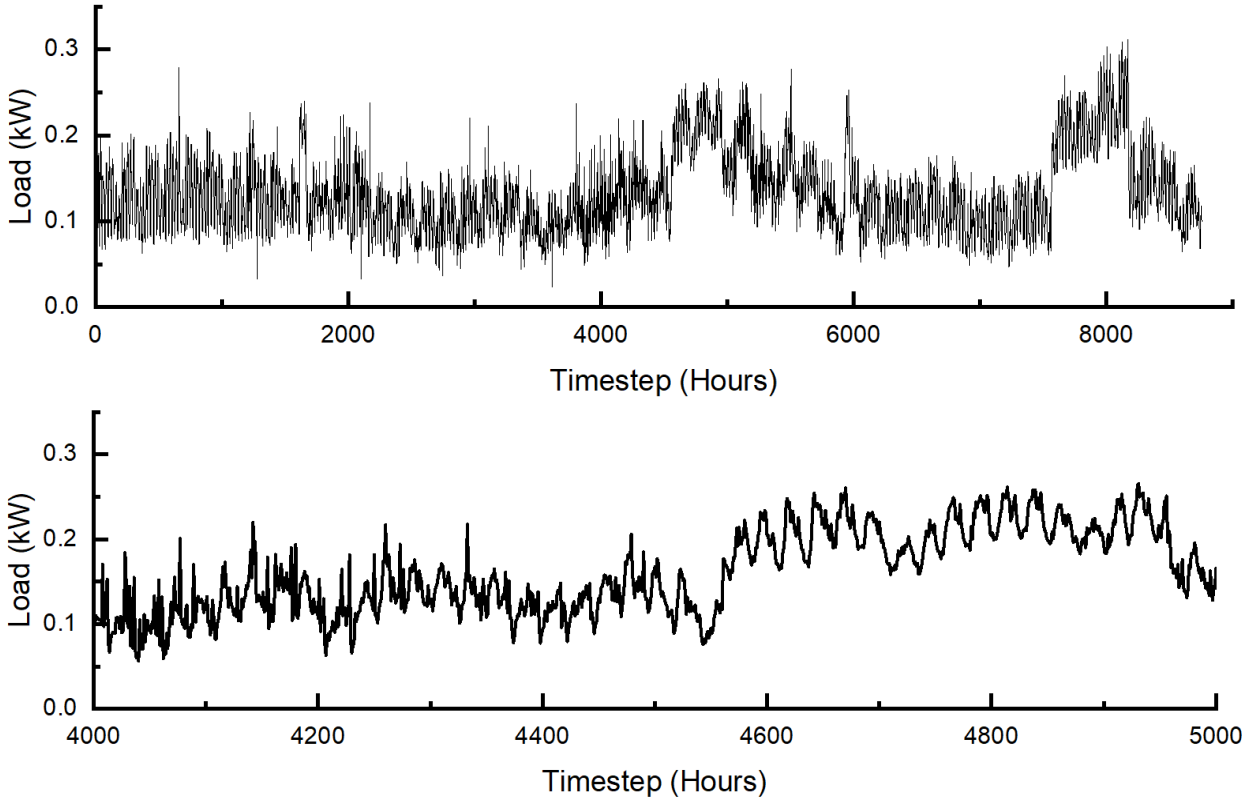

Figure 3: Power Demand (Load) Input Data

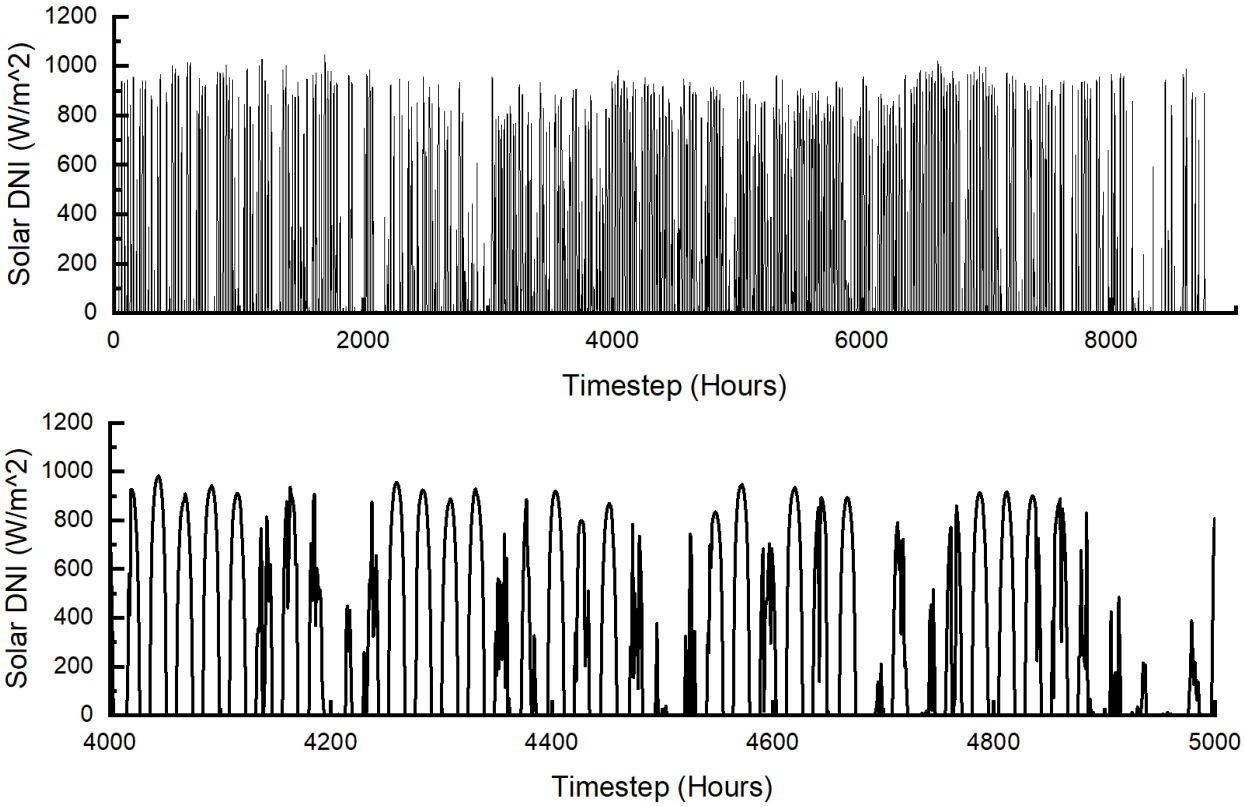

Figure 4: Direct Normal Solar Irradiance Input Data

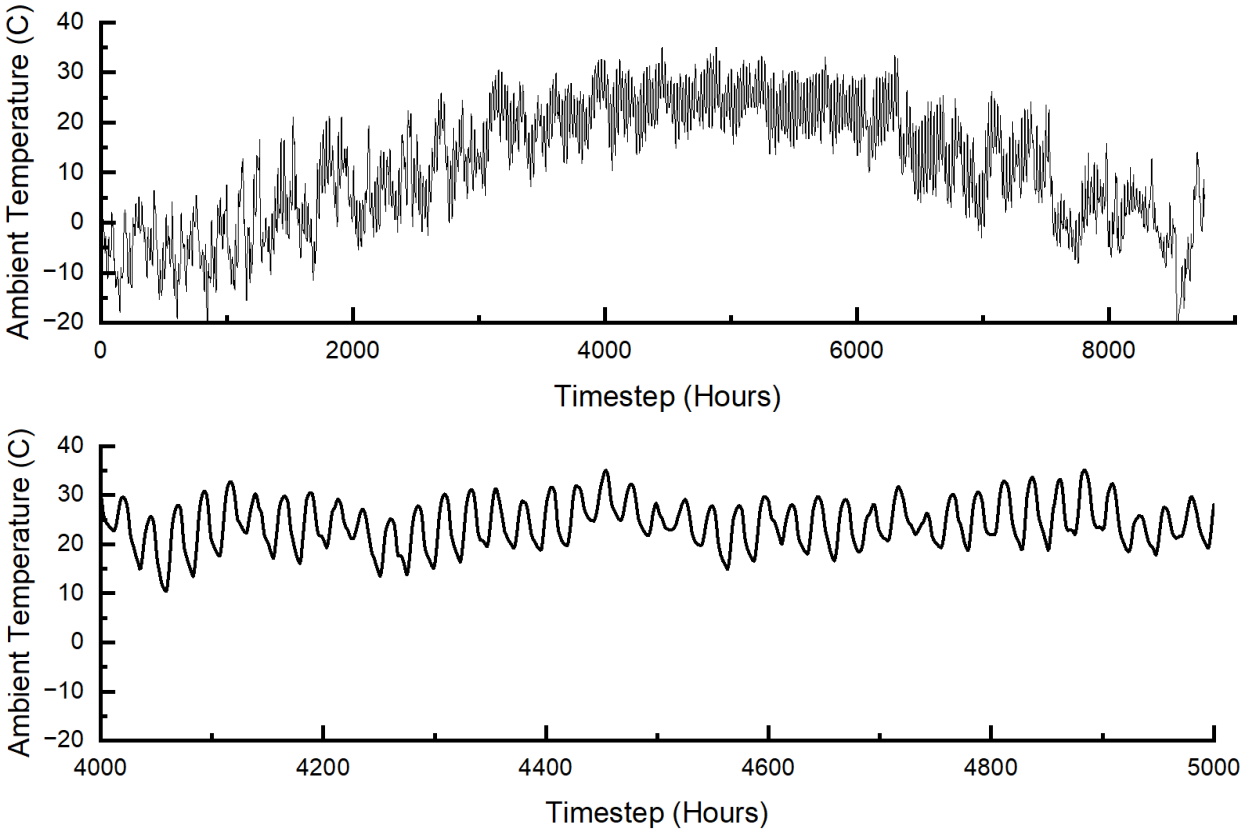

Figure 5: Ambient Temperature Input Data

CHAPTER 3: TEMPERATURE AND ENERGY GAIN AT RECEIVER OUTPUT

Mathematically modeling a parabolic trough CSP system first involves calculating the temperature of the working fluid at the outlet of the receiver tube. Due to the parabolic mirrors that concentrate solar radiation onto the receiver, energy is transferred to the working fluid as it flows through the receiver. The temperature, heat flux, and quantity of energy transferred at the receiver outlet depend on the size of the parabolic mirrors relative to the receiver and the working fluid flow rate.

Equation 5: Heat Flux into Receiver

$$q''_{absorber}[t] = \frac{S[t] * A_{aperture} * \eta_{thermal} * \eta_{optical} * \eta_{losses} * \kappa_{angle}}{A_{absorber,surface} * 1000} \quad (5)$$

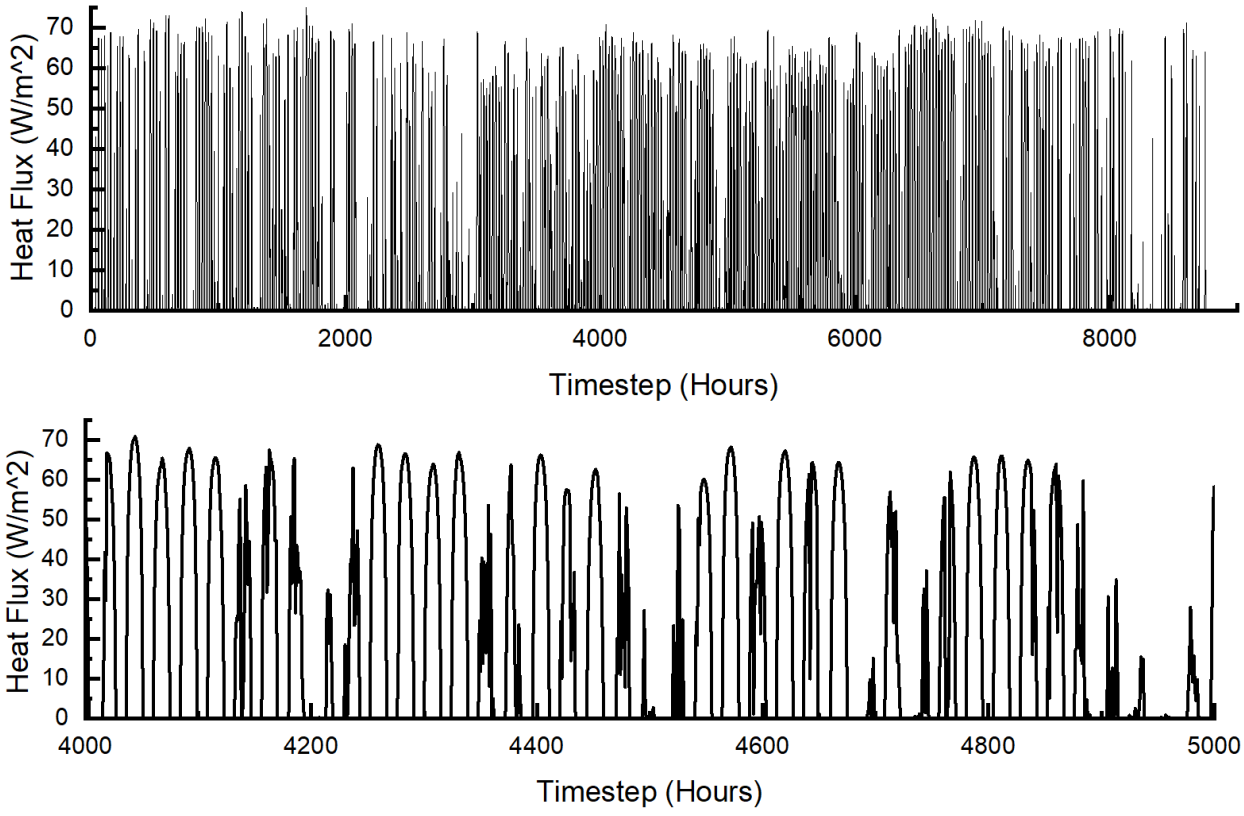

Figure 6: Heat Flux into Receiver

Equation 6: Mass Flow Rate of the Working Fluid

$$\dot{m} = \left(\frac{LE_{absorber}}{T_{wf}}\right) * A_{absorber,section} * \rho_{wf} \quad (6)$$

The hot working fluid from the outlet of the receiver is routed to a heat exchanger, where it heats water into steam. The steam powers a turbine connected to a generator to complete the transition of thermal energy to electrical energy. Heat exchangers are an essential component of concentrated solar power systems. A pipe heat exchanger is modeled in this calculation process, which has an outer diameter and an inner diameter to allow the flow of a hot working fluid and a cold fluid.

These pipes may be parallel flow, where the hot and cold fluid flow in the same direction, or counterflow, where the fluids flow in opposite directions. Once the output temperature of the working fluid from the receiver is known, the temperature of the water at the heat exchanger output can be calculated using the Effectiveness-NTU method. The temperature of the working fluid from the outlet of the receiver is treated as the "hot" fluid input temperature to the heat exchanger. The water at the heat exchanger input is treated as the "cold" fluid. For this stage of calculation, it is assumed that all the working fluid is routed toward the heat exchanger. None of the working fluid is routed toward thermal energy storage. The water must transition into steam in the heat exchanger to power the turbine, so the output temperature of the water from the heat exchanger must be at least 100 °C for the turbine to produce electricity.

Equation 7: Output Temperature of the Working Fluid from Receiver, Input to Heat Exchanger

$$T_{hot,in}[t] = \left(\frac{q''_{absorber}[t]}{\dot{m} * c_{p,hot}}\right) + T_{amb}[t] \quad (7)$$

Equation 8: Overall Heat Transfer Coefficient for the Heat Exchanger

$$U_{he} = \frac{1}{h_{hot}} + \frac{1}{h_{cold}} + \frac{w_{wall}}{k_{wall}} \quad (8)$$

Equation 9: NTU for the Heat Exchanger

$$NTU_{he} = \frac{U_{he} * A_{transfer}}{\min\left(c_{p,hot}\,, c_{p,cold}\right)} \tag{9}$$

Equation 10: C_r for the Heat Exchanger

$$C_{r,he} = \frac{\min\left(c_{p,hot}\,, c_{p,cold}\right)}{\max\left(c_{p,hot}\,, c_{p,cold}\right)} \tag{10}$$

Equation 11: Effectiveness of the Heat Exchanger

$$\varepsilon_{exchanger} = \frac{1 - e^{-NTU_{he}*\left(1-C_{r,he}\right)}}{1 - C_{r,he} * e^{-NTU_{he}*\left(1-C_{r,he}\right)}} \tag{11}$$

Equation 12: Output Temperature of the Working Fluid from the Heat Exchanger

$$T_{hot,out}[t] = T_{hot,in}[t] - \left(\frac{\varepsilon_{exchanger} * \min\left(c_{p,hot}\,, c_{p,cold}\right) * \left(T_{hot,in}[t] - T_{amb}[t]\right)}{c_{p,hot}}\right) \tag{12}$$

Equation 13: Output Temperature of the Water/Steam from the Heat Exchanger

$$T_{cold,out}[t] = \left(\frac{c_{p,hot}}{c_{p,cold}}\right) * \left(T_{hot,in}[t] - T_{hot,out}[t]\right) + T_{amb}[t] \tag{13}$$

The power output of the steam turbine is dependent on the output temperature of the steam from the heat exchanger, the mass flow rate of the steam, and various system efficiencies.

Equation 14: Expected Power Output of CSP System – Electric Power

$$P[t] = \eta_{system} * \dot{m} * c_{p,steam} * \left(T_{cold,out}[t] + 273\right) \tag{14}$$

Figure 7 shows the model's calculation for expected power output of the example CSP system. Expected power output is plotted over time alongside the input power demand (load). This plotted result assumes that thermal energy storage is not yet integrated into the example CSP system. The power output of the CSP system in this case is entirely dependent on intermittent solar irradiance, so it is frequently in surplus or shortage of the power demand. External energy storage or power control mechanisms would be necessary to support this CSP system to serve the current power demand profile. Integrating thermal energy storage into this

CSP system can address the problem as well, so the outcomes of this integration are covered in Section 4.

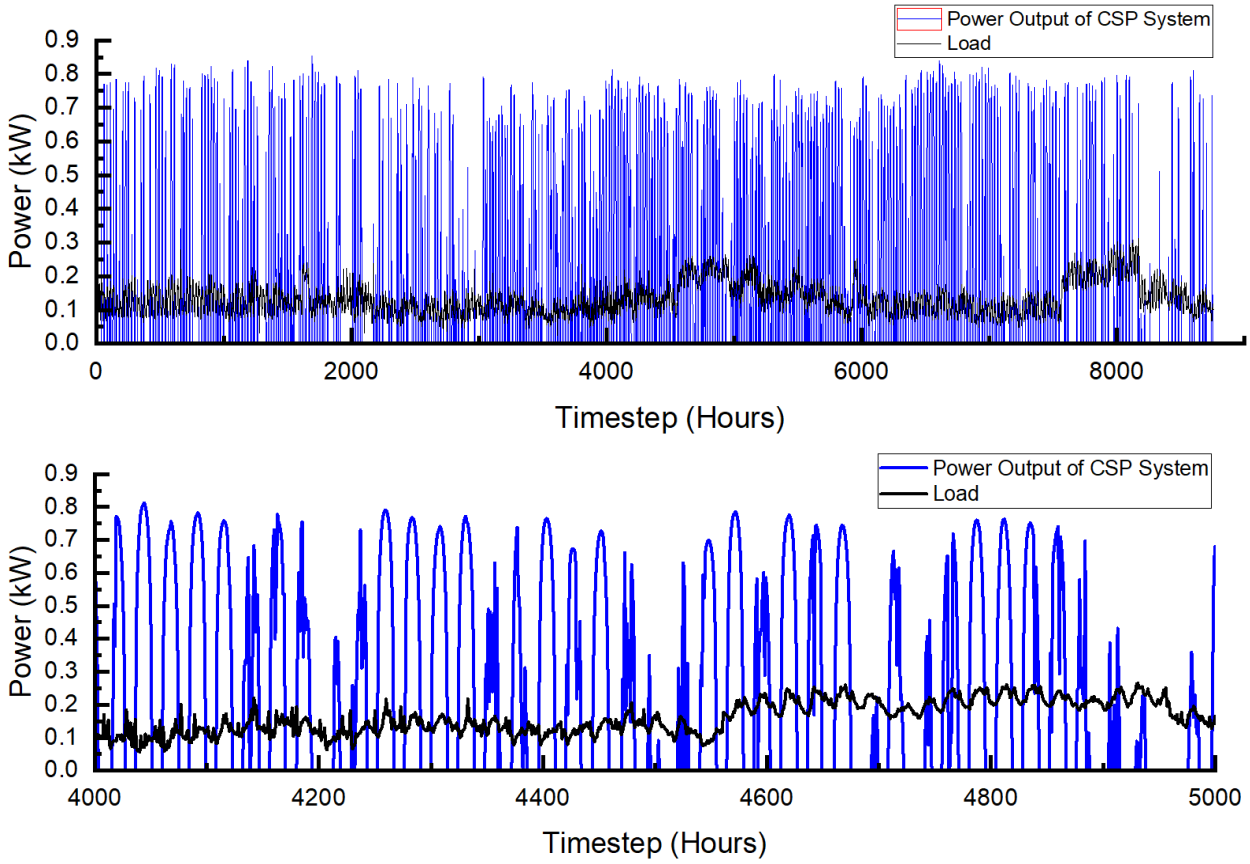

Figure 7: Power Demand (Load) vs Power Output of CSP System

External energy storage would capture the power output of the CSP system during periods of surplus power production and discharge power to the load during periods of a power production shortage. The surplus power production from the CSP system is calculated using Equation 15, where positive values represent a surplus of power in relation to the power demand and negative values represent a shortage. External energy storage is modeled in Equation 16. This formula considers the current state of power surplus and tracks the quantity of energy stored, considering a user-defined energy storage capacity.

Equation 15: Power Surplus from CSP System

$$P_{surplus} = P[t] - L[t] \tag{15}$$

Equation 16: Stored Energy within External Battery

$$\begin{gathered} If \quad E[t-1] + P_{surplus}[t] > E_{capacity} \quad , \quad E[t] = E_{capacity} \\ If \quad E[t-1] + P_{surplus}[t] < E_{capacity} \quad , \quad E[t] = 0 \\ else \quad E[t] = E[t-1] + P_{surplus}[t] \end{gathered} \tag{16}$$

CHAPTER 4: ADDING THERMAL ENERGY STORAGE

One purpose of thermal energy storage technologies in CSP systems is to regulate CSP power output to match current load. To model this output regulation, the next stage of this calculation process adds thermal energy storage to the CSP system. A controller can manage the proportion of working fluid from the receiver routed through the thermal energy storage versus directly to the heat exchanger. The proportion of working fluid routed through the thermal energy storage impacts the overall power output of the CSP system. Considering this, the proportion of working fluid routed through the thermal energy storage can be controlled to match the power output of the CSP system to the load.

When the temperature of the thermal energy storage material is higher than the temperature of the working fluid, the thermal energy storage system will provide additional energy to any proportion of working fluid that is routed to pass through the thermal energy storage system. This would raise the working fluid temperature and can manage expected power production shortages. When the temperature of the thermal energy storage material is lower than the temperature of the working fluid, any working fluid routed to the thermal energy storage will charge the storage system. This would lower the working fluid temperature and can manage expected power production surplus.

The following set of calculation steps determine the proportion of working fluid that must be routed to the thermal energy storage at each timestep to match the electrical power output to the load. The first step is to find the desired output temperature of the steam that is needed to match the correspondent load data point. This is directly calculated from each load data point.

Equation 17: Desired Steam Output Temperature from Heat Exchanger to Match Load

$$T_{cold,out}^{des}[t] = \frac{L[t]}{\eta_{system} * \dot{m} * c_{p,steam}} - 273 \quad (17)$$

Using the effectiveness-NTU method, the next step is to find the needed working fluid temperature at the input of the heat exchanger to achieve the desired steam output temperature. This working fluid temperature is also at the output of the thermal energy storage system, so it can also be expressed as the desired temperature at the output of the thermal energy storage system. The effectiveness of the heat exchanger found previously is used for this step.

Equation 18: Desired Working Fluid Input Temperature to Heat Exchanger / Output Temperature from Energy Storage to Match Load

$$T_{hot,esout}^{des}[t] = T_{hot,in}^{des}[t] = \frac{c_{p,cold} * \left(T_{cold,out}[t] - T_{amb}[t]\right)}{\varepsilon_{exchanger} * \min\left(c_{p,hot}, c_{p,cold}\right)} + T_{amb}[t] \quad (18)$$

The output temperature of the working fluid from the receiver ($T_{hot,in}$) is calculated in the previous section. In a CSP system with thermal energy storage as an intermediate stage of power production, the output temperature from the receiver becomes the input temperature to the thermal energy storage system ($T_{hot,esin}$) rather than directly to the heat exchanger. Equation 19 reflects this change.

Equation 19: Output Temperature of the Working Fluid from Receiver, Input to Thermal Energy Storage System

$$T_{hot,esin}[t] = \left(\frac{q''_{absorber}[t]}{\dot{m} * c_{p,hot}}\right) + T_{amb}[t] \quad (19)$$

The effectiveness of the thermal energy storage system must be calculated. To do so, Equations 23 through 26 calculate NTU and C_r based on user-defined energy storage system parameters. In a sensible system, these properties are treated as constants. In a latent system, material properties such as heat transfer coefficient, specific heat, and density change as the

energy storage material experiences phase changes. These material properties are treated as dynamic variables that depend on the material's phase at each timestep.

Equation 20: Dynamic Heat Transfer Coefficient of the Phase Change Material

$$h_{PCM}[t] = h_{PCM,s} \quad for \quad T_{PCM}[t] < T_m \quad else \quad h_{PCM}[t] = h_{PCM,l} \tag{20}$$

Equation 21: Dynamic Specific Heat of the Phase Change Material

$$c_{p,PCM}[t] = c_{PCM,s} \quad for \quad T_{PCM}[t] < T_m \quad else \quad c_{p,PCM}[t] = c_{PCM,l} \tag{21}$$

Equation 22: Dynamic Density of the Phase Change Material

$$\rho_{PCM}[t] = \rho_{PCM,s} \quad for \quad T_{PCM}[t] < T_m \quad else \quad \rho_{PCM}[t] = \rho_{PCM,l} \tag{22}$$

Phase-dependent material characteristics contribute to the effectiveness of a latent thermal energy storage system. Effectiveness is a time-domain variable due to the phase dependency.

Equation 23: Dynamic Overall Heat Transfer Coefficient for the Energy Storage System

$$U_{es}[t] = \frac{1}{h_{hot}} + \frac{1}{h_{PCM}[t]} + \frac{w_{wall,es}}{k_{wall,es}} \tag{23}$$

Equation 24: Dynamic NTU for the Energy Storage System

$$NTU_{es}[t] = \frac{U_{es}[t] * A_{transfer,es}}{\min\left(c_{p,hot}\,, c_{p,PCM}[t]\right)} \tag{24}$$

Equation 25: Dynamic C_r for the Energy Storage System

$$C_{r,es}[t] = \frac{\min\left(c_{p,hot}\,, c_{p,PCM}[t]\right)}{\max\left(c_{p,hot}\,, c_{p,PCM}[t]\right)} \tag{25}$$

Equation 26: Dynamic Effectiveness of the Energy Storage System

$$\varepsilon_{es}[t] = \frac{1 - e^{-NTU_{es}[t]*\left(1-C_{r,es}[t]\right)}}{1 - C_{r,es}[t] * e^{-NTU_{es}[t]*\left(1-C_{r,es}[t]\right)}} \tag{26}$$

This effectiveness can be used to calculate the output temperature of the working fluid from the thermal energy storage system, the heat flux into the energy storage material, and the temperature change in the thermal energy storage material. The thermal energy storage material can be a sensible material that maintains its phase during temperature fluctuations, or it can be a

latent material with a melting point that enables phase change. Once heat flux into the thermal energy storage material is calculated in Equation 28, Equation 29 calculates the temperature of the energy storage material using derivations of heat flux formulas. This equation applies the derivation of the sensible heat flux formula to find temperature when the calculated temperature indicates that no phase change occurs between the current and previous timestep. When the sensible formula indicates that the material will phase change from solid to liquid or from liquid to solid, this equation instead applies the latent heat flux derivation to find the temperature of the thermal energy storage material.

Equation 27: Working Fluid Output Temperature from the Energy Storage System

$$T_{hot}^{esout}[t] = T_{hot}^{esin}[t] - \left(\frac{\varepsilon_{es}[t] * \min\left(C_{p,hot}, C_{p,PCM}[t]\right) * \left(T_{hot}^{esin}[t] - T_{PCM}[t-1]\right)}{C_{p,hot}} \right) \quad (27)$$

Equation 28: Total Heat Transfer Rate and Heat Flux into Energy Storage Material

$$\dot{Q}[t] = \dot{m} * C_{p,hot} * \left(T_{hot,esin}[t] - T_{hot,esout}[t]\right) \quad (28a)$$

$$q"[t] = \frac{\dot{Q}[t]}{A} \quad (28b)$$

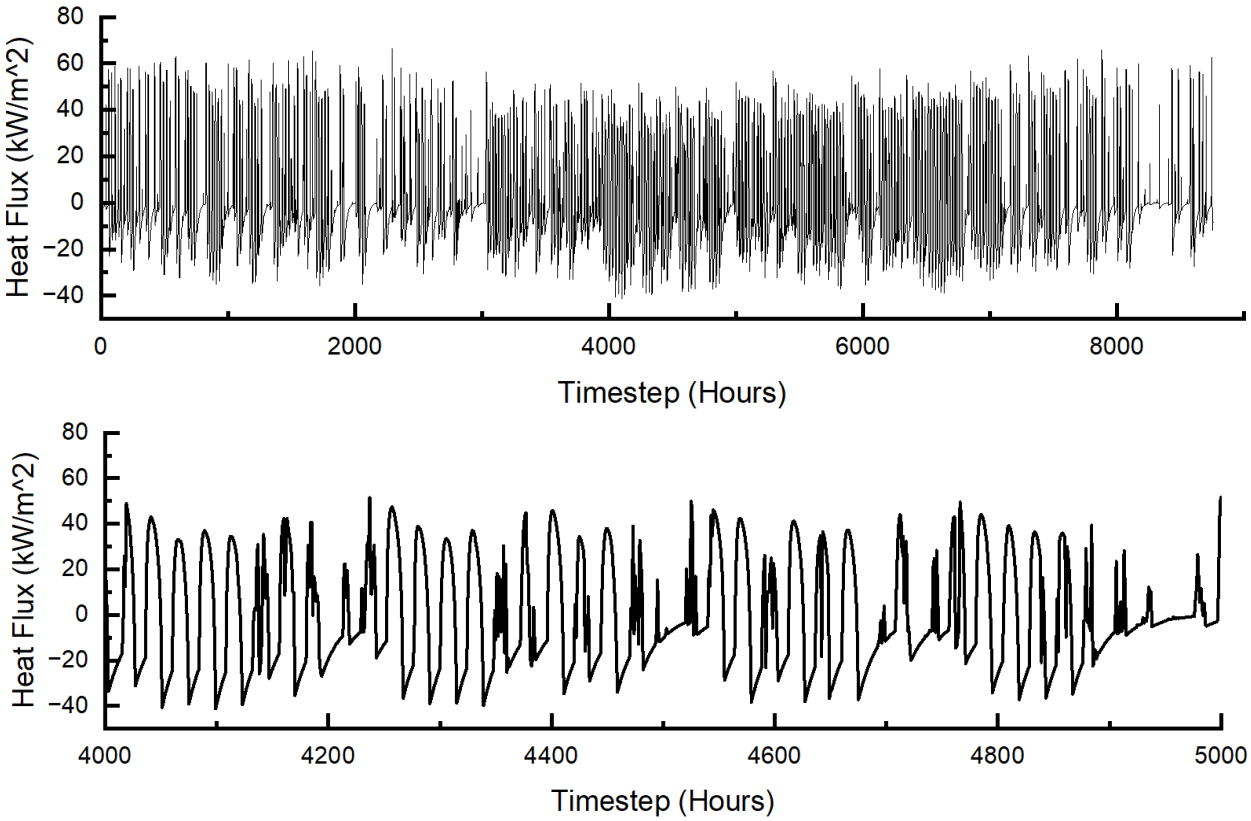

Figure 8: Heat Flux into Thermal Energy Storage Material

Equation 29: Dynamic Temperature of the Thermal Energy Storage PCM

$$For \quad T_{PCM}[t-1] > T_m \quad and \quad T_{PCM,sensible}[t] < T_m \quad \text{(phase change to solid)}$$

$$\dot{Q}[t] = -\left(\dot{m} * c_{PCM,s} * (T_m - T_{PCM}[t]) + \dot{m} * L + \dot{m} * c_{PCM,l} * (T_{PCM}[t-1] - T_m)\right)$$

$$T_{PCM}[t] = T_m + \frac{\left(q''[t] + \dot{m} * L + m_{dot} * c_{PCM,l} * (T_{PCM}[t-1] - T_m)\right)}{m_{dot} * c_{PCM,s}} \tag{29a}$$

$$Phase = -1$$

$$For \quad T_{PCM}[t-1] < T_m \quad and \quad T_{PCM,sensible}[t] > T_m \quad \text{(phase change to liquid)}$$

$$\dot{Q}[t] = \left(\dot{m} * c_{PCM,s} * (T_m - T_{PCM}[t-1]) + \dot{m} * L + \dot{m} * c_{PCM,l} * (T_{PCM}[t] - T_m)\right)$$

$$T_{PCM}[t] = T_m + \frac{\left(q''[t] - \dot{m} * L - \dot{m} * c_{PCM,s} * (T_m - T_{PCM}[t-1])\right)}{\dot{m} * c_{PCM,l}} \tag{29b}$$

$$Phase = 1$$

$$For \quad T_{PCM}[t-1] > T_m \quad and \quad T_{PCM,sensible}[t] > T_m \quad \text{(remains in liquid state)}$$

$$\dot{Q}[t] = \left(\dot{m} * c_{PCM,l} * (T_{PCM}[t] - T_{PCM}[t-1])\right)$$

$$T_{PCM}[t] = T_{PCM}[t-1] + \frac{q''[t]}{\dot{m} * c_{PCM,l}} \tag{29c}$$

$$Phase = 0$$

$$For \quad T_{PCM}[t-1] < T_m \quad and \quad T_{PCM,sensible}[t] < T_m \quad \text{(remains in solid state)}$$

$$\dot{Q}[t] = \left(\dot{m} * c_{PCM,s} * (T_{PCM}[t] - T_{PCM}[t-1])\right)$$

$$T_{PCM}[t] = T_{PCM}[t-1] + \frac{q''[t]}{\dot{m} * c_{PCM,s}} \tag{29d}$$

$$Phase = 0$$

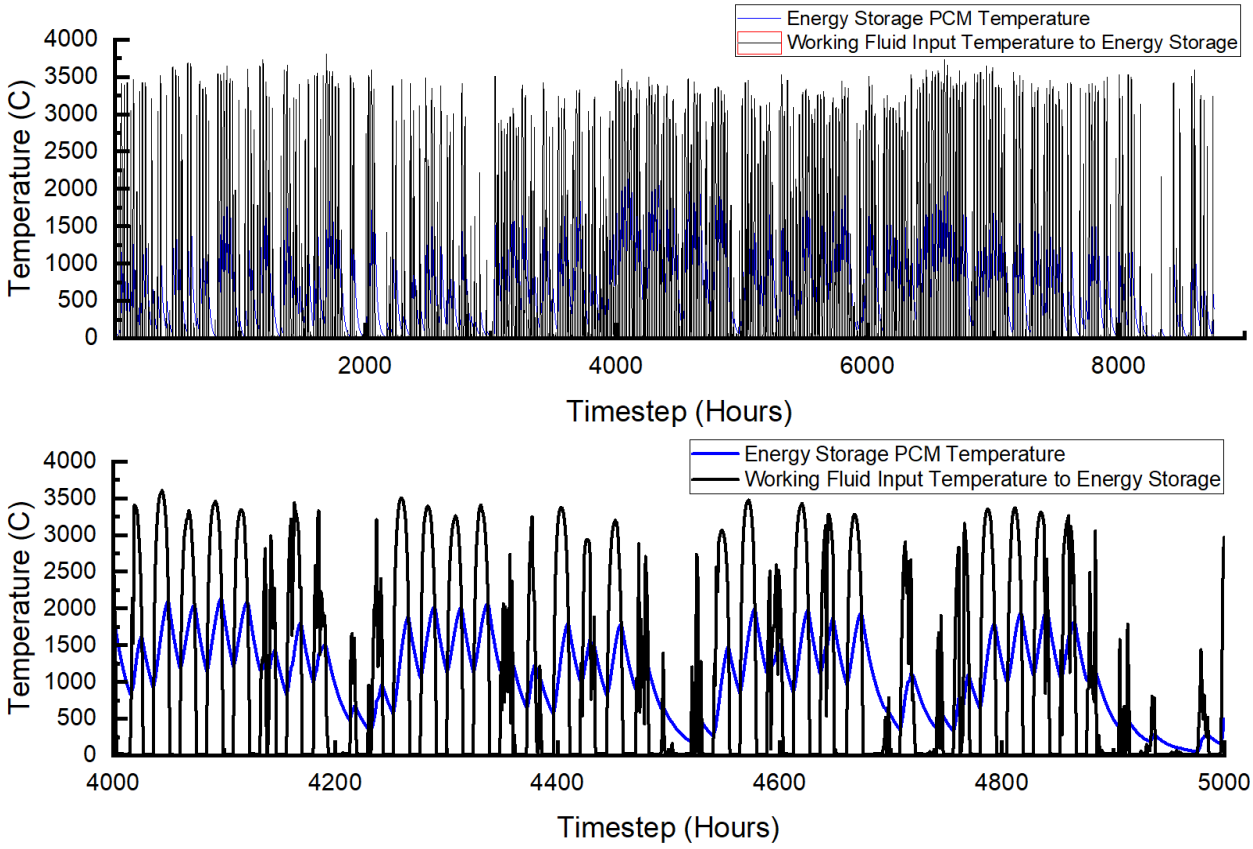

Figure 9: Working Fluid Input Temperature vs Temperature of the PCM

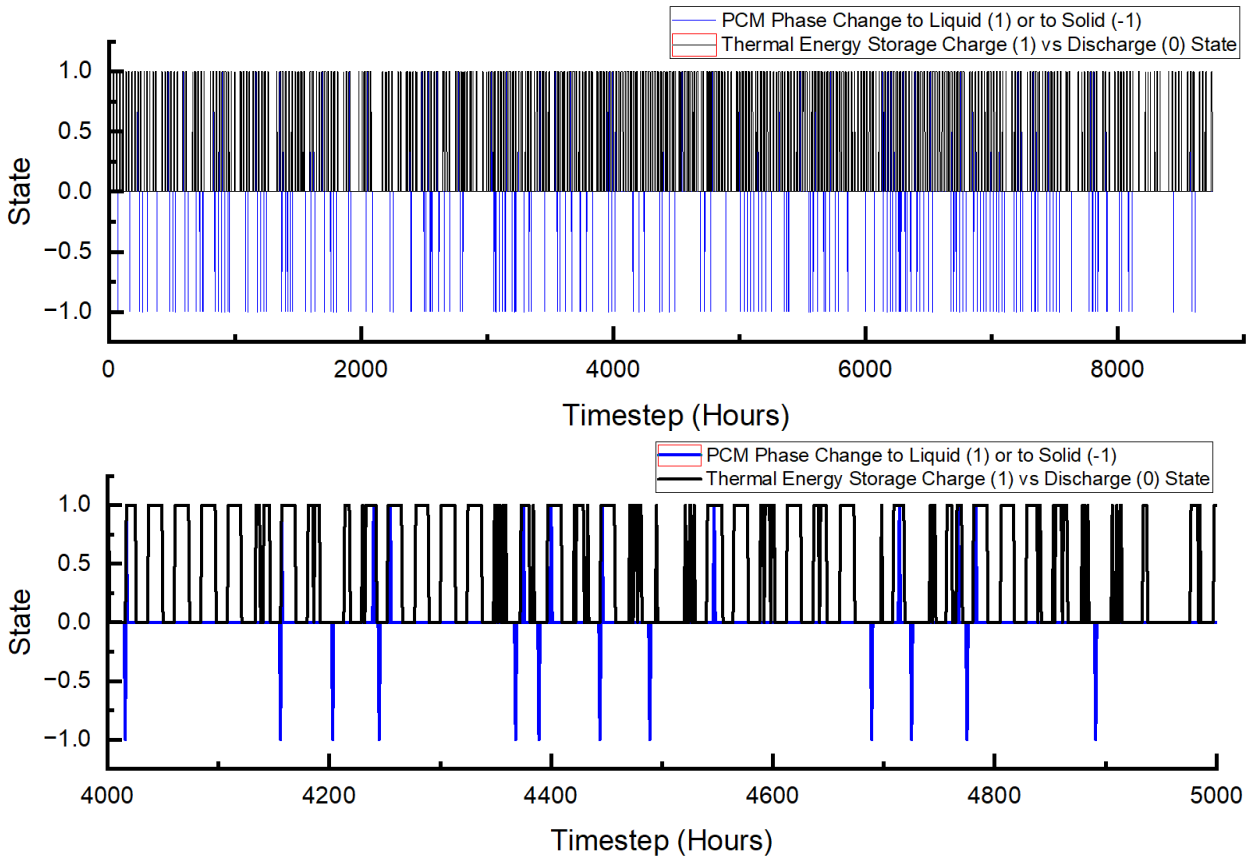

Figure 10: Thermal Energy Storage PCM Charge State and Phase Changes

The temperature of the energy storage material is necessary to calculate the output temperature of the working fluid from the thermal energy storage system in Equation 27. At each timestep, this allows the calculation process to determine what proportion of the working fluid must be routed to the energy storage system before it reaches the heat exchanger to match the output power of the system to the load.

Equation 30: Proportion of Working Fluid Routed to the Energy Storage System

$$PR_{hot}[t] = \frac{T^{des}_{hot,esout}[t] - T_{hot,esin}[t]}{T_{hot,esout}[t] - T_{hot,esin}[t]} \tag{30}$$

Timesteps for which this proportion is between 0 and 1 indicate that the CSP system can use its thermal energy storage to match its power output to the current load. These timesteps are marked as “Matches Load.” When the proportion is greater than 1, the CSP system is incapable

of matching its power output to the current load. In a technical sense, this means that a greater quantity of working fluid than the available working fluid would have to be diverted to the energy storage for the CSP system to match load. There are three potential causes for a proportion greater than 1:

1. The power output capability of the CSP system is too small relative to the load
2. The load is high relative to the energy in the working fluid and there isn't enough stored thermal energy to transfer into the working fluid

$$T_{hot,esout}^{des}[t] > T_{hot,esin}[t]$$

3. The load is low relative to the energy in the working fluid and the thermal energy storage system is at a temperature too high to accept energy discharged into the system

$$T_{hot,esin}[t] > T_{hot,esout}^{des}[t]$$

These conditions impact how instances of PR_{hot} greater than 1 are classified as shown in Equation 31.

Equation 31: Outcomes of Proportion of Working Fluid Routed to Energy Storage

$$\begin{matrix} t \rightarrow \text{"Matches Load"} \quad for \quad 1 > PR_{hot}[t] > 0 \\ t \rightarrow \text{"Insufficient"} \quad for \quad PR_{hot}[t] > 1 \quad and \quad T_{hot,esout}^{des}[t] > T_{hot,esin}[t] \\ t \rightarrow \text{"Excess Power"} \quad for \quad PR_{hot}[t] > 1 \quad and \quad T_{hot,esin}[t] > T_{hot,esout}^{des}[t] \end{matrix} \tag{31}$$

In a small portion of timesteps, the direction of heat transfer between the working fluid and the phase change material in the thermal energy storage system can be opposite of the direction of heat transfer needed to match the load on the CSP system. Ideally, the CSP system should be designed to minimize the proportion of time that this contradiction occurs. This contradiction is characterized by the "Mismatch" outcome, which overrides all other outcomes

assigned to the timestep. When the first condition in this equation is true, the temperature of the working fluid traveling into the energy storage is greater than the desired output temperature to match load. This means that the working fluid must charge the phase change material in the energy storage system to match load. When the second condition in this equation is true, the working fluid is charging the phase change material in the energy storage system. When both conditions are true, the energy storage system is charged during a timestep in which it is demanded. When both conditions are false, the stored thermal energy system is being dispatched during a timestep in which it is demanded. The "Mismatch" outcome is assigned to timesteps where only one condition or the other is met.

Equation 32: Mismatch Outcome of Proportion of Working Fluid Routed to Energy Storage

$$t \rightarrow \text{"Mismatch"} \quad for \quad T_{hot,esin}[t] > T^{des}_{hot,esout}[t] \quad xor \quad T_{PCM}[t] > T_{PCM}[t-1] \tag{32}$$

Due to these conditions, it is rare to design a solar CSP system that can frequently match the load as a stand-alone system. The actual proportion of working fluid that would be routed through the thermal energy storage system is a positive value that cannot exceed 1, so the next equation applies this condition.

Equation 33: Actual Proportion of Working Fluid Routed Through Energy Storage

$$PR_{hot,actual}[t] = 1 \quad for \quad PR_{hot}[t] > 1 \quad else$$
$$PR_{hot,actual}[t] = 0 \quad for \quad PR_{hot}[t] < 0 \quad else \quad PR_{hot,actual}[t] = PR_{hot}[t] \tag{33}$$

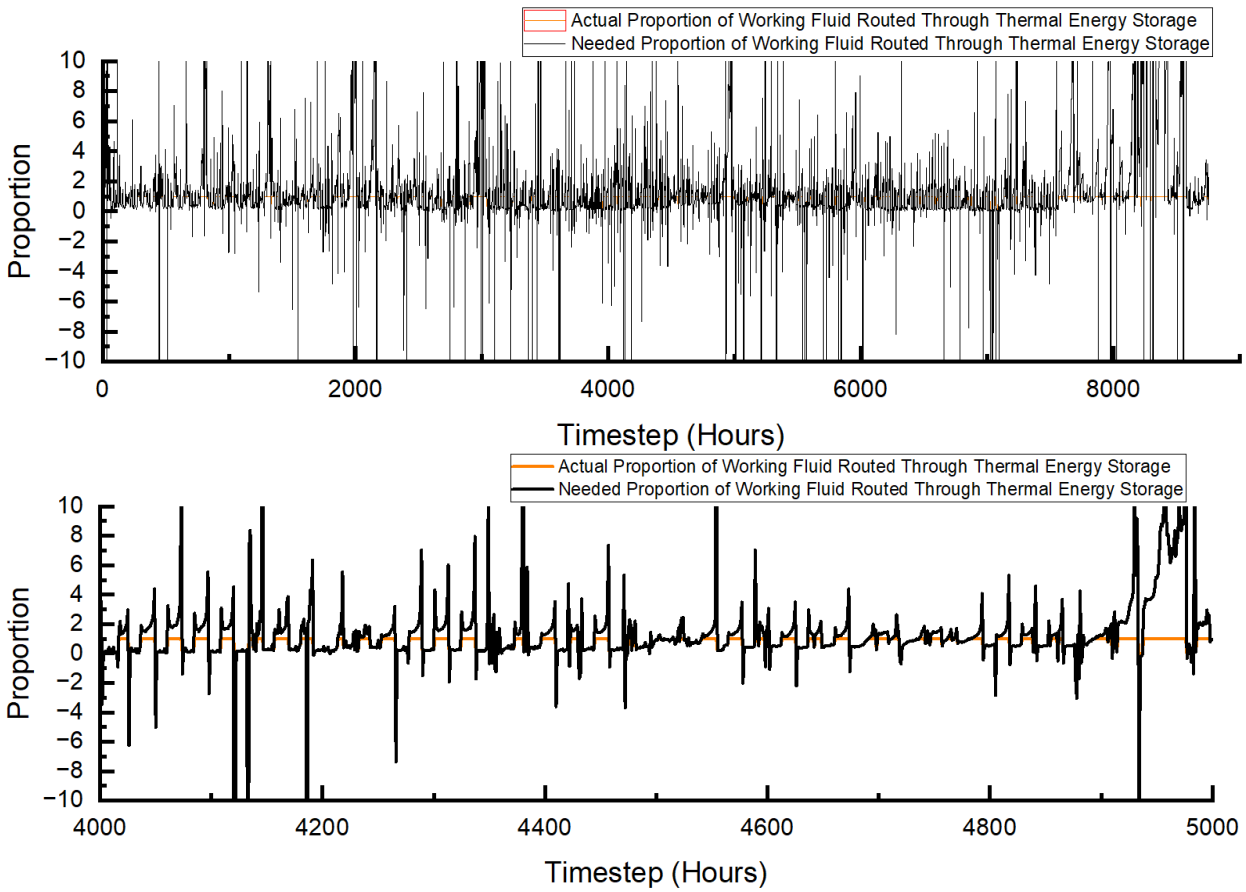

Figure 11: Proportion of Working Fluid Through Thermal Energy Storage

This algorithm assumes that the working fluid routed directly to the heat exchanger and the working fluid routed through the thermal energy storage system reconverge to enter the heat exchanger. The proportion of working fluid routed through the thermal energy storage system versus the proportion routed directly to the heat exchanger determines the output temperature of the reconverged working fluid. This means that the temperature of the working fluid input to the heat exchanger is a function of this actual proportion of working fluid routed through the energy storage system. This working fluid input temperature and the previously calculated effectiveness of the heat exchanger are used to calculate the output temperature of the steam from the heat exchanger that travels to the turbine.

Equation 34: Temperature of Reconverged Working Fluid into the Heat Exchanger

$$T_{hot,in}^{actual}[t] = \left(\left(1 - PR_{hot,actual}[t]\right) * T_{hot,in}[t]\right) + \left(PR_{hot,actual}[t] * T_{hot,esout}[t]\right) \quad (34)$$

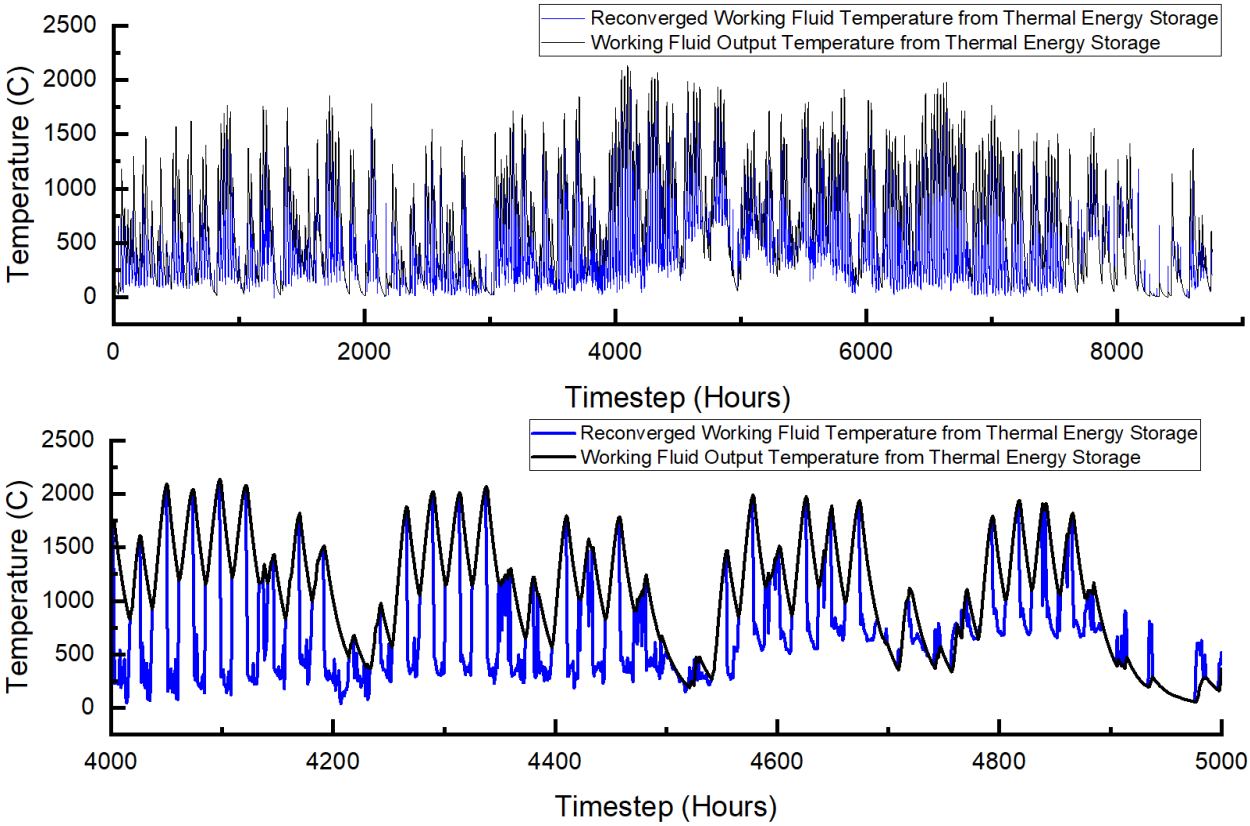

Figure 12: Reconverged Working Fluid Output Temperature

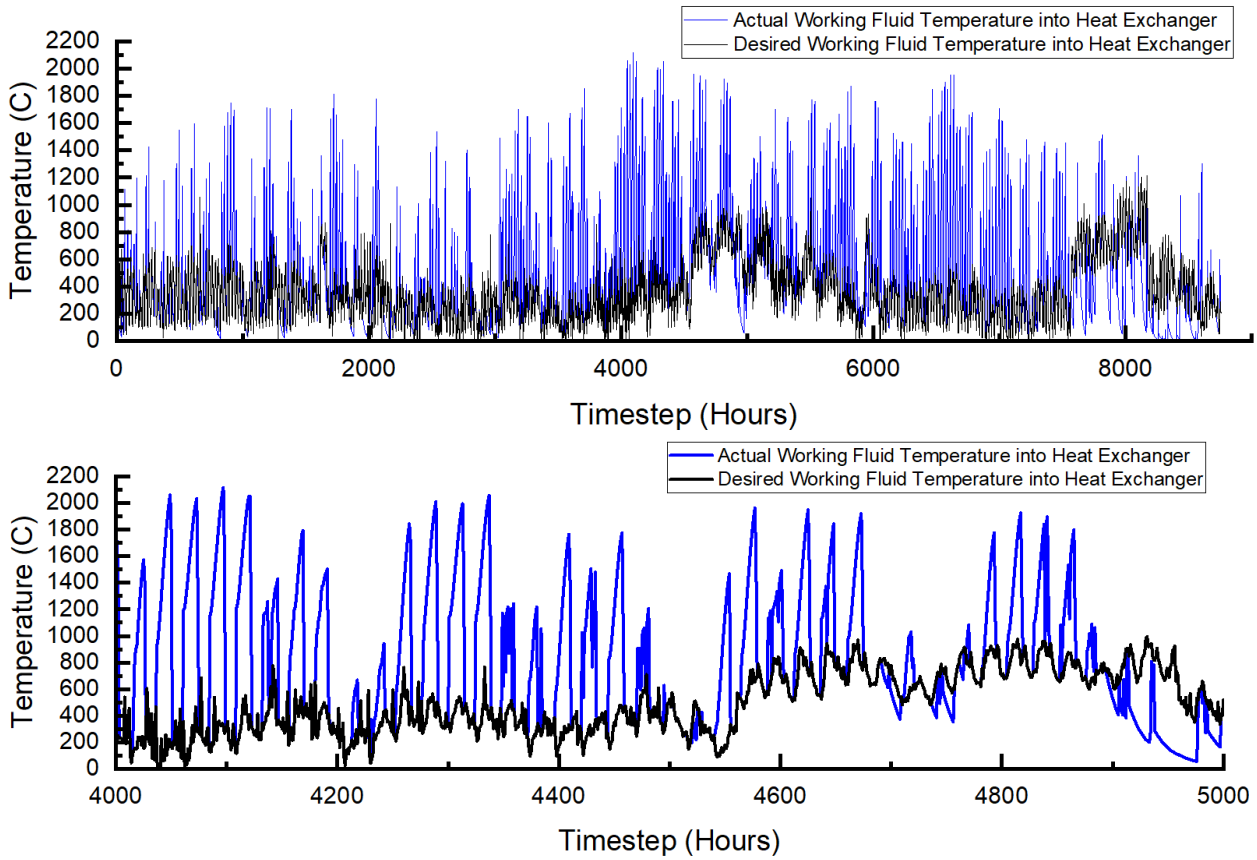

Figure 13: Desired vs Actual Working Fluid Temperature into Heat Exchanger

Equation 35: Temperature of Working Fluid Out of the Heat Exchanger

$$T_{hot,out}^{actual} = T_{hot,in}^{actual} - \left(\varepsilon_{exchanger} * \min\left(c_{p,hot}, c_{p,cold}\right) * \frac{T_{hot,in}^{actual} - T_{amb}[t]}{c_{p,hot}} \right) \quad (35)$$

Equation 36: Actual Steam Output Temperature from Heat Exchanger

$$T_{cold,out}^{actual} = \frac{c_{p,hot}}{c_{p,cold}} * \left(T_{hot,in}^{actual} - T_{hot,out}^{acutal}\right) + T_{amb}[t] \quad (36)$$

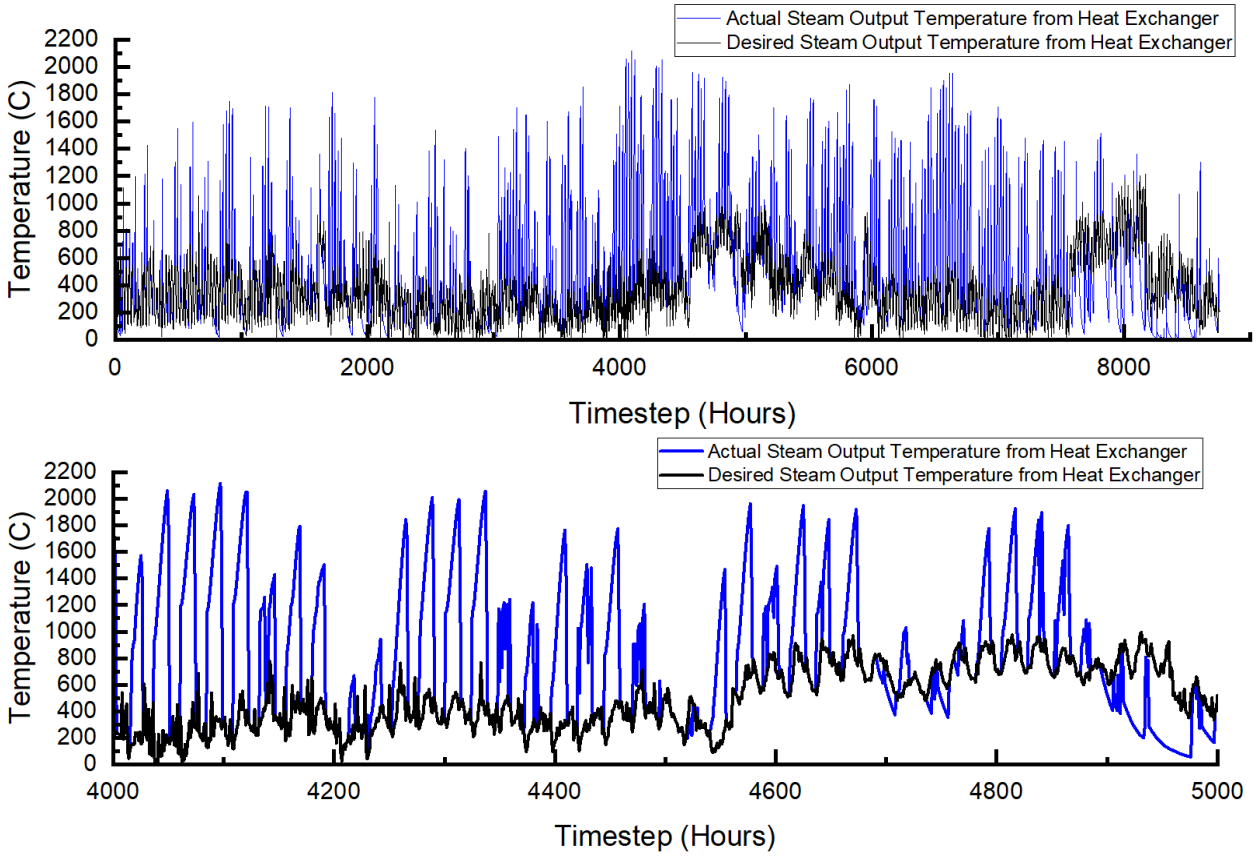

Figure 14: Desired vs Actual Steam Output Temperature

CHAPTER 5: POWER AVAILABILITY OF PARABOLIC TROUGH CSP SYSTEMS

The superheated steam output from the heat exchanger travels to a turbine, which powers an engine. The steam, the turbine, and the type of engine used at the end of the system determine the electric power output of the parabolic trough solar CSP system. The most common types of heat engines for parabolic trough solar thermal systems are the Stirling engine or the Brayton Cycle engine (Zhu, 2019). The electric power produced by the engine is directly related to the output temperature of the steam, the heat energy within it, and the efficiency of the turbine and engine. Equation 37 calculates the electric power produced at every timestep, considering the condition that water only turns to steam above 100 C.

Equation 37: Electric Power Output of CSP System

$$P[t] = \eta_{system} * \dot{m} * c_{p,steam} * \left(T_{cold,out}^{actual}[t] + 273\right) \quad for \quad T_{cold,out}^{actual}[t] > T_{steam,min} \quad else \quad P[t] = 0 \tag{37}$$

Figure 15 shows example results for the electric power output of a CSP system with and without thermal energy storage. The first plot is the time-domain output of Equation 10; the CSP system power output (orange line) compared to an example load profile (blue line) assuming that no thermal energy storage is included. This plot shows that the power output of a CSP system without thermal energy storage is dependent on solar irradiance patterns, so it cannot match load patterns. The second plot is the time-domain output of Equation 37; the CSP system power output compared to the load profile if the CSP system has thermal energy storage. This algorithm assumes that the CSP system can control the proportion of working fluid routed through the thermal energy storage channel. This allows the CSP system to modulate its power output to match the load when possible. Due to this power output modulation, the second plot shows instances for which the power output of the CSP system matches the user-input electric load.

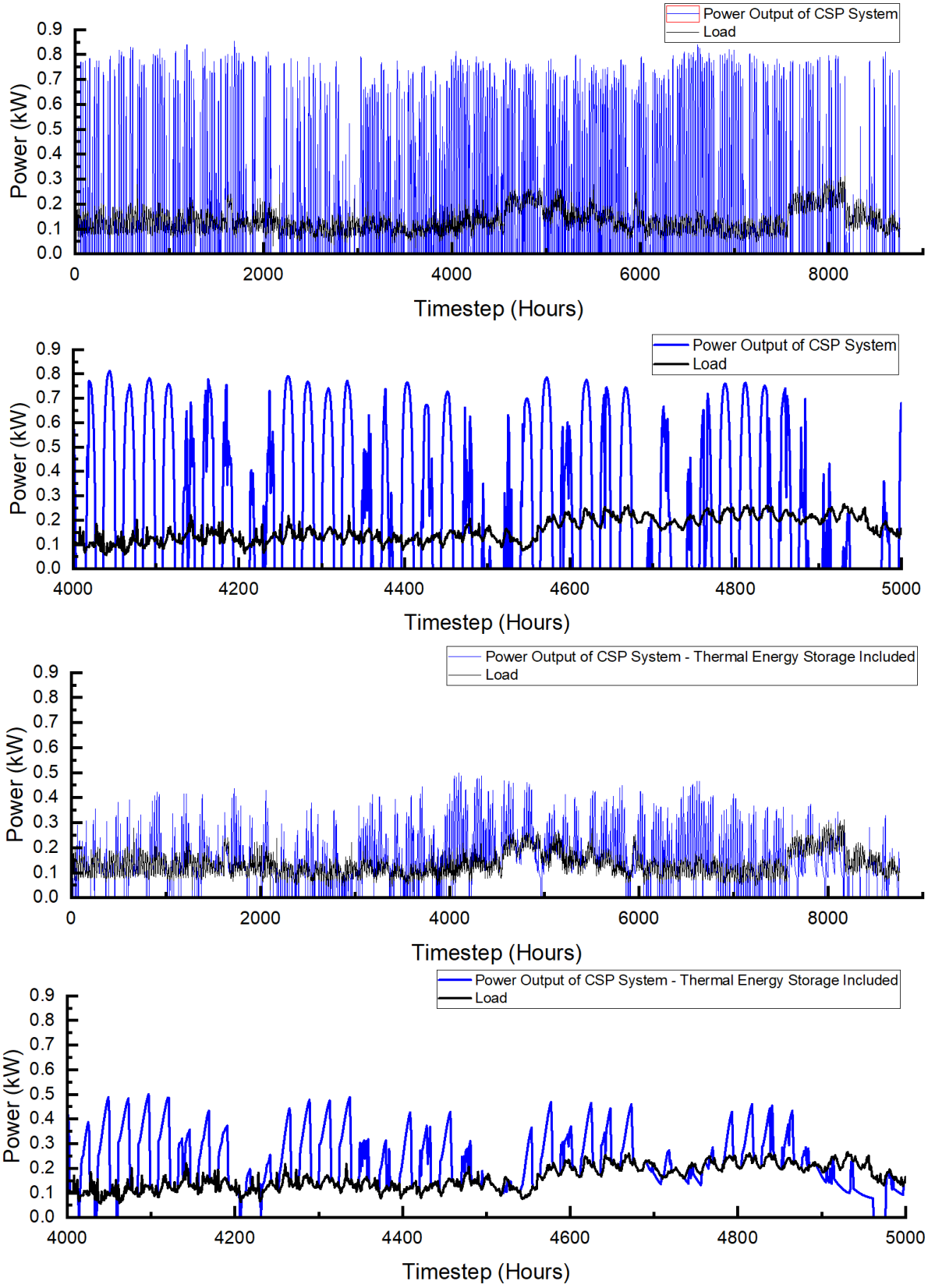

Figure 15: Plotted Power Demand (Load) vs CSP System Power Output With and Without Thermal Energy Storage

The calculated electric power output of the CSP system at each timestep can be exported to AMPeRRe. This allows for the modeling of a CSP system and its behavior when integrated into a microgrid with other intermittent renewable energy resources and dispatchable power. AMPeRRe provides several reliability and resilience-related metrics, which presents the opportunity to quantify how the incorporation of a CSP system with DynPCM thermal energy storage impacts microgrid reliability and resilience. The AMPeRRe calculation process will allow for the pairing of the CSP system electric power output with a user-input load profile at every timestep. AMPeRRe will use this load profile to determine when the CSP system would charge an external energy storage system (ESS) and when the ESS must discharge to account for a shortage of the intermittent power resources, including the CSP system.

This algorithm assumes that the proportion of working fluid passing through the thermal energy storage system can modulate the power output of the CSP system to match a load as closely as possible. Equation 38 compares the power output of the CSP system to the load demand, with positive values being a surplus of CSP-produced power (S[t] > 0) and negative values being a shortage (S[t] < 0). When the CSP system matches the load at any given timestep, S[t] = 0.

Equation 38: Surplus of Produced CSP Power

$$S[t] = P[t] - L[t] \tag{38}$$

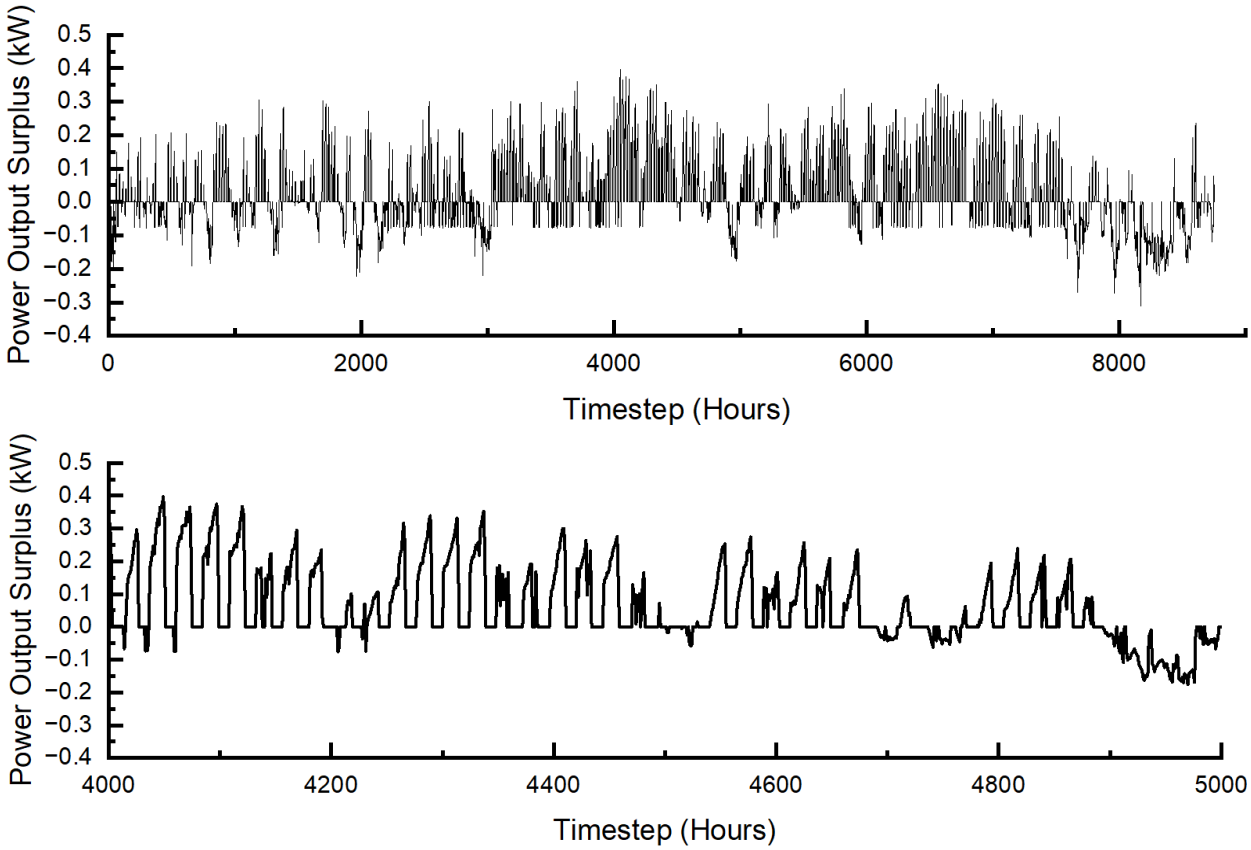

Figure 16: CSP System Power Output Surplus

The power availability of a CSP system can be quantified as the proportion or percentage of time that the CSP system meets or exceeds the load demand that it supplies power to. Equation 39 reflects this.

Equation 39: Percent Power Availability of the CSP System

$$AV_{CSP} = \frac{\sum_{t=1}^{n}(1 \quad for \quad S[t] \geq 0 \quad else \quad 0)}{n} * 100 \tag{39}$$

If external battery energy storage is incorporated to support the CSP system, the battery energy storage can account for periods of energy surplus and shortages characterized by the "Insufficient" and "Excess Power" timesteps. Given a specified capacity of the battery energy storage and initial state of charge, Equation 40 tracks stored energy at every timestep.

Equation 40: Stored Energy in an External Battery Energy Storage System

$$E[t] = S[t] + E[t-1] \quad for \quad 0 < E[t] < E_{capacity} \quad else \quad E[t] = 0 \quad for \quad E[t] < 0 \quad else \quad E[t] = E_{capacity} \quad for \quad E[t] > E_{capacity} \tag{40}$$

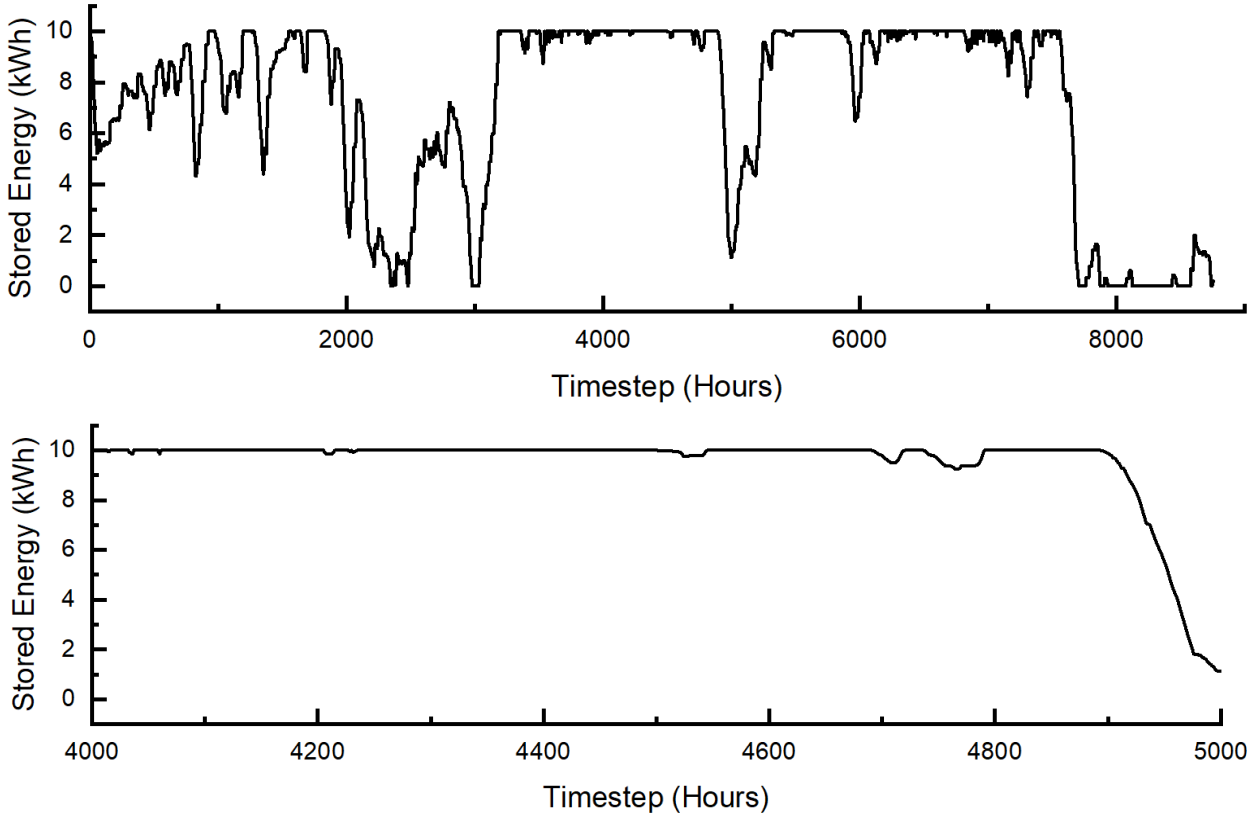

Figure 17: External Battery Energy Stored

External battery energy storage can provide additional capacity to manage discrepancies between produced CSP power and load. This would increase the power availability of the CSP system. Equation 41 calculates the power availability of the CSP system with external battery energy storage. Table 2 shows the calculated power availability results for the example CSP system with latent thermal energy storage and the number of phase changes that occur throughout the modeled time period.

Equation 41: Percent Power Availability of CSP System with External Battery Energy Storage

$$AV_{battery} = \frac{\sum_{t=1}^{n}(1 \quad for \quad E[t] > 0 \quad or \quad S[t] > 0 \quad else \quad 0)}{n} * 100 \tag{41}$$

Table 2: Power Availability Results for a CSP System with Latent Thermal Energy Storage

Result	**Without Battery Energy Storage**	**With Battery Energy Storage**
# of Phase changes	346	346
Power Availability (%)	68.6	92.3

Power availability is a valuable metric that can be used to gauge the feasibility of incorporating CSP systems with different system features, parameters, materials, and sensible or latent thermal energy storage with dynamic phase change materials.

CHAPTER 6: INTEGRATING DYNPCMS IN CSP THERMAL ENERGY STORAGE

CSP systems use sensible or latent thermal energy storage to modulate their power output. Latent thermal energy storage presents the opportunity to incorporate dynamic phase change materials (dynPCMs). The working fluid can flow through a channel for which the boundary connects to a tank containing an energy storage PCM. The PCM rests at the bottom of the tank when it is in its solid phase, and the bottom of the tank shares a boundary with the working fluid channel. When the solar CSP system is producing excess thermal energy, some of the heated working fluid can be routed through the channel bordering the energy storage PCM tank. The heated fluid enables the charge cycle within the PCM tank. When the solar CSP system is not producing enough thermal energy, any thermal energy stored in the PCM tank can be used by routing the cold working fluid through the bordering channel to enable the discharge cycle.

If a dynPCM is incorporated into the thermal energy storage system, pressure would be applied to the solid-state PCM to push it against the boundary heated by the working fluid and transition it from a solid to a liquid state. The pressure would minimize the liquid boundary layer, maximize the heat flux, and maximize the thermal energy captured due to heat transfer during the PCM charge cycle. The application of dynPCM pressure solves a problem that conventional latent thermal energy storage systems commonly face. When the solid phase PCM is pressed against the heated boundary, the transition into the liquid phase begins at the point of contact and propagates away from the boundary. The propagation of the melt front is defined through the Stefan problem as heat is transferred into the PCM. When no pressure is applied to the solid-state PCM, the Stefan problem dictates that the thickness of the liquid layer expands until it reaches a steady-state or the boundary of the space within the thermal energy storage

system. The difference between the temperature of the PCM at the boundary and the temperature of the heated boundary narrows, decreasing heat flux into the PCM and the effectiveness of the charge cycle. DynPCMs are a conceptual solution that would negate the Stefan problem. The pressure applied to the solid-state material keeps the material pressed against the heated boundary, minimizing the thickness of the liquid boundary layer and causing it to reach a steady state. The higher the pressure applied to the solid-state PCM, the smaller the steady state liquid boundary layer and the greater the heat flux from the heated boundary surface into the solid-state PCM.

A dynPCM thermal energy storage system would operate in the following stages:

1. The working fluid flows through a channel adjacent to the chamber with the energy storage PCM (such as salt, which can phase change into molten salt).
2. Heat transfer occurs through the boundary layer that sits between the working fluid in the channel and the PCM in the thermal energy storage chamber.
3. During the thermal energy storage charge cycle, some of the working fluid is routed from the receiver to flow through the energy storage chamber. The hot working fluid transfers its thermal energy to the PCM within the thermal energy storage chamber.
4. Pressure is applied to the top of the solid state PCM to push it against the boundary and maximize heat flux between the hot working fluid and the PCM – increases speed and efficiency of the charge cycle.
5. During the thermal energy storage discharge cycle, some of the cold working fluid is routed from the receiver to flow through the energy storage chamber. The hot PCM in the thermal energy storage chamber transfers its thermal energy to the cold working fluid.

6. The working fluid routed through the thermal energy storage system reconverges with the fluid routed directly to the heat exchanger. The reconverged fluid enters the heat exchanger to generate steam for the turbine.

Figure 18 visually represents how the dynPCM would contribute to the charge (stage 3) and discharge (stage 5) cycles.

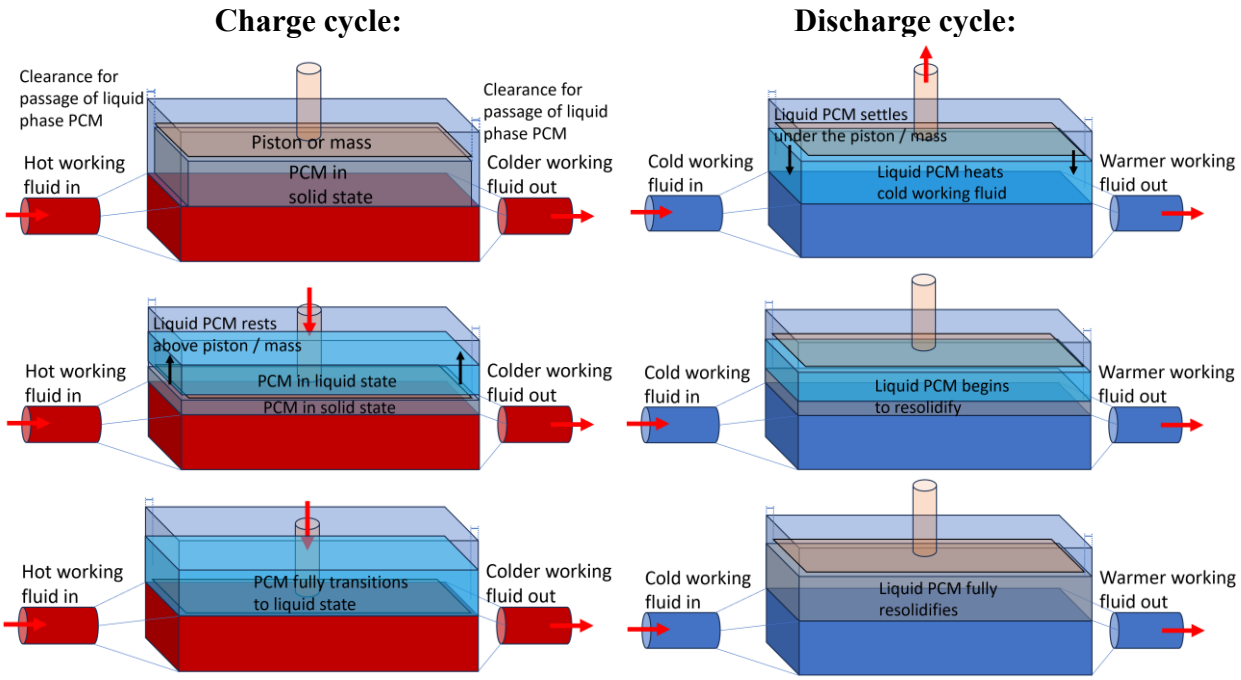

Figure 18: Stages of the Charge and Discharge Cycle of DynPCM Thermal Energy Storage

In a thermal energy storage system with a dynPCM, the constant pressure applied to the solid-state PCM against the heated boundary would allow for greater heat flux and a higher efficiency charge cycle. The heat flux of a system with a dynPCM is dependent on the pressure applied to the PCM and the difference between the melting point of the PCM and the temperature of the working fluid. As a necessary condition of the dynPCM system, there will be a small liquid layer of height δ defined by Equation 3 between the heated boundary and the solid portion of PCM, which we account for in this model. The greater the pressure, the closer the

calculated heat flux values approach ideal heat transfer. This occurs because the liquid layer is smaller when a greater pressure is pushing away the liquid layer to keep the solid side connected to the heated boundary.

Calculating results for a CSP system with a dynPCM in thermal energy storage is similar to the calculation method for a CSP system with conventional latent thermal energy storage (from the previous sections). Most formulas from the conventional latent thermal energy storage calculation process are common to the DynPCM calculation process, so this section only shows formulae for which the DynPCM calculation process deviates. Equation 43, for example, shows that during the charge cycle, the output temperature of the working fluid is determined by the difference between the hot working fluid temperature and the melting point of the material pressed against the heated boundary.

Equation 42: Specific Heat of the PCM at Different Phases

$$\begin{gathered} If \quad T_{PCM}[t] > T_m \quad then \\ c_{p,PCM}[t] = c_{PCM,l} \\ else \\ c_{p,PCM}[t] = c_{PCM,s} \end{gathered} \tag{42}$$

Equation 43: Output Temperature of the Working Fluid from Thermal Energy Storage

$$\begin{gathered} If \quad T_{PCM}[t] > T_{PCM}[t-1] \\ T_{hot,esout}[t] = T_{hot,esin}[t] - (\varepsilon_{es} * \min\left(c_{p,PCM}[t], c_{p,hot}\right) * \frac{T_{hot,esin}[t] - T_m}{c_{p,hot}} \\ else \\ T_{hot,esout}[t] = T_{hot,esin}[t] - (\varepsilon_{es} * \min\left(c_{p,PCM}[t], c_{p,hot}\right) * \frac{T_{hot,esin}[t] - T_{PCM}[t]}{c_{p,hot}} \end{gathered} \tag{43}$$

Equation 44 shows the heat flux from the working fluid into the thermal energy storage material. During the charge cycle, an alternate heat flux formula is applied that accounts for the pressure applied to the solid phase energy storage material. Since this heat flux formula only applies during the charge cycle, the condition for its use is that the current temperature of the PCM must be greater than the previous timestep. The second condition for its use is that at least

part of the PCM is in its solid state. When the solid PCM runs out, shown as h[t] = 0, the heat flux reverts to the sensible formula.

Equation 44: Heat Flux into the PCM

$$If \quad T_{PCM}[t] > T_{PCM}[t-1] \quad and \quad h[t-1] > 0$$

$$q"[t] = 1.24\left(k_l * \left(T_{hot}^{esin} - T_m\right)\right)^{\frac{3}{4}} * \left(\frac{\rho_{PCM}^{s} * (L + (T_m - T_{PCM}[t-1]) * c_{PCM}^{s}) * Pr}{A_{transfer,es} * \mu_l}\right)^{\frac{1}{4}} \tag{44}$$

$$else$$

$$\dot{Q}[t] = \dot{m} * c_{p,hot} * (T_{hot,esin}[t] - T_{hot,esout}[t])$$

$$q"[t] = \frac{\dot{Q}[t]}{A}$$

The following results show an example case with identical parameters to the case from the previous section, but under the assumption that the thermal storage system is capable of operating in the dynamic mode. These results are dependent on the pressure applied to the PCM. For example, increasing the pressure applied to the PCM increases the heat flux from the working fluid into the thermal energy storage during timesteps of battery charge. Figures 19-21 show plots of this time-based heat flux at different pressures. Figure 19 shows a case that applies 10 Pa of pressure to the PCM, Figure 20 shows a case applying 1,000 Pa, and Figure 21 shows a case applying 100,000 Pa. As the pressure condition increases, subsequent figures show progressively higher heat flux peaks at specific timesteps for which the thermal energy storage charge cycle takes place.

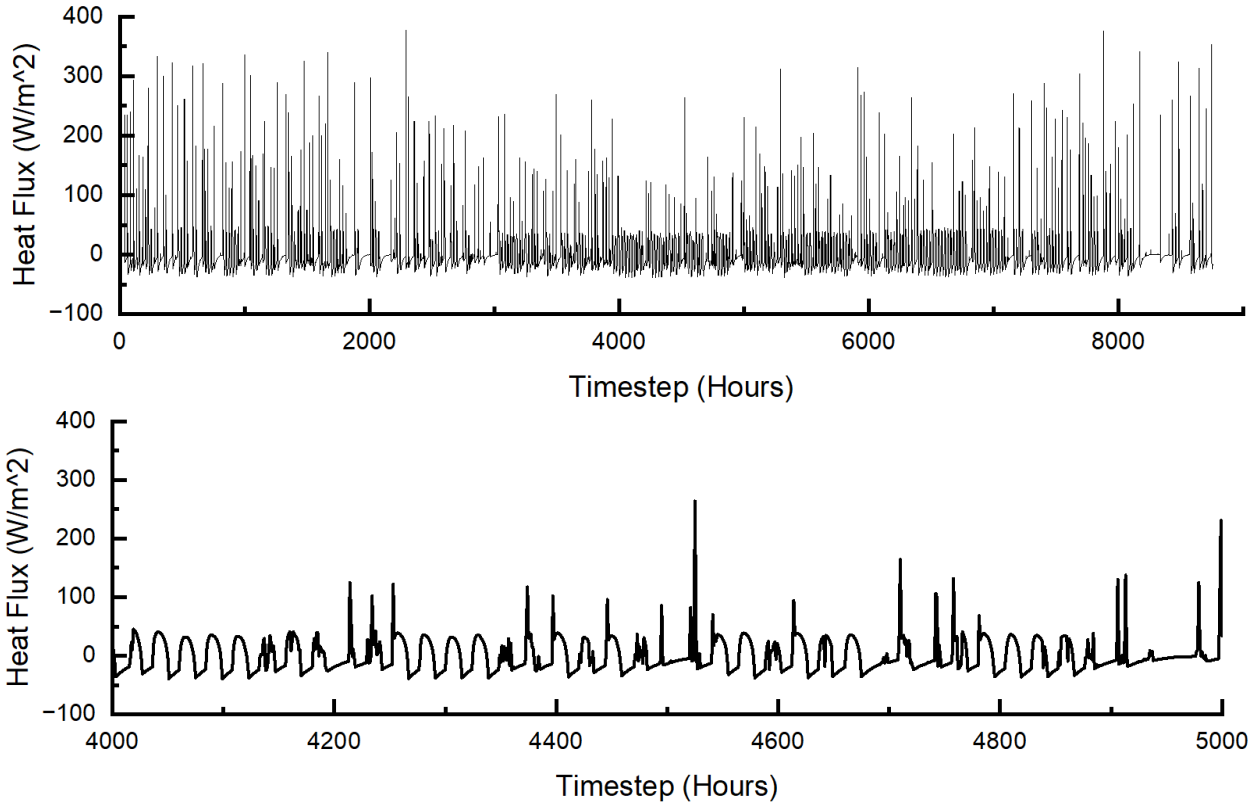

Figure 19: Heat Flux into Thermal Energy Storage – 10 Pa

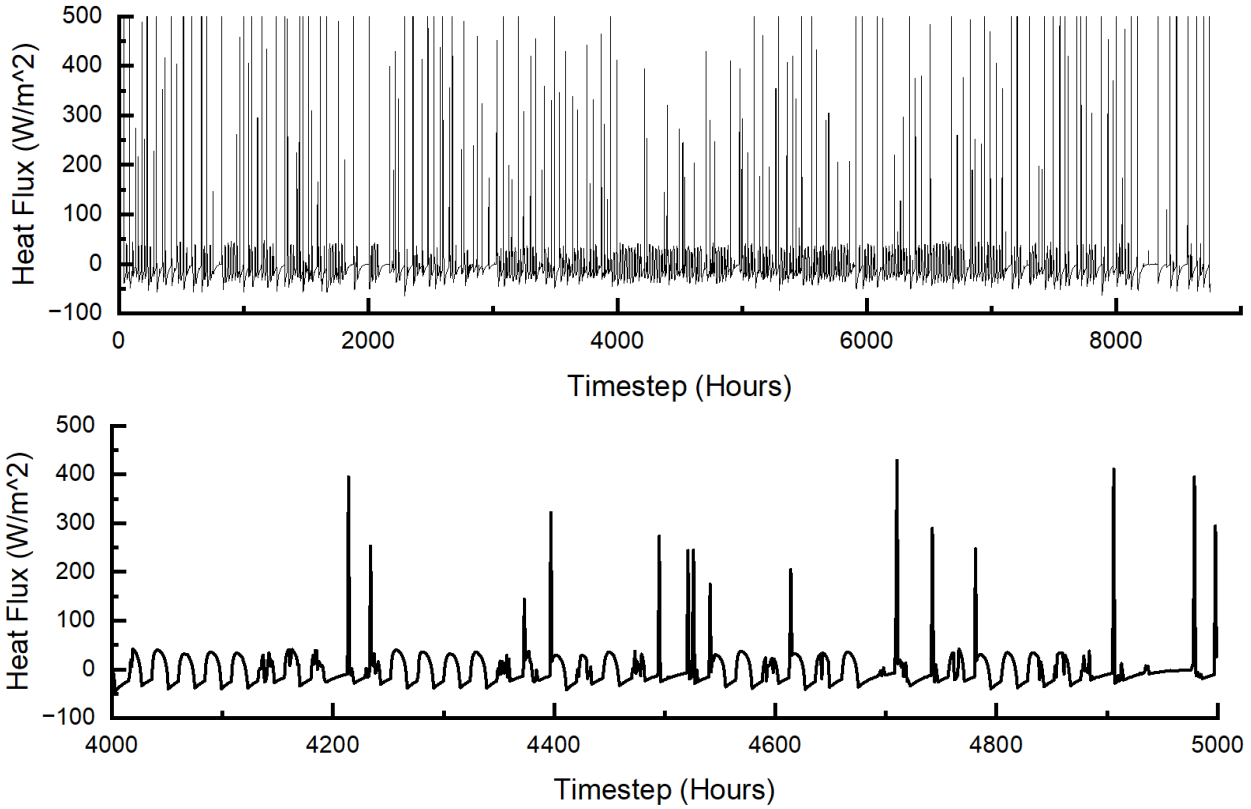

Figure 20: Heat Flux into Thermal Energy Storage – 1000 Pa

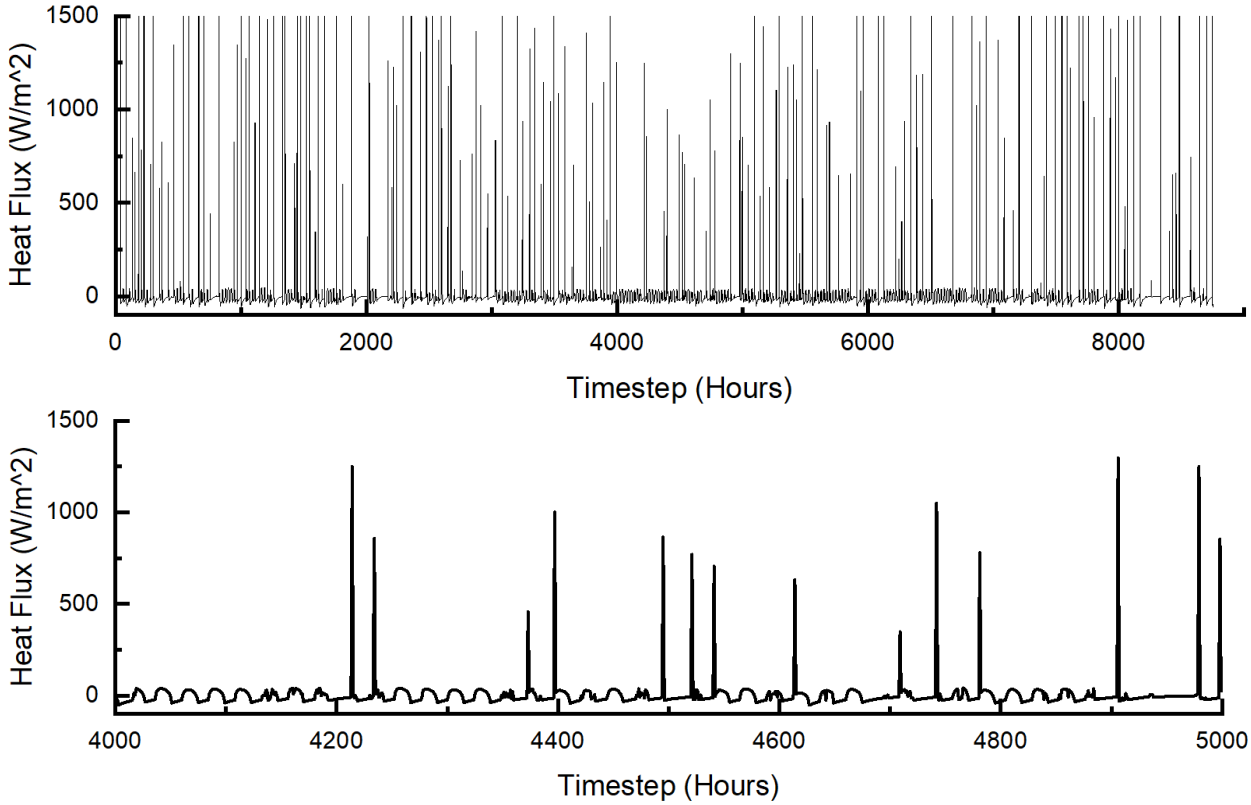

Figure 21: Heat Flux into Thermal Energy Storage – 100,000 Pa

Similar to the conventional latent model, different heat flux formulas are used to determine the temperature of the energy storage material depending on whether the material changes to a solid phase, liquid phase, or experiences no phase change. As confirmed by the plots above, higher applied pressures also lead to higher heat flux into the thermal energy storage material and a more effective charge cycle.

Equation 45: Dynamic Temperature of the PCM and Total Heat Transfer Rate

$$For \quad T_{PCM}[t-1] > T_m \quad and \quad T_{PCM,sensible}[t] < T_m \quad \text{(phase change to solid)}$$

$$\dot{Q}[t] = -\left(\dot{m} * c_{PCM,s} * (T_m - T_{PCM}[t]) + \dot{m} * L + \dot{m} * c_{PCM,l} * (T_{PCM}[t-1] - T_m)\right)$$

$$T_{PCM}[t] = T_m + \frac{\left(q''[t] + \dot{m} * L + \dot{m} * c_{PCM,l} * (T_{PCM}[t-1] - T_m)\right)}{\dot{m} * c_{PCM,s}} \qquad (45a)$$

$$Phase = -1$$

$$For \quad T_{PCM}[t-1] < T_m \quad and \quad T_{PCM,sensible}[t] > T_m \quad \text{(phase change to liquid)}$$
$$\dot{Q}[t] = \left(\dot{m} * c_{PCM,s} * (T_m - T_{PCM}[t-1]) + \dot{m} * L + \dot{m} * c_{PCM,l} * (T_{PCM}[t] - T_m)\right)$$
$$T_{PCM}[t] = T_m + \frac{\left(q''[t] - \dot{m} * L - \dot{m} * c_{PCM,s} * (T_m - T_{PCM}[t-1])\right)}{\dot{m} * c_{PCM,l}} \tag{45b}$$
$$Phase = 1$$

$$For \quad T_{PCM}[t-1] > T_m \quad and \quad T_{PCM,sensible}[t] > T_m \quad \text{(remains in liquid state)}$$
$$\dot{Q}[t] = \left(\dot{m} * c_{PCM,l} * (T_{PCM}[t] - T_{PCM}[t-1])\right)$$
$$T_{PCM}[t] = T_{PCM}[t-1] + \frac{q''[t]}{\dot{m} * c_{PCM,l}} \tag{45c}$$
$$Phase = 0$$

$$For \quad T_{PCM}[t-1] < T_m \quad and \quad T_{PCM,sensible}[t] < T_m \quad \text{(remains in solid state)}$$
$$\dot{Q}[t] = \left(\dot{m} * c_{PCM,s} * (T_{PCM}[t] - T_{PCM}[t-1])\right)$$
$$T_{PCM}[t] = T_{PCM}[t-1] + \frac{q''[t]}{\dot{m} * c_{PCM,s}} \tag{45d}$$
$$Phase = 0$$

Figures 22-24 show the temperature of the PCM as it changes with time compared to the working fluid input temperature to the energy storage system. Similar to the results from the conventional latent thermal energy storage model, these dynPCM system results show expected behavior between the two quantities. When the working fluid input temperature is higher than the PCM temperature, the PCM temperature increases due to heat flux from the working fluid. When the working fluid input temperature is lower than the PCM temperature, the PCM temperature decreases. Pressure added to the PCM results in higher PCM temperature peaks than the conventional latent model during charge cycles within the time series. The higher the pressure applied to the PCM in a dynPCM system, the higher the PCM temperature peaks.

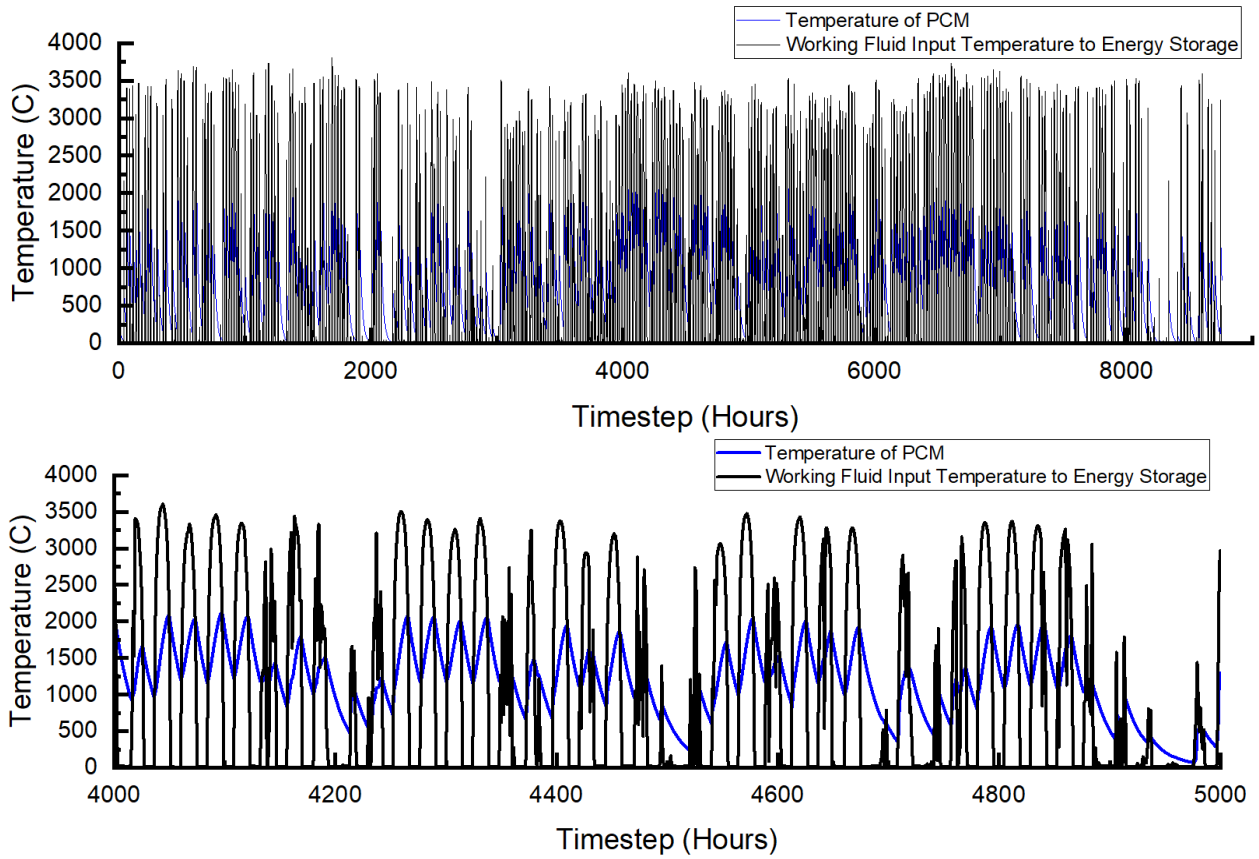

Figure 22: Working Fluid Input Temperature to Energy Storage vs PCM Temperature – 10 Pa

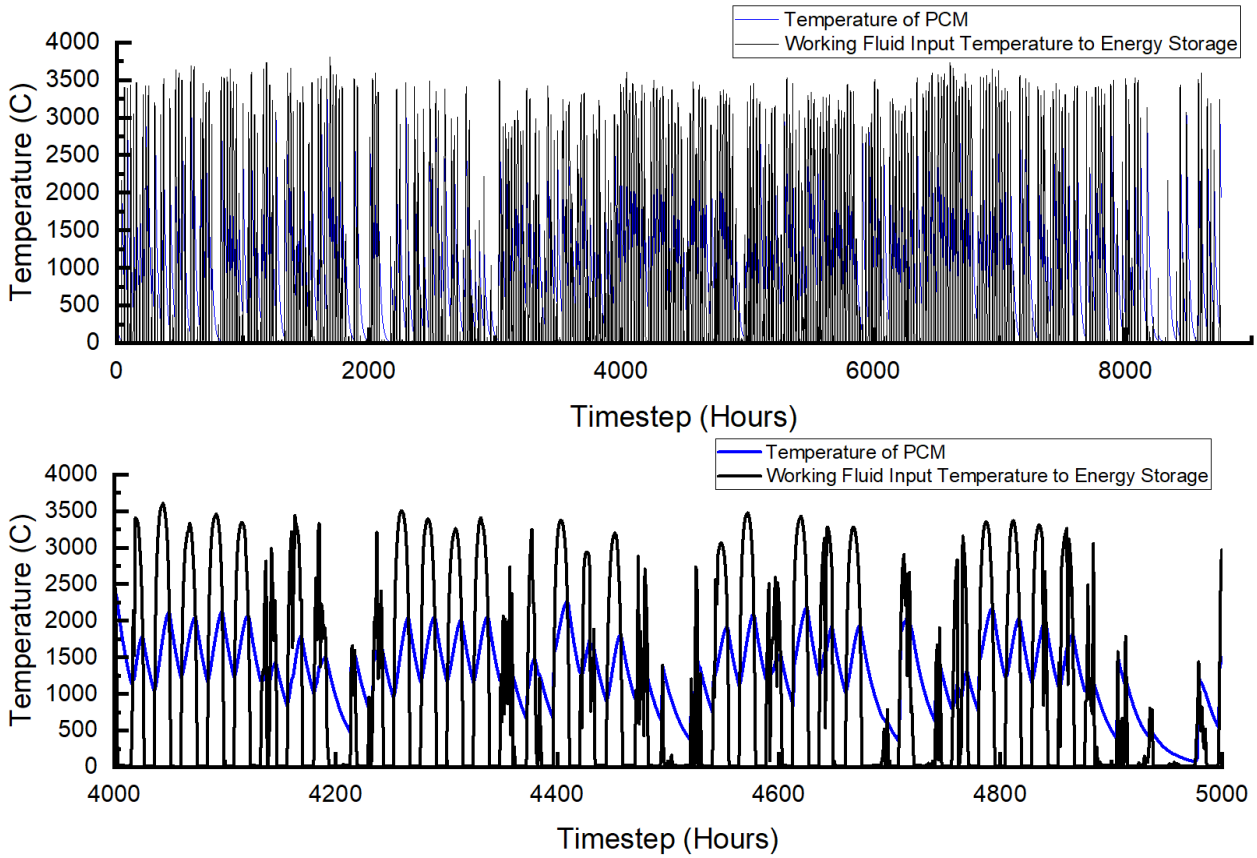

Figure 23: Working Fluid Input Temperature to Energy Storage vs PCM Temperature – 1000 Pa

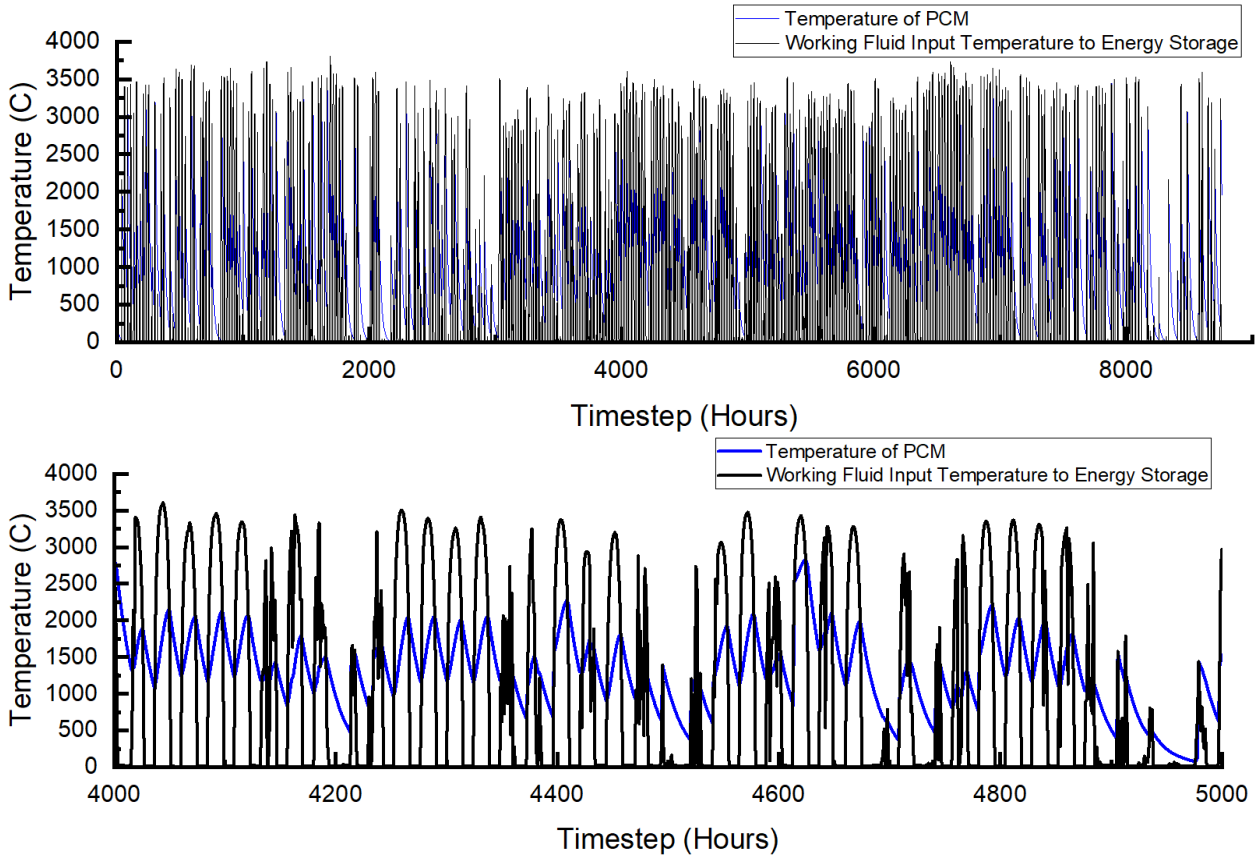

Figure 24: Working Fluid Input Temperature to Energy Storage vs PCM Temperature – 100,000 Pa

Figures 25-27 track whether the thermal energy storage system is in a charge cycle or a discharge cycle at any given timestep, as well as timesteps for which a phase change occurs. These figures allow for evaluation of certain heat flux and temperature behaviors in the context of whether the system is in a charge or discharge cycle and whether the PCM is in solid or liquid phase. Given that the dynamic pressure mechanism only applies during the charge cycle, system behavior is expected to differ depending on cycle. Only minimal differences arise in the timing of charge vs discharge cycles and the phase of the PCM across the time period depending on the pressure applied to the PCM.

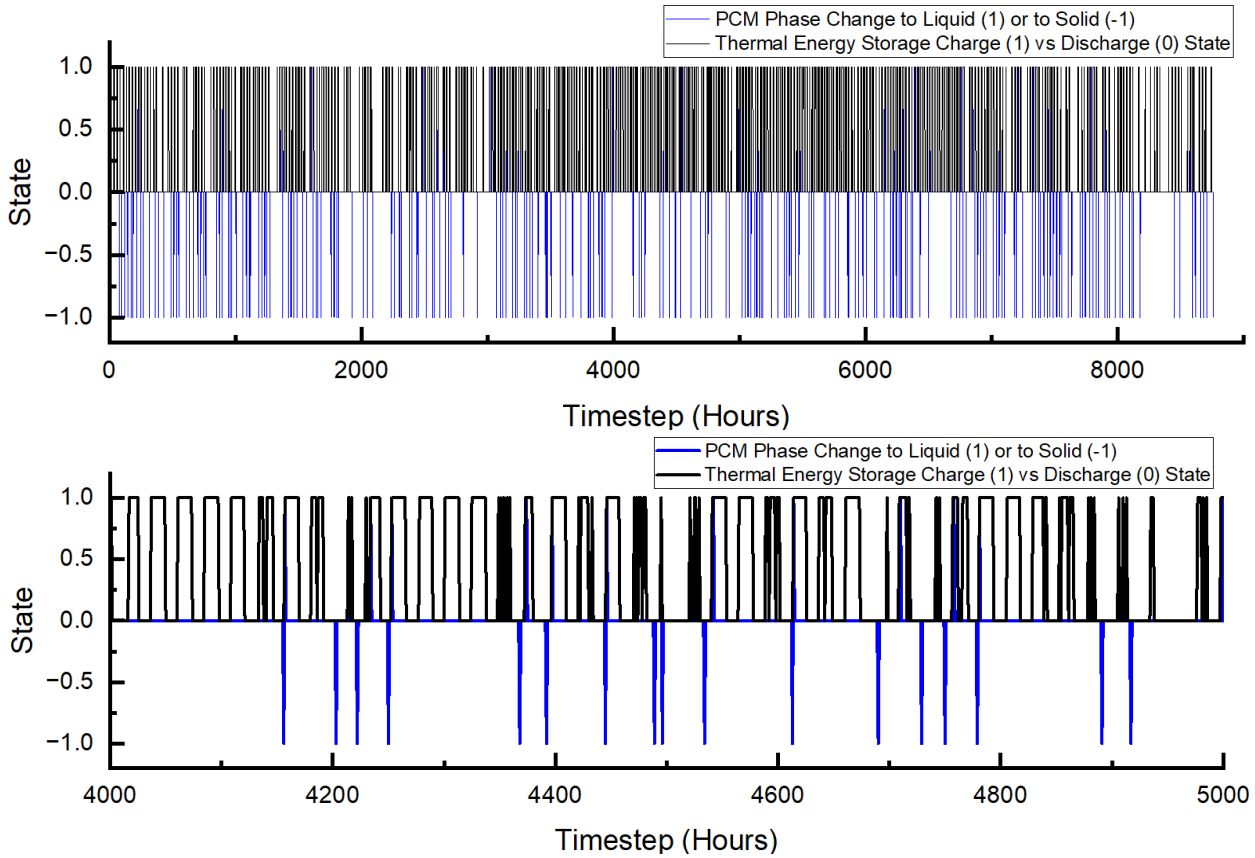

Figure 25: Thermal Energy Storage Charge vs Discharge State and Phase Changes – 10 Pa

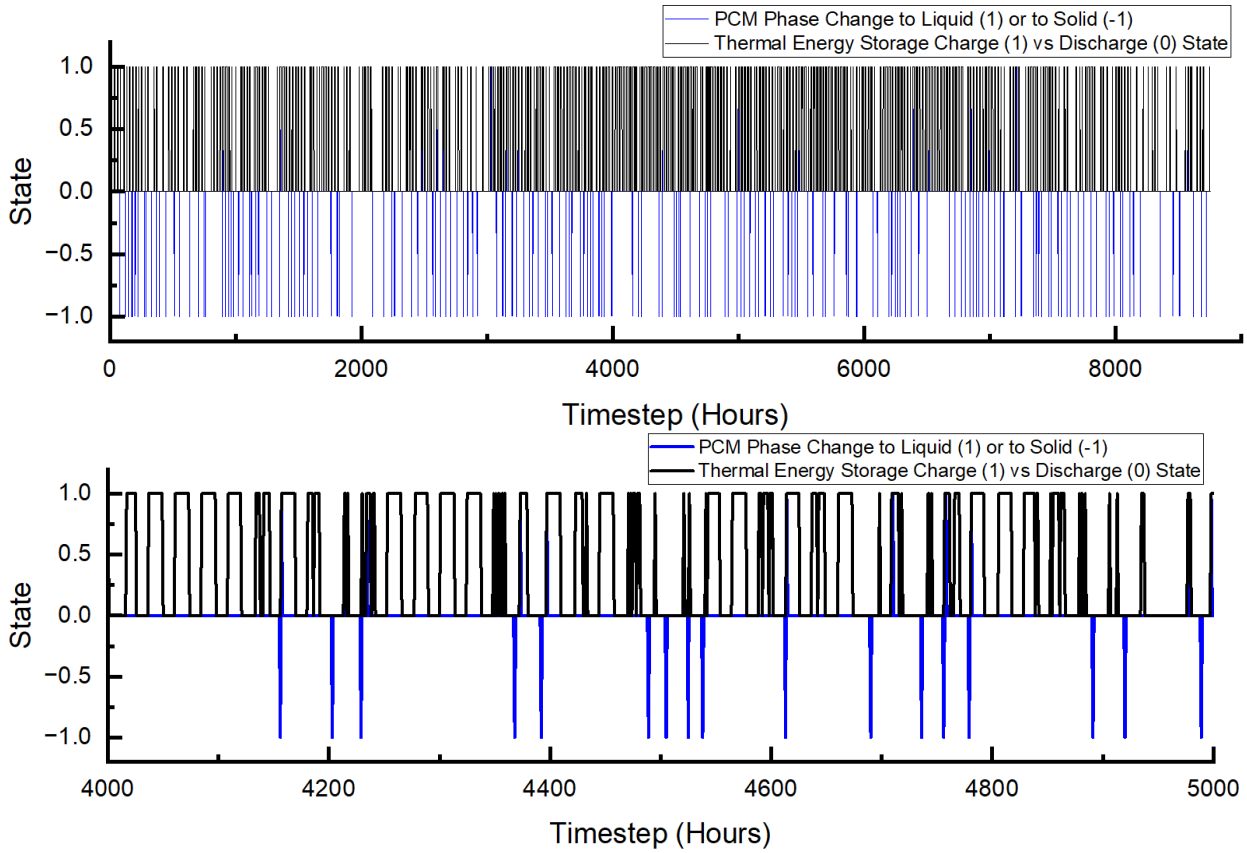

Figure 26: Thermal Energy Storage Charge vs Discharge State and Phase Changes – 1000 Pa

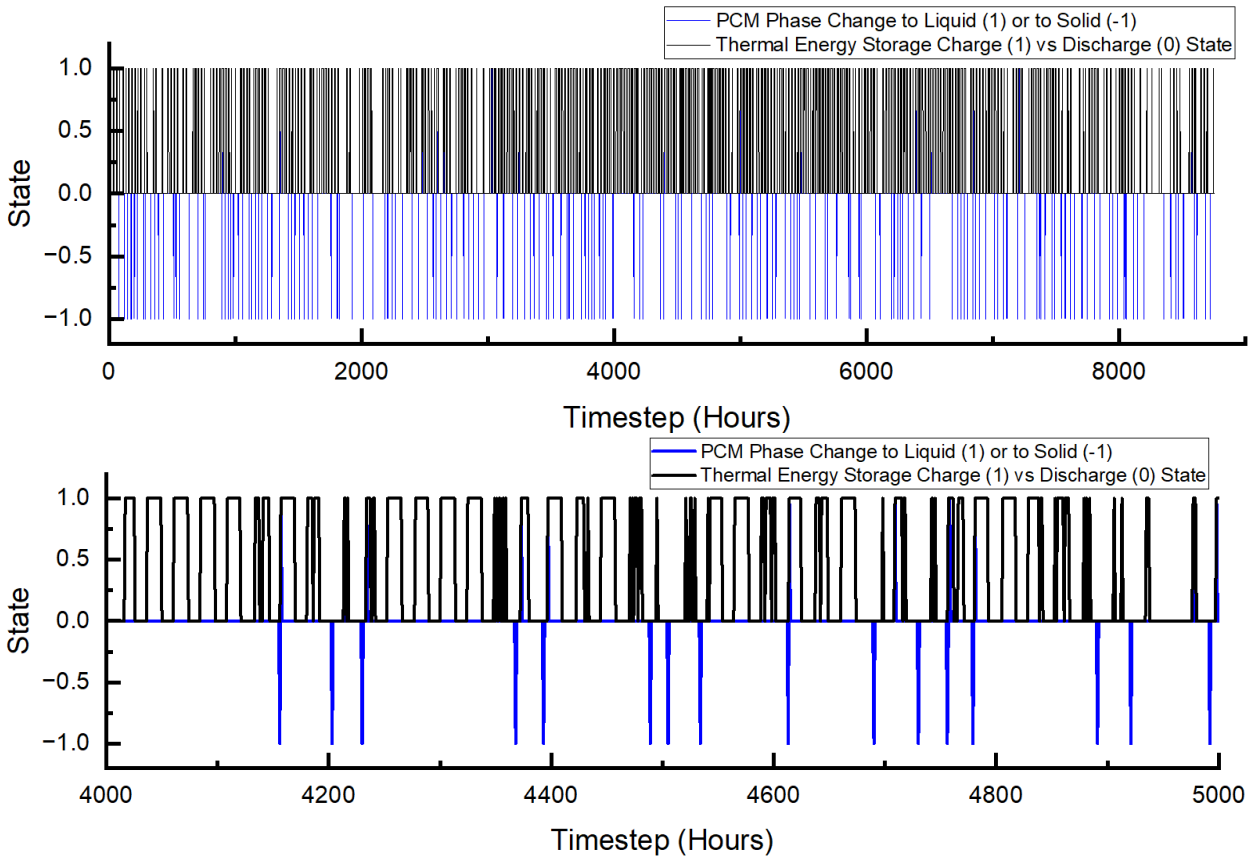

Figure 27: Thermal Energy Storage Charge vs Discharge State and Phase Changes – 100,000 Pa

During a charge cycle, the solid PCM begins to melt and the solid phase of the material depletes as pressure is applied. The temperature of the PCM rises during this cycle, however, given the constant replenishment of the solid PCM at the heated boundary, there is not a substantial change in temperature of the solid PCM which is not in contact with the heated boundary. Rather, the liquid PCM layer experiences a temperature increase before being expelled from the melt region. The PCM is both solid and liquid until the solid PCM is fully depleted, and the PCM rapidly transitions into a fully liquid state when the overall PCM temperature exceeds the melting point. When the discharge cycle causes the temperature to drop below the melting point, this indicates that the material begins to solidify again. Equation 46 calculates the number of timesteps in which the PCM experiences a phase change by counting each timestep that the

PCM temperature crosses the melting point threshold. The more phase changes, the more the thermal energy storage system takes advantage of the latent heat transfer pressure mechanism to maximize the heat energy stored in the system.

Equation 46: Number of Phase Changes

$$Phases = \sum_{t=1}^{n}(1 \quad for \quad Phase = 1 \quad or \quad Phase = -1 \quad else \quad 0) \tag{46}$$

The solid PCM in the thermal energy storage system is a finite material that will melt during the dynPCM charge cycle. Ideally, the solid PCM has a height large enough to ensure it is rarely or never fully depleted during a charge cycle. This means that the pressure mechanism can press the solid edge of the PCM against the heated boundary to maximize heat flux throughout the full charge cycle. A charge cycle can fully deplete the solid PCM, however, when it lasts long enough at a high enough melting speed. When the solid PCM is fully depleted, it is in full liquid phase and the sensible heat flux formula determines heat flux into the PCM. This is reflected in Equation 44.

To track the state (current height) of the solid PCM, Equation 47 calculates the melting speed of the PCM. The melting speed is dependent on the melting point of the material, the temperature of the PCM at the current timestep, the heat flux between the heated boundary and the PCM, and material properties.

Equation 47: Melting Speed of Solid PCM

$$u[t] = \frac{q''[t]}{\rho_{PCM,s}L + (T_m - T_{PCM}[t-1]) * \rho_{PCM,s}c_{PCM,s}} \tag{47}$$

The melting speed determines the height of the PCM at each timestep as shown by Equation 44. Equation 47 calculates melting speed in terms of meters per second, so Equation 48 converts this value to meters per hour to account for hour-long timesteps.

Equation 48: Height of Solid PCM

$$ht[t] = ht[t-1] - (u[t] * 3600) \quad for \quad ht_{peak} > ht[t-1] - (u[t] * 3600) > 0$$
$$ht[t] = ht_{peak} \quad for \quad ht[t-1] - (u[t] * 3600) \geq ht_{peak} \tag{48}$$
$$ht[t] = 0 \quad for \quad ht[t-1] - (u[t] * 3600) \leq 0$$

Appendix B contains the next set of plots for this dynPCM case, including the proportion of working fluid through thermal energy storage, the working fluid temperature input to the heat exchanger, and the power output of the CSP system. These results consider the same dynPCM thermal energy storage system as the plots above with different quantities of pressure applied to the PCM. The formulas and methodology used to produce these plots are the same as the formulas shown for conventional latent thermal energy storage in the previous section, but the results are different due to the incorporation of the pressure on the PCM. Each of the plots in Appendix A represent intermediate calculations that lead to the calculation of an actionable result–the expected electric power output of the CSP system for the dynPCM case. Figures 28 through 30 show this expected power output at each timestep given different pressures on the solid-state PCM. The power output of the CSP system is plotted against the power demand (load) to visualize how, similar to the conventional latent case, the CSP system power output is controlled to match the power demand as closely as possible.

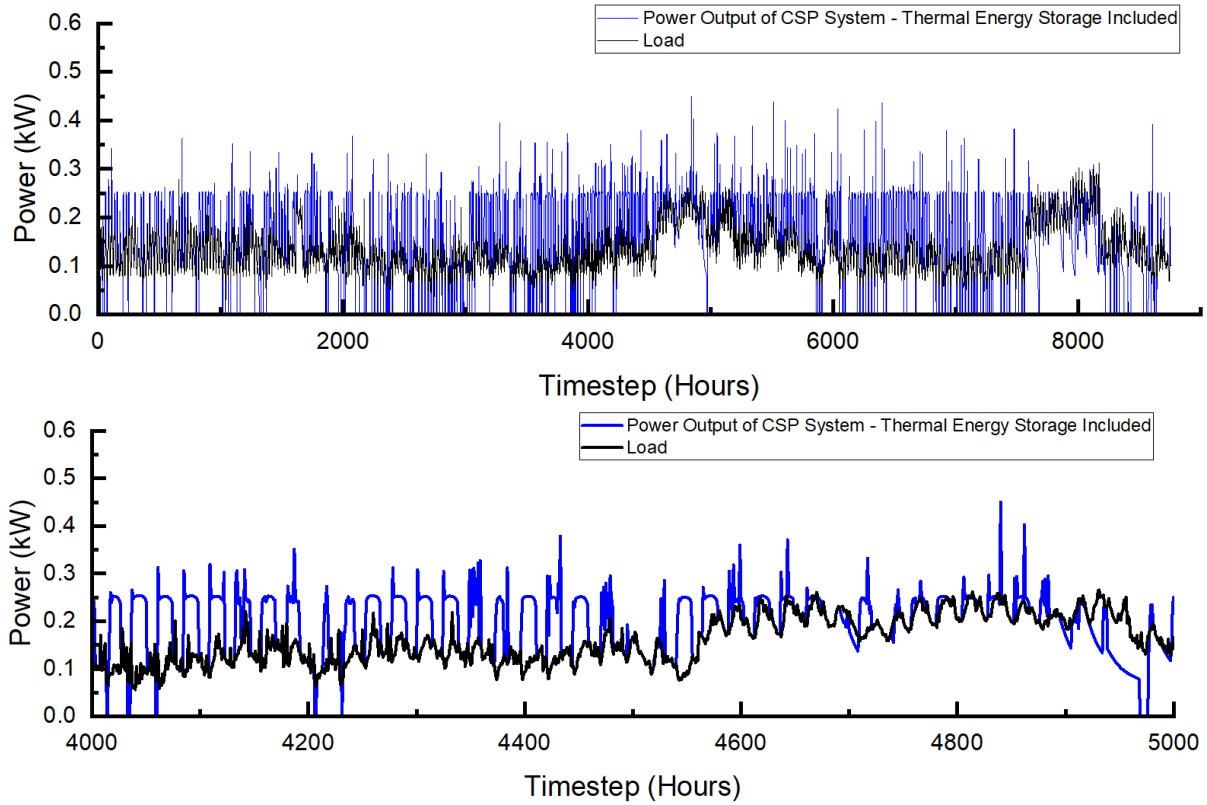

Figure 28: Power Demand (Load) vs Power Output of CSP System – 10 Pa

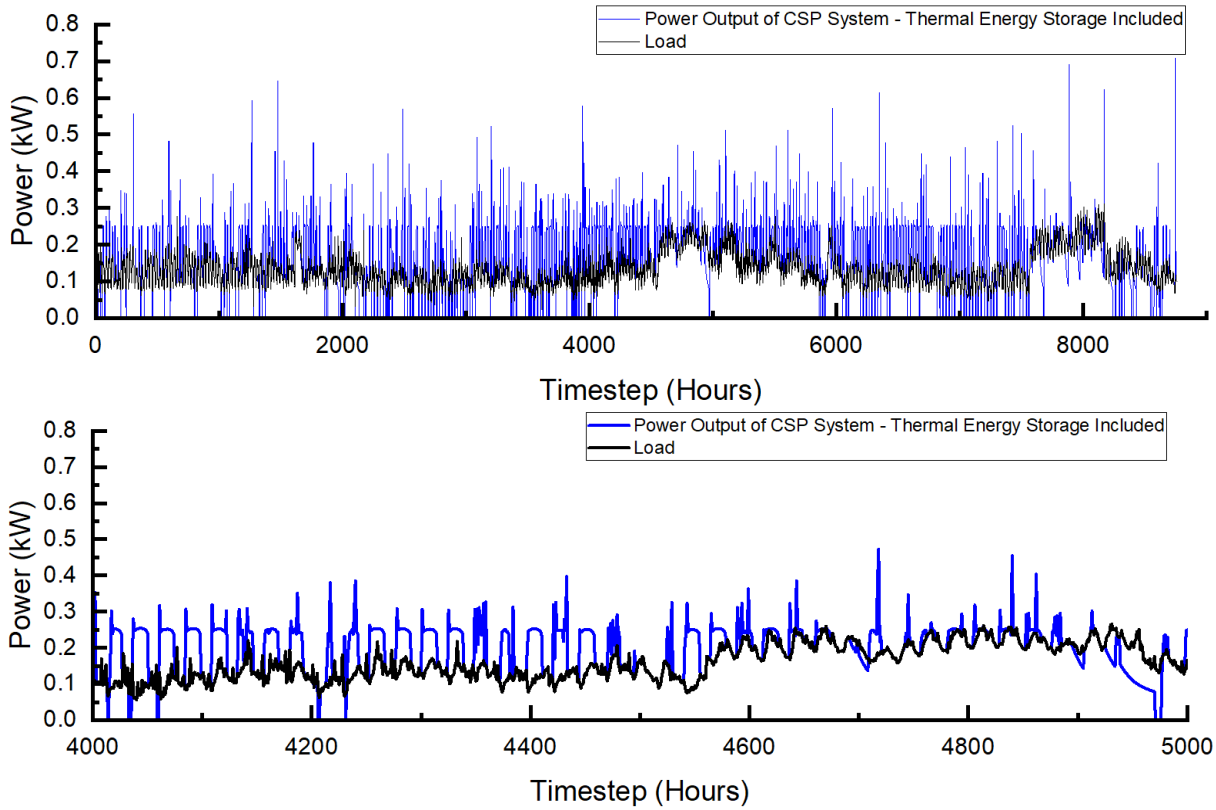

Figure 29: Power Demand (Load) vs Power Output of CSP System – 1000 Pa

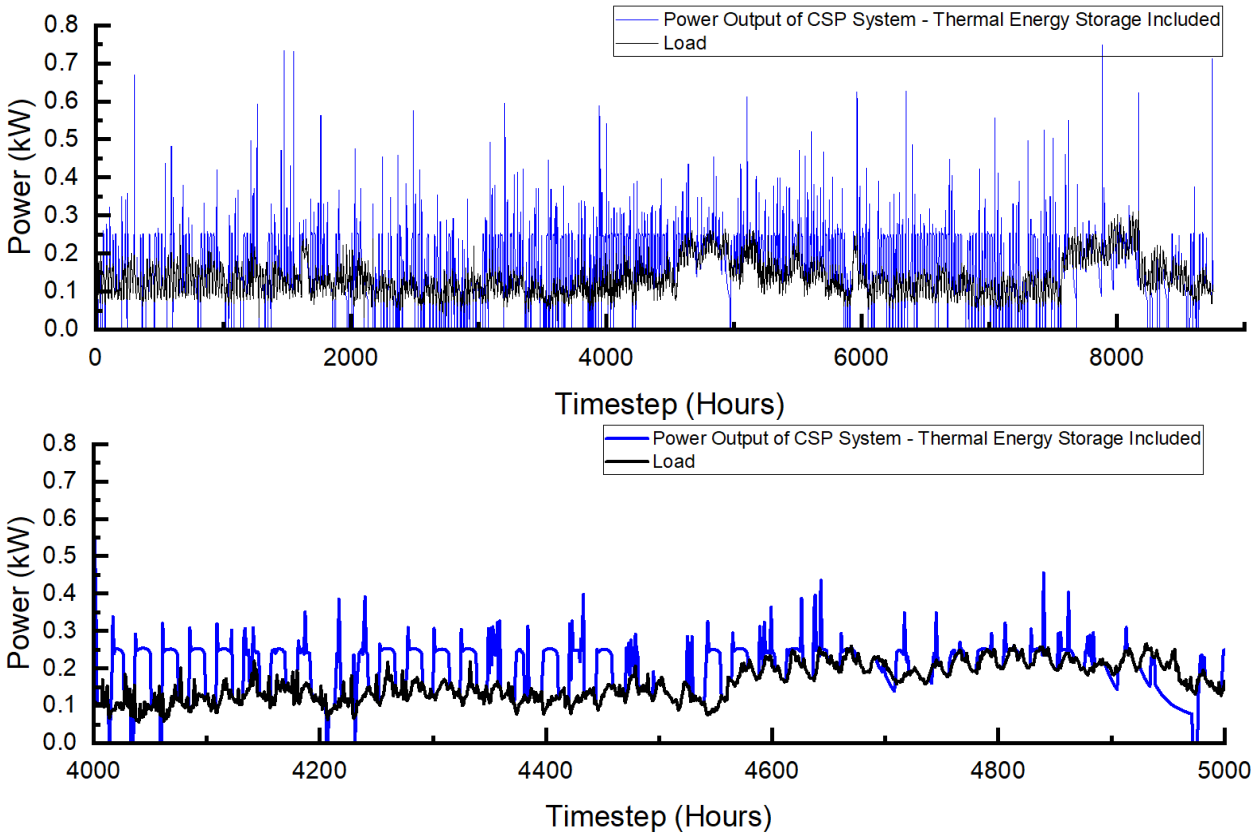

Figure 30: Power Demand (Load) vs Power Output of CSP System – 100,000 Pa

As in the conventional latent case, the dynPCM case assumes that an external battery energy storage system supports the CSP system. Figures 31 through 33 show the external battery energy stored for the dynPCM case at different pressures. At some timesteps, variation can be seen in how much energy is stored. Higher pressures cause higher-efficiency thermal energy storage charge cycles, increasing the electric power output of the CSP system when the thermal energy storage discharges. This excess electric power associated with higher pressures is routed to battery energy storage, contributing to higher stored electric energy at some timesteps.

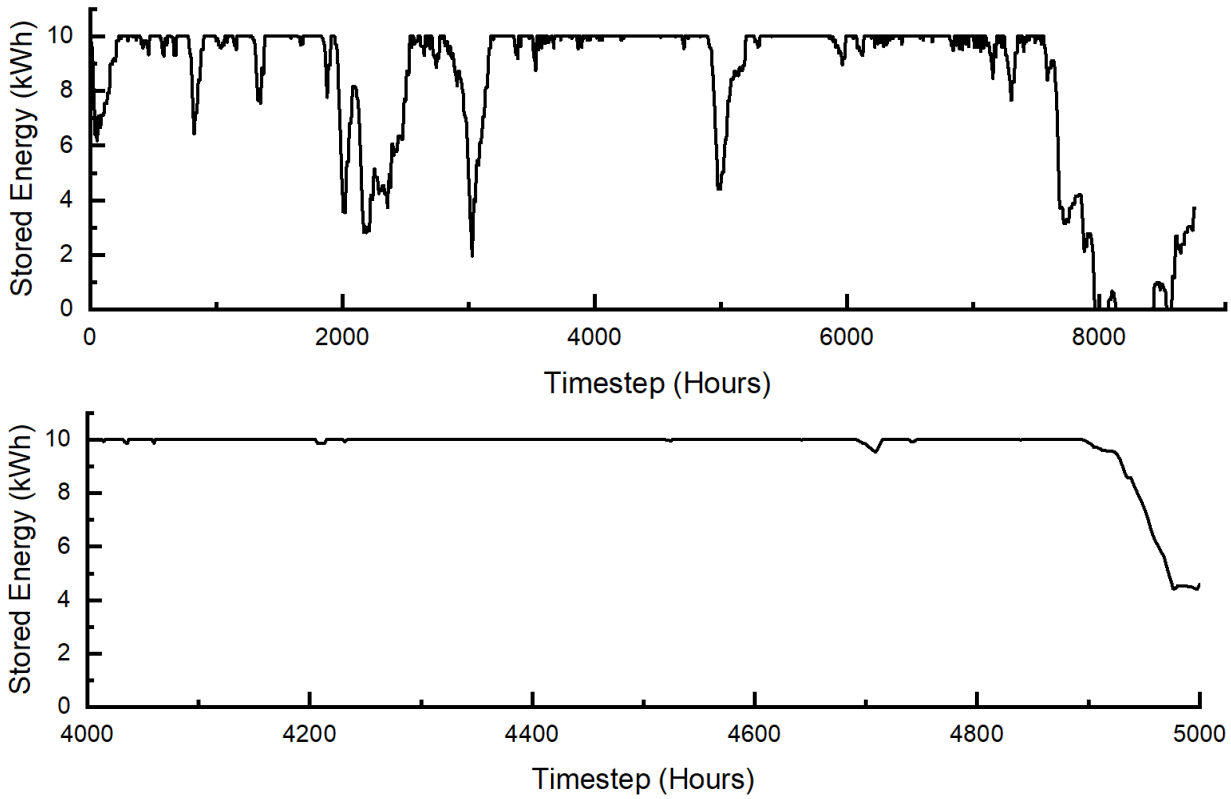

Figure 31: External Battery Stored Energy – 10 Pa

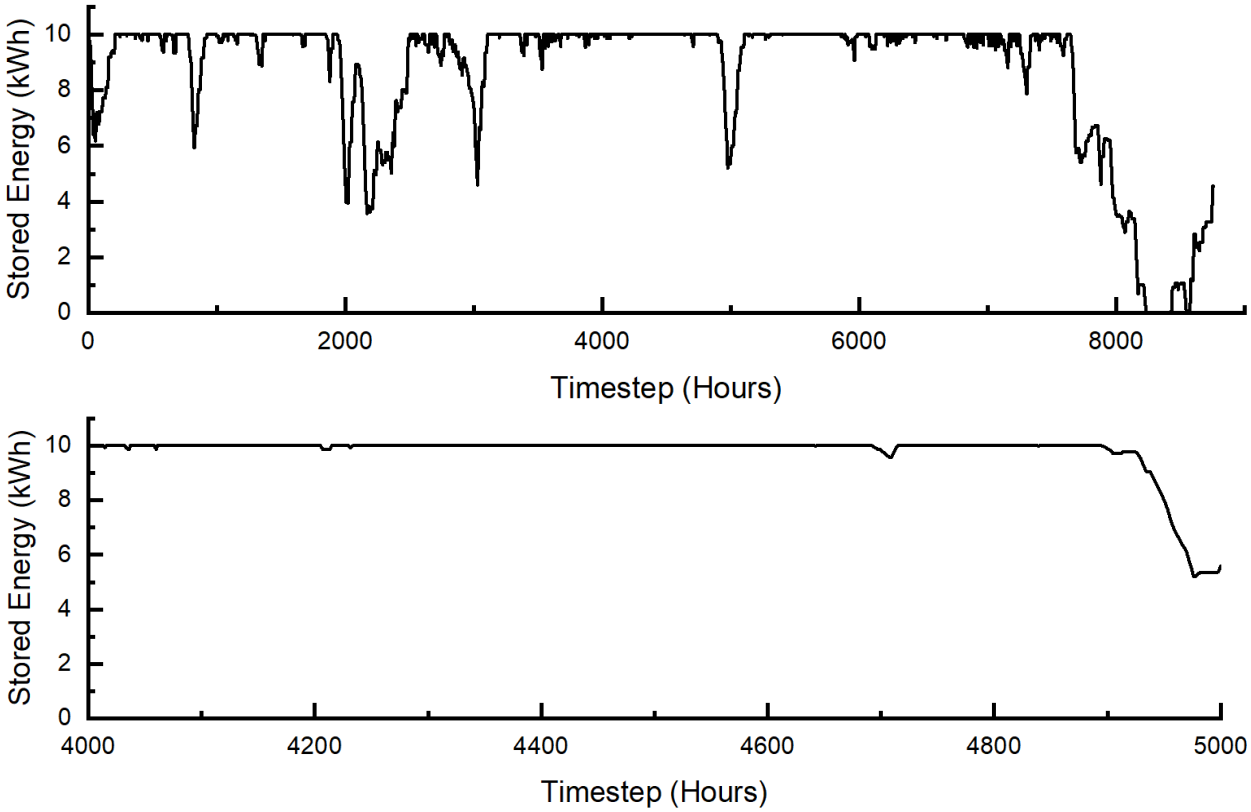

Figure 32: External Battery Stored Energy – 1000 Pa

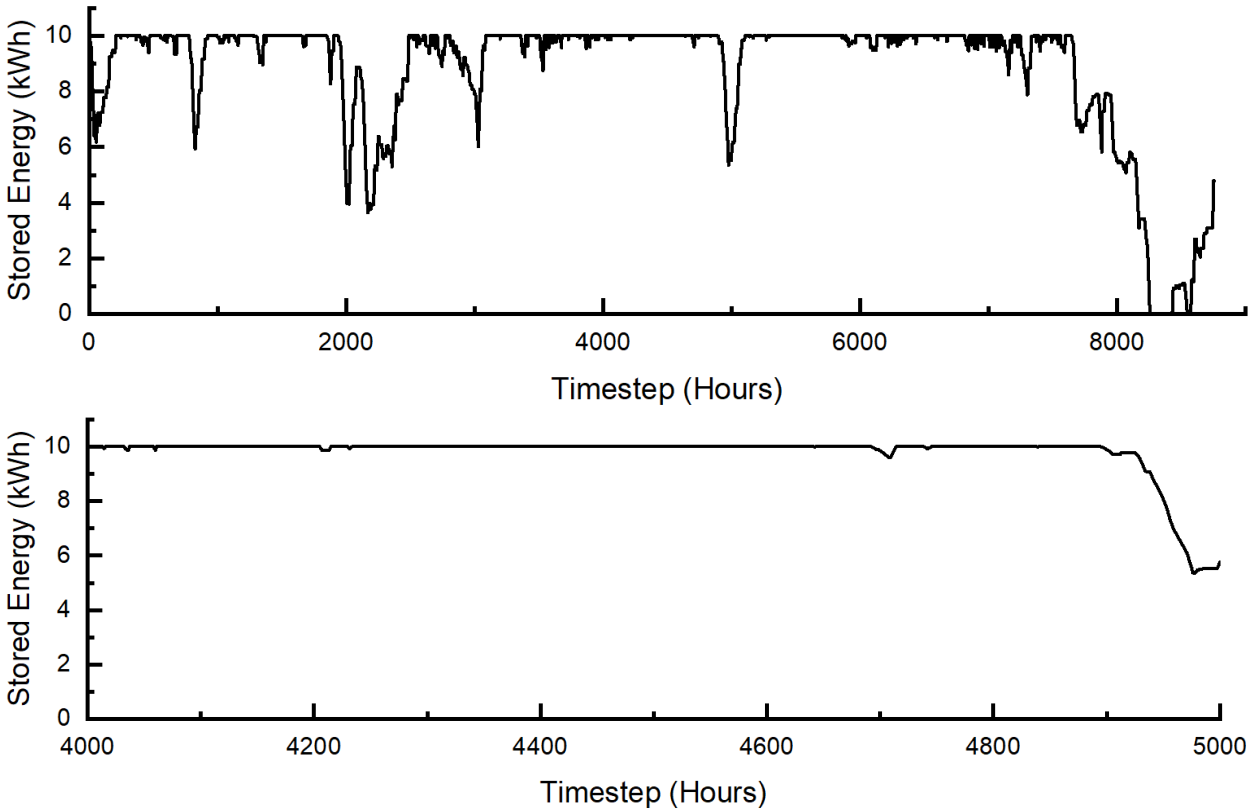

Figure 33: External Battery Stored Energy – 100,000 Pa

Modeling this system has allowed for the calculation of power output and power availability of an example CSP system with sensible, latent, and dynPCM thermal energy storage. The power availability of this solar CSP system with latent thermal energy storage is 68.6, and its power availability becomes 92.3 with external battery energy storage. Given a dynPCM system, power availability increases with an increase in pressure applied to the PCM. This increase follows an approximately logarithmic trend, meaning that the pressure on the PCM must increase exponentially with each increment to achieve approximately equal increments of increase in power availability. The increase in power availability due to increased pressure on the PCM can be attributed to the increased heat flux from pressing the solid edge of the material to the heated boundary from the working fluid. The greater the pressure on the PCM, the smaller

the liquid boundary layer between the solid PCM and the heated boundary. The smaller the boundary, the greater the heat flux during charge cycles.

The power availability of the CSP system with dynPCM thermal energy storage is calculated using the same method as for the conventional latent thermal energy system. Since the pressure applied to the PCM during the charge cycle impacts the heat flux into the PCM, the working fluid temperature dynamics, and the electric power output of the CSP system, the pressure has an impact on the overall power availability of the CSP system. Figure 34 presents calculated results from this model that show the power availability of the CSP system is expected to be higher when higher pressures are applied to the PCM. Figure 35 shows that when an external battery is applied as a supporting power resource, power availability is higher in every case with a similar trend of increased power availability given higher pressure.

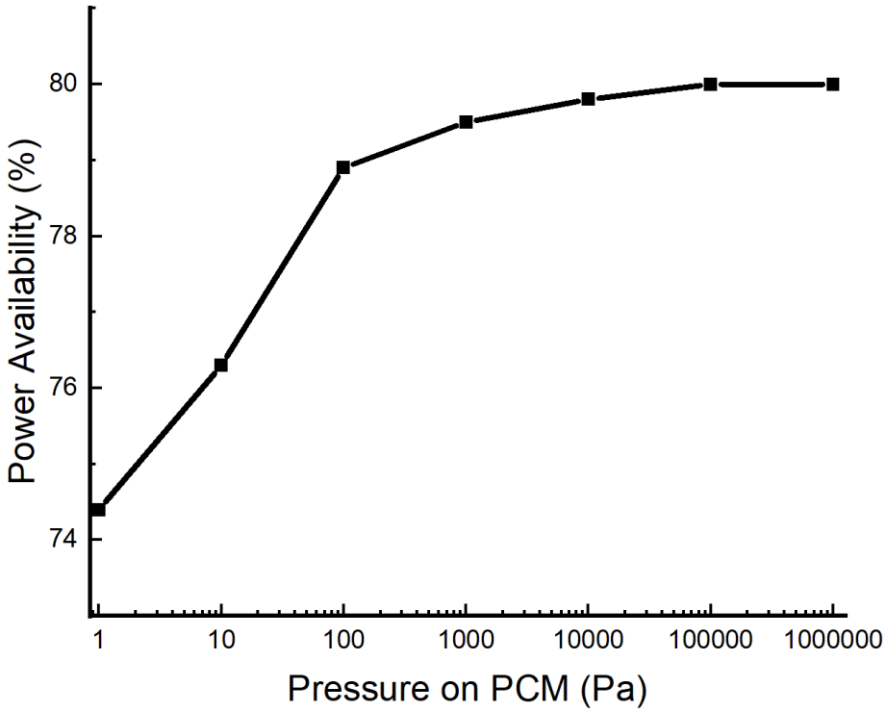

Figure 34: Power Availability of the CSP System at Different Pressures on the Solid PCM

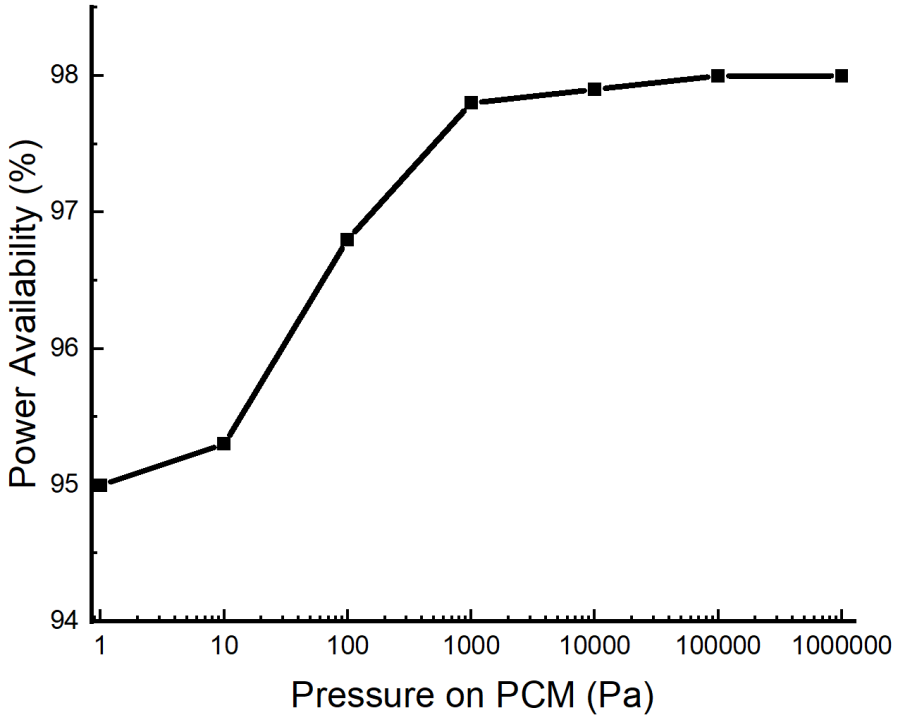

Figure 35: Power Availability of the CSP System with a Supporting External Battery

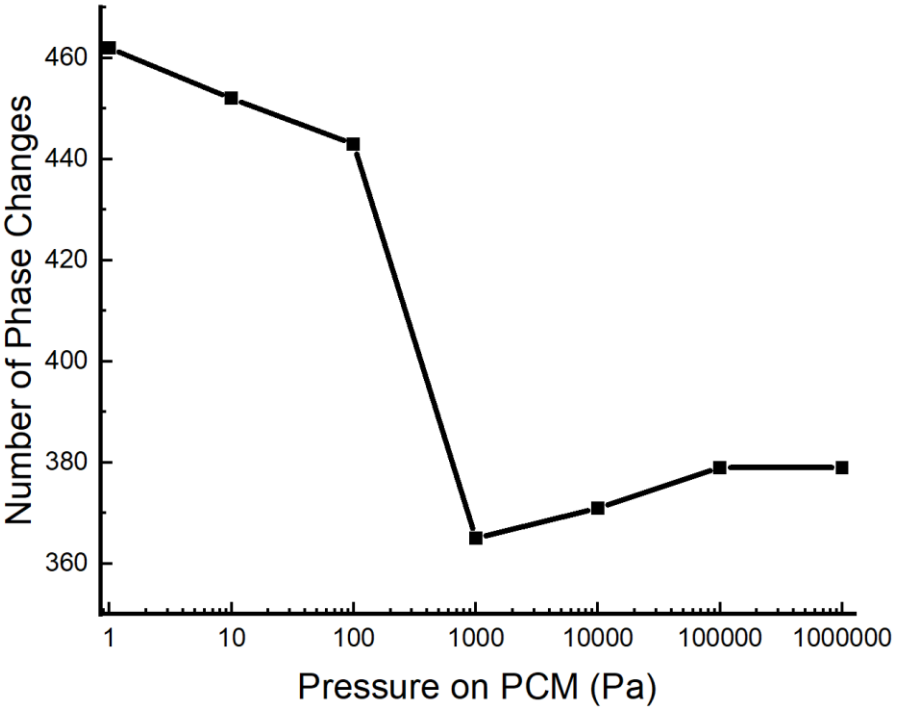

Figure 36: Number of PCM Phase Changes in the CSP Thermal Energy Storage

CHAPTER 7: CONCLUSION

The model presented in this study quantifies the expected performance and power availability of CSP systems with conventional thermal energy storage and dynPCM thermal energy storage. It is a valuable planning-stage analysis tool that decision makers can use to determine expected outcomes for a variety of planned thermal energy storage technologies and CSP systems, reducing uncertainty associated with the incorporation of these technologies in a microgrid. Results from this model consist of critical analytical information needed to build business cases and make investment decisions about power components. The use of this model will enable power system planners to design and invest in technologies for CSP systems that yield measurable benefits to the systems' reliability, performance, and cost. It will enable informed investment decisions, optimizing the outcomes associated with implementation of thermal energy storage and CSP systems in microgrids.

This study applied the computational model to an example CSP system with thermal energy storage. The example results demonstrate the model's capability to inform decision-makers and quantify the benefit of applying dynPCMs in a thermal energy storage system. The expected power availability is a numerical result from this model that allows decision-makers to gauge the expected reliability of different investment plans. Plotted results give decision-makers a more in-depth, quantified understanding of how individual components within the system will behave under a variety of conditions. The results in this study show that a CSP system with dynPCMs is expected to have higher power output and power availability compared to a system with conventional latent thermal energy storage, particularly at higher pressures. Higher power

availability indicates that a CSP system with dynPCMs will need less support from external power resources to maintain continuous power supply to a demand profile.

The next stage of this work is to develop the computational model into a MATLAB program. This program will be incorporated into the existing Analysis of Microgrid Performance, Reliability, and Resilience (AMPeRRe) computational model (Nicholson, 2024), which will quantify the expected reliability and resilience outcomes of placing CSP systems and thermal energy storage in microgrids. This includes forecasted outcomes such as power availability, fuel consumption, excess energy over a time period, and survival time in the event of various resource disconnection scenarios. Incorporation of this model into AMPeRRe will expand its analysis capabilities to emulate the interaction of CSP systems and different types of thermal energy storage with other power resources in a microgrid such as PV solar, wind power, generators, and battery energy storage.

This study represents a significant step towards modeling thermal energy storage and CSP systems to reduce uncertainty around their implementation in microgrids. By modeling dynPCMs, it also provides a critical comparison of this conceptual technology to conventional thermal energy storage systems. This study advances the understanding of how CSP systems behave when supplying to a power demand, and how different thermal energy storage systems behave within CSP systems to modulate power output and maximize power availability. The computational model presented in this work is broadly applicable and repeatable so it can benefit a wide variety of power planning projects that involve CSP systems and thermal energy storage. For many projects, it will provide quantified analytics on the expected behavior of these systems, measure the benefits and tradeoffs of incorporating new technologies such as dynPCMs, and

create improved reliability and performance outcomes when the model-driven analytics inform planning and development.

REFERENCES

Ayalew, B. S. (2025). Recent Advancements in Latent Thermal Energy Storage and Their Applications for HVAC Systems in Commercial and Residential Buildings in Europe - Analysis of Different EU Countries' Scenarios. *Energies*.

Bellos, E. T. (2016). A detailed working fluid investigation for solar parabolic trough collectors. *Applied Thermal Engineering*.

Bozorg, M. C. (2023). Thermal energy storage in a tightly packed bed with sodium as the heat transfer fluid: A numerical study. *Applied Energy*.

Chen, J. e. (2019). Effects of different phase change material thermal management strategies on the cooling performance of the power lithium ion batteries: a review. *J. Power Sources*.

Fu, W. e. (2022). High Power and energy density dynamic phase change materials using pressure-enhanced close contact melting. *Nature Energy, vol. 7*, 270-280.

Gasa, G. e. (2022). Life cycle assessment (LCA) of a concentrating solar power (CSP) plant in tower configuration with different storage capacity in molten salts. *Journal of Energy Storage, vol. 53*, 105219.

Iwayemi, T. e. (2025). Hybrid Energy Storage Systems for Renewable Integration: Combining Batteries, Supercapacitors, and Flywheels. *International Journal of Latest Technology in Engineering Management & Applied Science*.

Kirincic, M. e. (2024). Latent thermal energy storage performance enhancement through optimization of geometry parameters. *Applied energy, vol. 365*, 123255.

Knysh, L. (2018). Modeling of the turbulent heat and mass transfer in the receiver systems of the solar parabolic trough modules. *Applied Solar Energy, vol. 54*, 444-447.

Kulacki, F. (2020). Handbook of Thermal Science and Engineering. *Springer International Publishing*.

Mansouri, L. B. (2017). One-dimensional time-dependent modeling of conductive heat transfer during the melting of an initially subcooled semi-infinite PCM. *Congrès Français de Mécanique*.

Mehta, P. e. (2025). Performance assessment of thermal energy storage system for solar thermal applications. *Scientific Reports, vol. 15*.

Mehta, P. e. (2025). Performance assessment of thermal energy storage system for solar thermal applications. *Scientific Reports, vol. 15*.

Moya, E. Z. (2012). Parabolic trough concentrating solar power (CSP) systems. *Concentrating Solar Power Technology*, 197-239.

Nicholson, J. J. (2024). Analysis of Microgrid Performance, Reliability, and Resilience (AMPeRRe) Computational Model. *ERDC Library*.

Oshilalu, A. Z. (2015). Design of a CSP-based heat tracking system for combustion of food waste in a downdraft bio-digester. *13th International Energy Conversion Engineering Conference*.

Qureshi, Z. A. (2018). Recent Advances on Thermal Conductivity enhancement of phase change materials for energy storage system: a review. *International Journal of Heat and Mass Transfer*, 838-856.

Saito, A. U. (1986). Basic research on the latent heat thermal energy storage utilizing the contact melting phenomena. *JSME*, 2946-2952.

Sharma, P. e. (2025). A Comprehensive Review of Sensible Heat Thermal Energy Storage for High Temperature Applications. *Journal of Energy Storage*.

Sharma, P. e. (2025). A Comprehensive Review of Sensible Heat Thermal Energy Storage for High Temperature Applications. *Journal of Energy Storage*.

Sharopov, U. e. (2025). New challenges for lithium fluoride: From dosimeter to solid-state batteries. *Next Materials*.

Si, H. e. (2025). Solid-State Sodium-Ion Batteries: Theories, Challenges, and Perspectives. *Chemistry - A European Journal*.

Sivalingam, e. a. (2024). Optimizing thermal performance in Parabolic Trough Solar Power Systems: An experimental design and analysis. *E3S Web of Conferences*, 02005.

Yang, T. K. (2021). Phase change material-based thermal energy storage. *Cell Rep. Phys. Sci.*

Yang, X. H. (2018). Finned heat pipe assisted low melting point metal PCM heat sink against extremely high power thermal shock. *Energy Conversion Management*, 467-476.

Zhu, S. e. (2019). A free-piston Stirling generator integrated with a parabolic trough collector for thermal-to-electric conversion of solar energy. *Journal of Applied Energy*.

APPENDIX A: VARIABLES AND SUBSCRIPTS

Variables

q" = Heat flux

$\dot{Q}$ = Total heat transfer rate

$S[t]$ = Direct normal solar irradiance data

$L[t]$ = Time-based power demand (load) profile

n = Number of timesteps

A = Area

w = Width

η = Efficiency

κ_{angle} = Incident angle modifier

$\dot{m}$ = Working fluid mass flow rate

LE_{absorber} = Length of the receiver tube

τ_{wf} = Time for the working fluid to pass through the receiver

ρ = Density

$T[t]$ = Dynamic temperature

c_{p} = Specific heat

k = Thermal conductivity

h = Heat transfer coefficient

U = Overall heat transfer coefficient

L = Latent heat of fusion of the PCM

μ_{l} = PCM viscosity

T_{m} = Melting point of the PCM

$T_{\text{steam,min}}$ = Boiling point of water (100 C)

C_{r} = Coefficient for Effectiveness-NTU method

ε = Effectiveness for the Effectiveness-NTU method

$P[t]$ = Electric power output of the CSP system

$P_{\text{surplus}}[t]$ = Power surplus from CSP system

$E[t]$ = Stored energy within an external battery

$E_{capacity}$ = Capacity of battery energy storage

$PR_{hot}[t]$ = Proportion of working fluid routed to the thermal energy storage system

AV_{CSP} = Percent power availability of the CSP system

$AV_{battery}$ = Percent power availability of the CSP system with external battery energy storage

$ht[t]$ = Height of the remaining solid-state PCM during a charge cycle

ht_{peak} = Maximum height of the solid-state PCM when the full material is solidified

Pr = Pressure applied to the PCM during a charge cycle

Phases = Number of phase changes

Phase = Numerical representation of whether a phase change occurs within a given timestep

$u[t]$ = Melting speed of solid-state PCM

Subscripts

absorber = CSP system receiver

aperture = Parabolic trough mirror aperture

surface = Surface area

section = Cross-sectional area

transfer = Area of heat transfer

thermal = Thermal efficiency of the solar CSP system

optical = Optical efficiency of the solar CSP system

losses = Efficiency value to represent the energy conversion losses of the CSP system

system = Overall efficiency of the turbine and generator system

wf = Working fluid

hot = Material treated as “hot” working fluid (working fluid from receiver)

cold = Material treated as “cold” working fluid (water / steam)

in = At the input to the heat exchanger

out = At the output from the heat exchanger

esin = At the input to the energy storage system

esout = At the output from the energy storage system

steam = Steam thermophysical properties

amb = Ambient / surroundings

he = Heat exchanger

es = Thermal energy storage

wall = Heat transfer boundary wall

des = Desired value

actual = Actual value

PCM = Phase change material in the thermal energy storage

s = Solid phase

l = Liquid phase

sensible = For sensible heat transfer

Abbreviations

PCM = Phase Change Material

DynPCM = Dynamic Phase Change Material

CSP = Concentrated Solar Power

NTU = Number of Thermal Units

APPENDIX B: ADDITIONAL PLOTS

The following plots are a continuation of the results from Section 6. They are produced using the same methodology as the latent case in Section 4, but the results are different as they consider a dynPCM thermal energy storage system under different pressures.

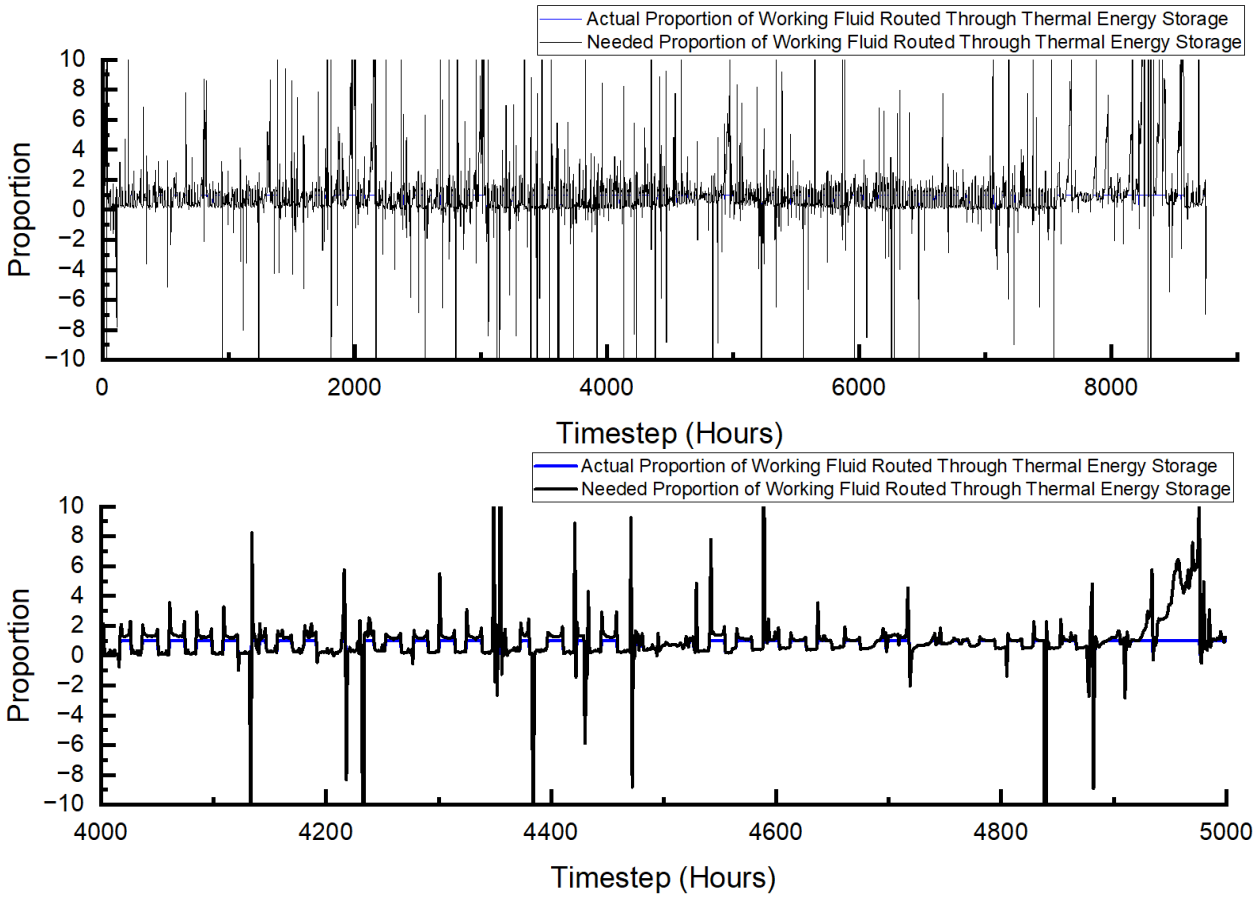

Figure 37: Proportion of Working Fluid Through Energy Storage – 10 Pa

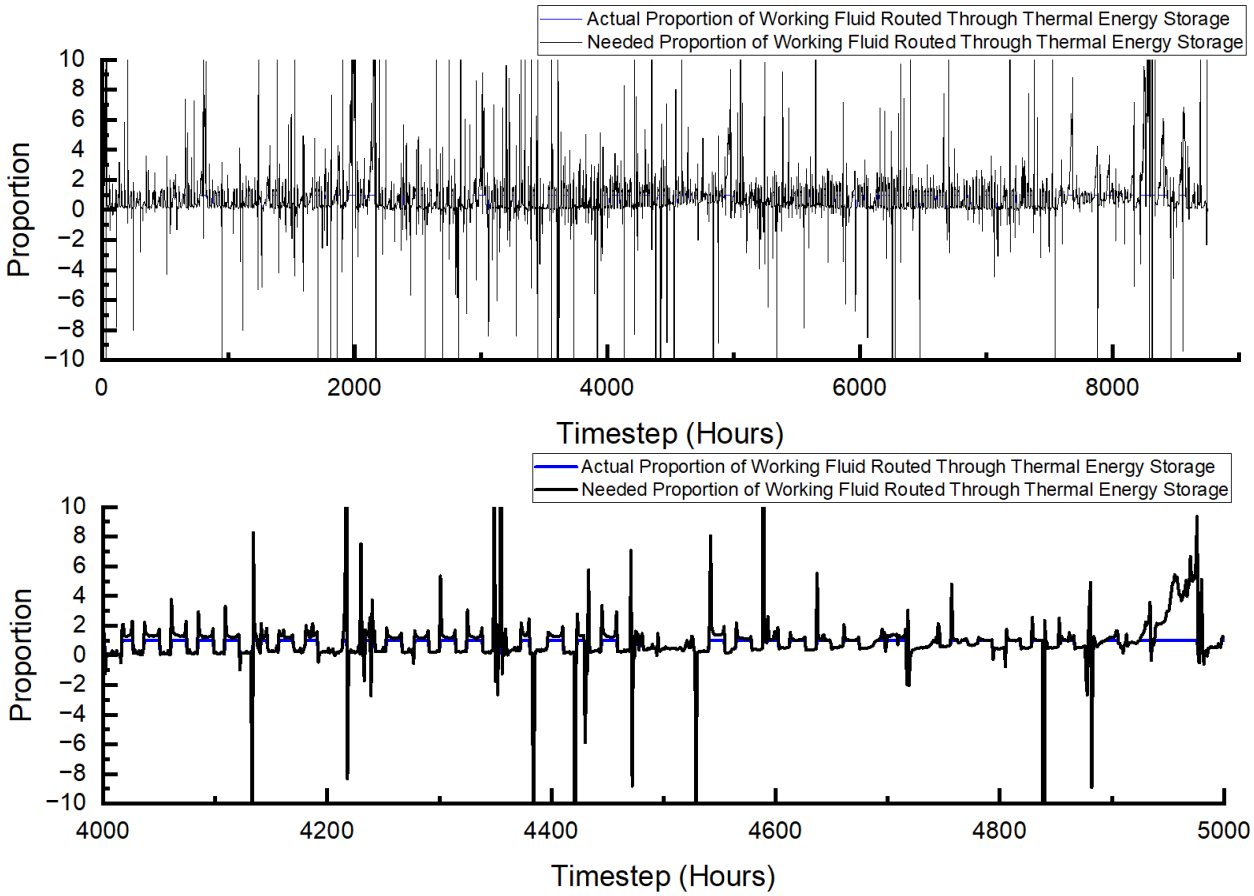

Figure 38: Proportion of Working Fluid Through Energy Storage – 1000 Pa

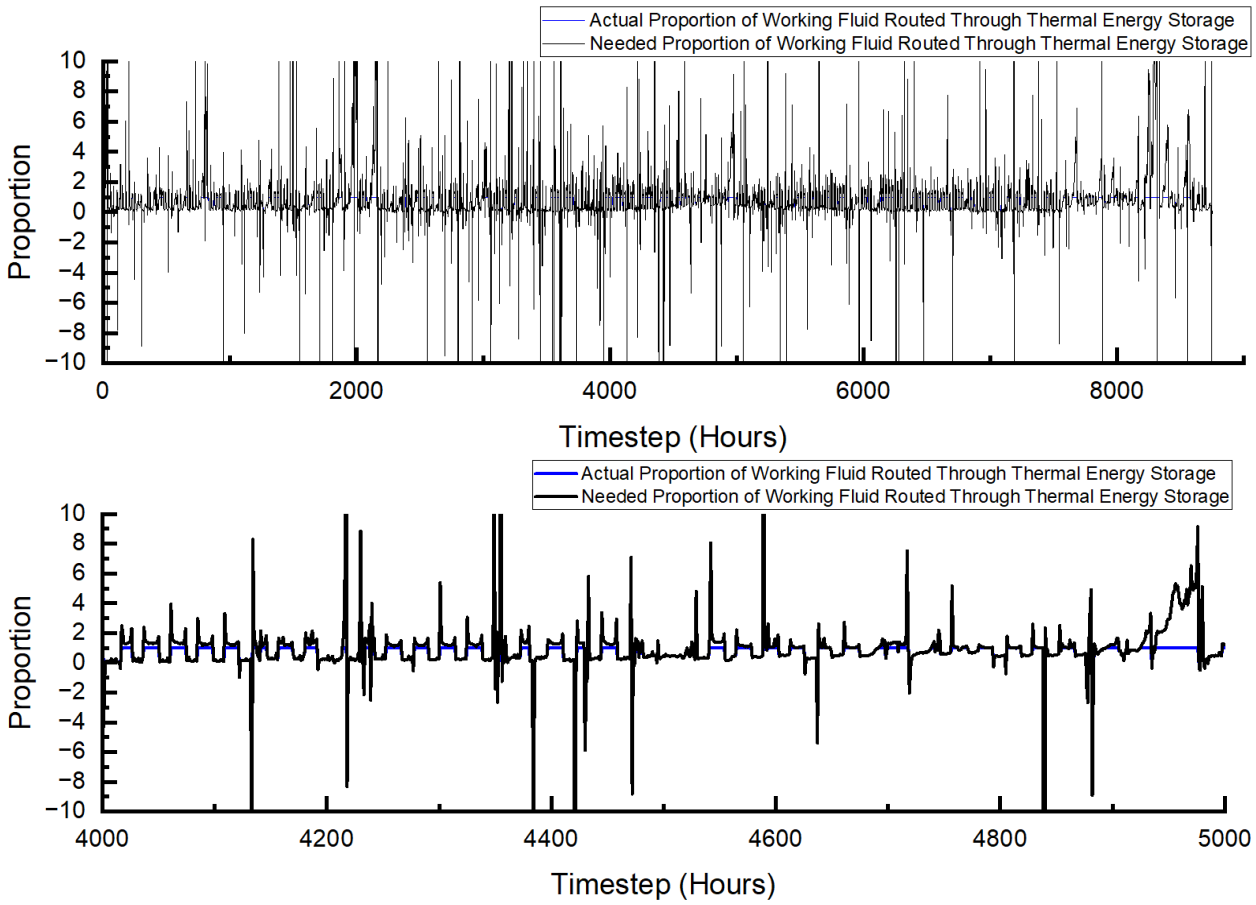

Figure 39: Proportion of Working Fluid Through Energy Storage – 100,000 Pa

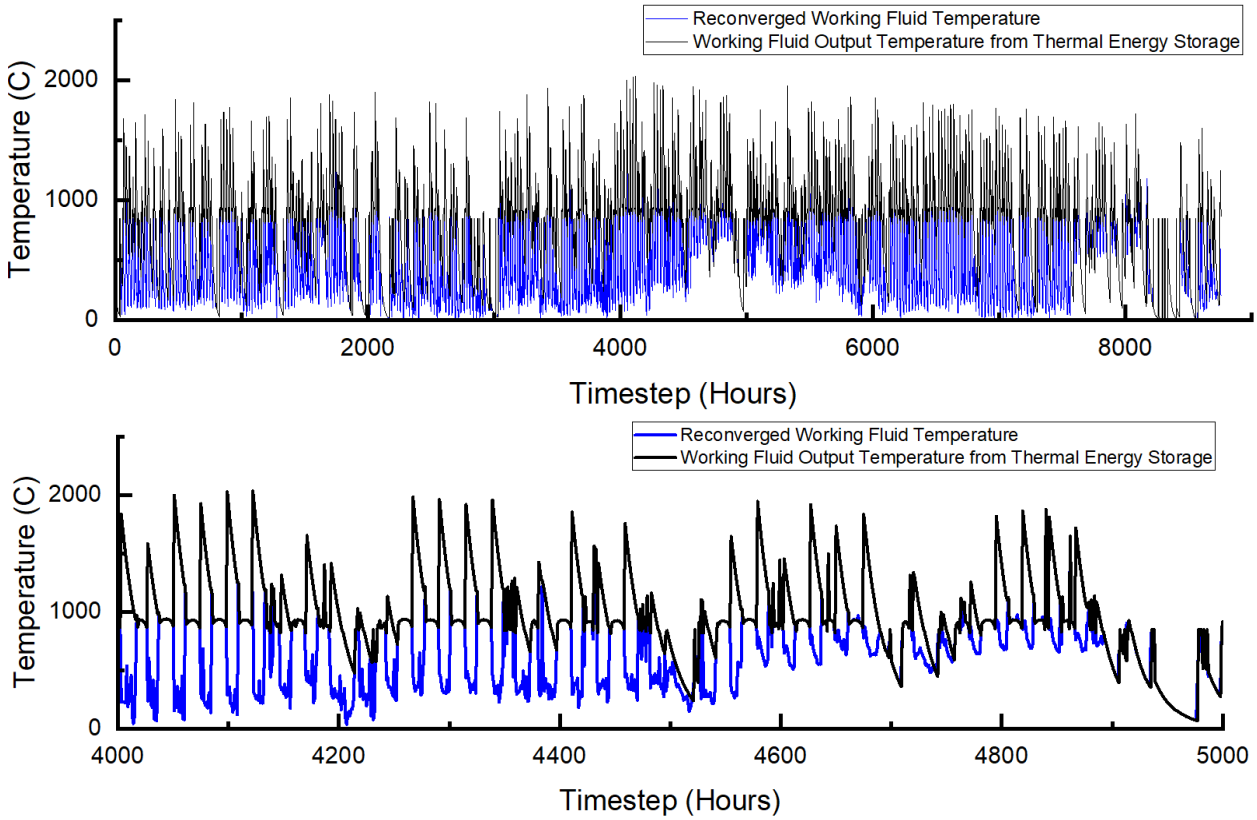

Figure 40: Reconverged Working Fluid Output Temperature – 10 Pa

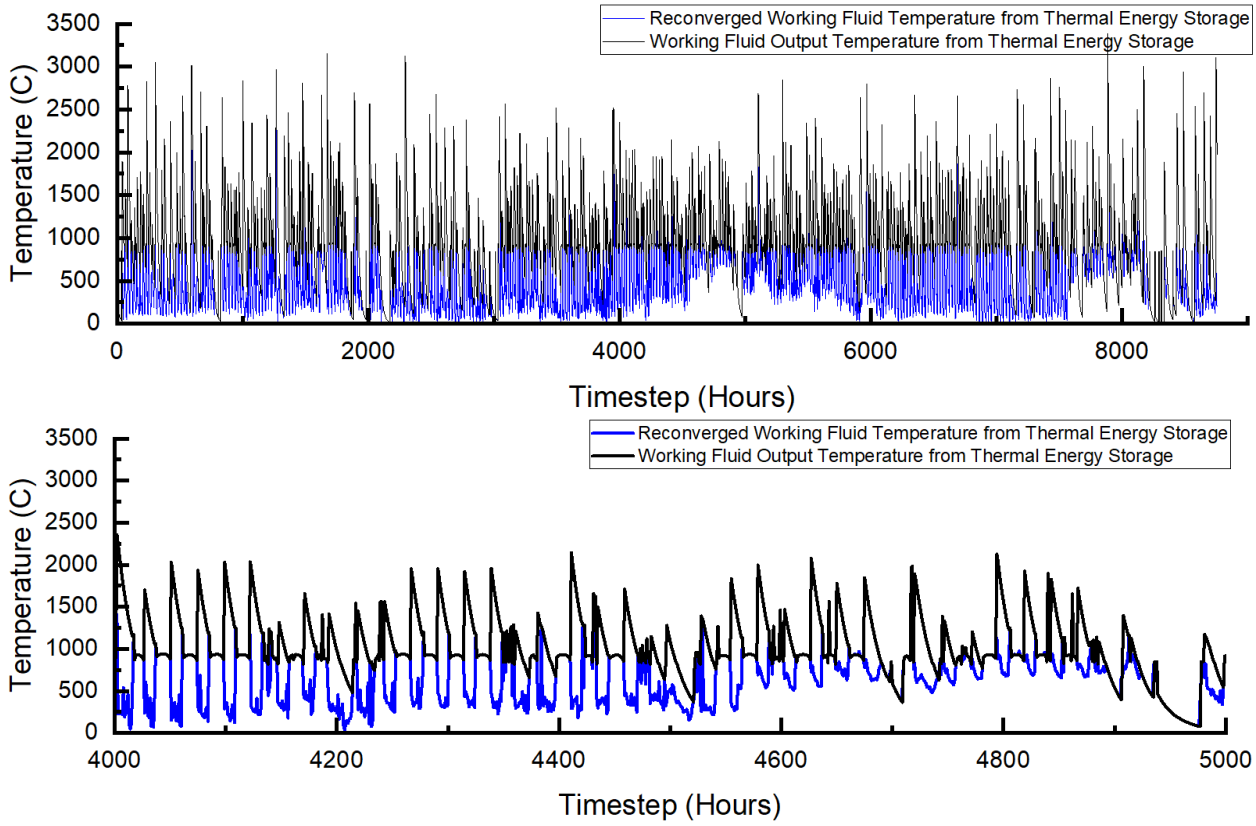

Figure 41: Reconverged Working Fluid Output Temperature – 1000 Pa

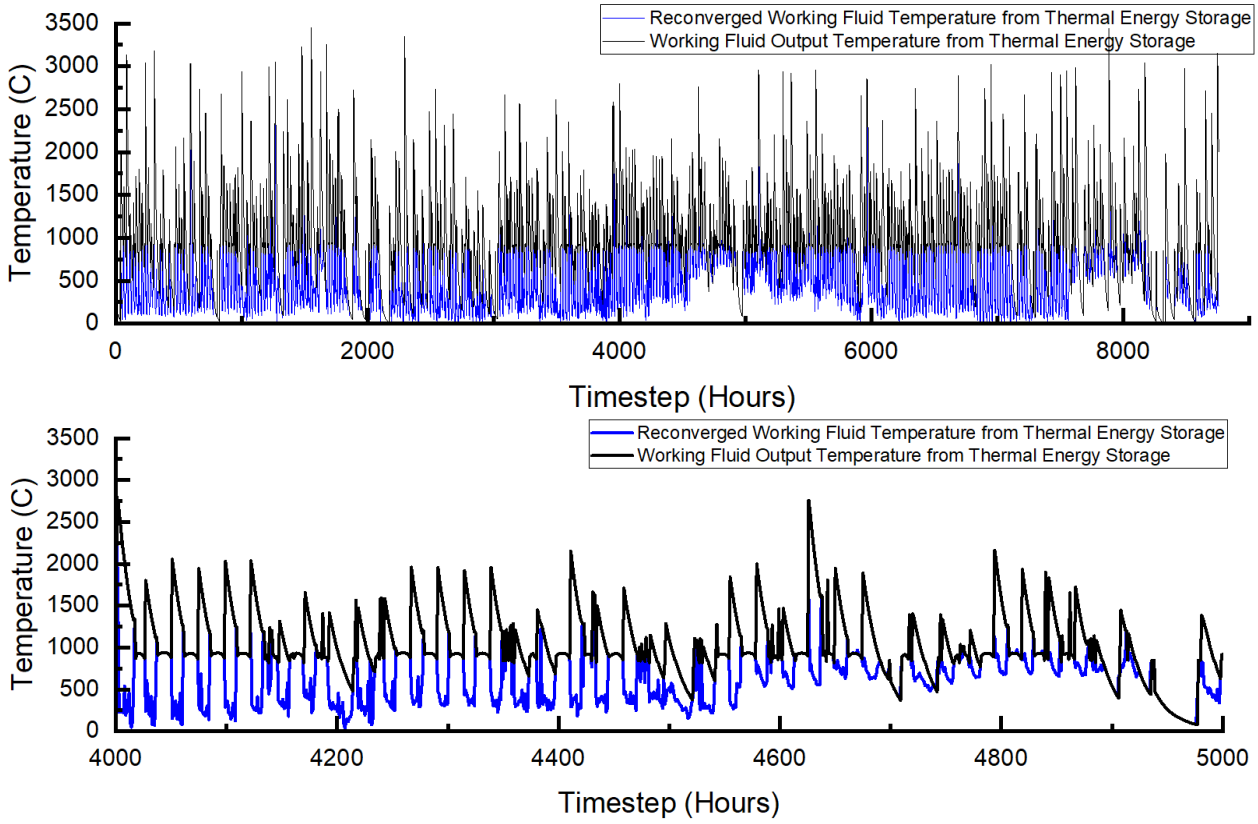

Figure 42: Reconverged Working Fluid Output Temperature – 100,000 Pa

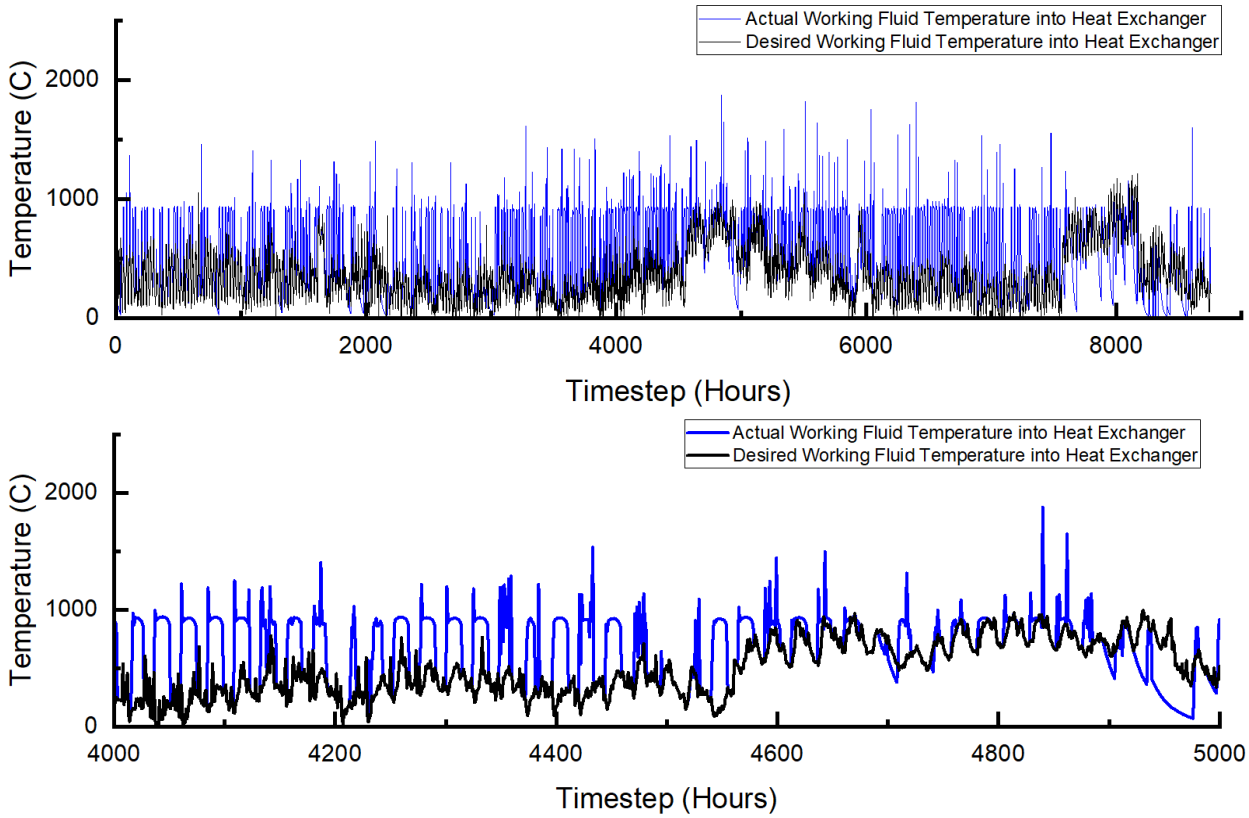

Figure 43: Working Fluid Temperature into Heat Exchanger – 10 Pa

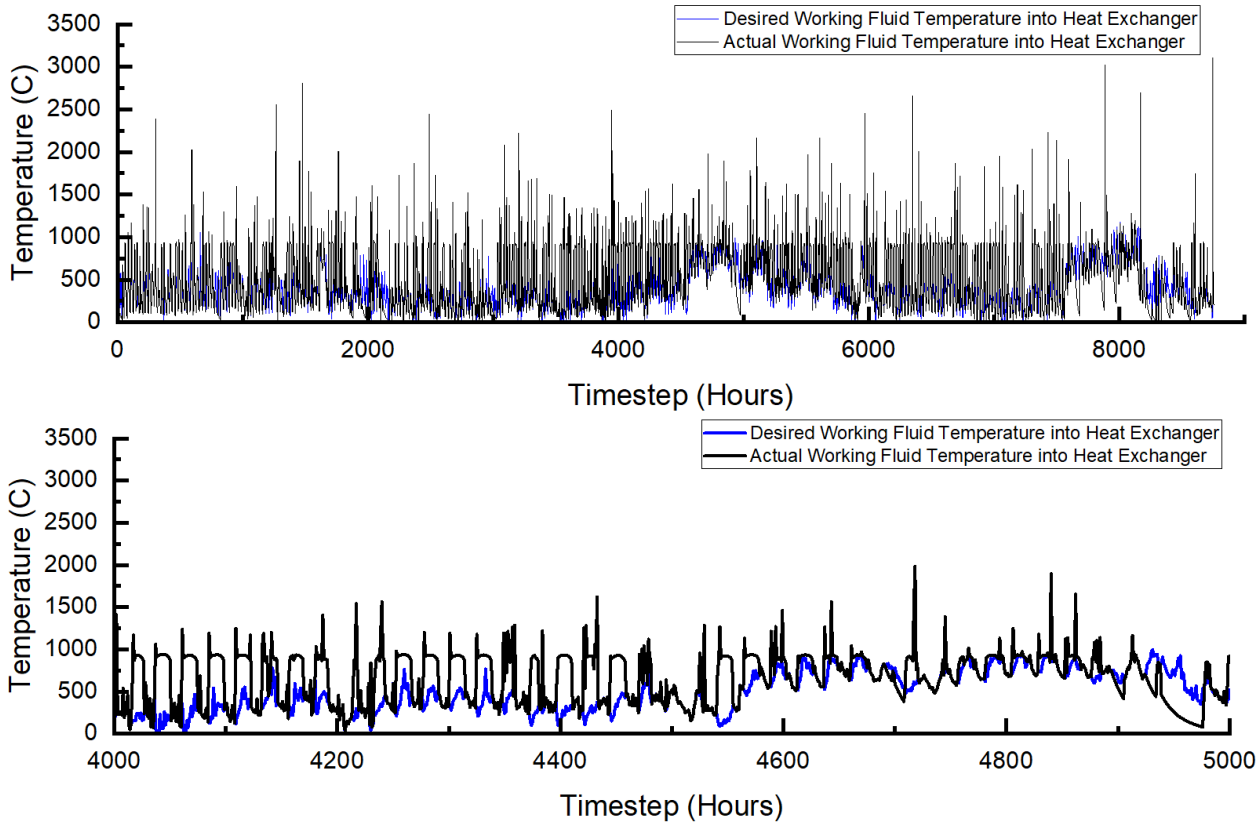

Figure 44: Working Fluid Temperature into Heat Exchanger – 1000 Pa

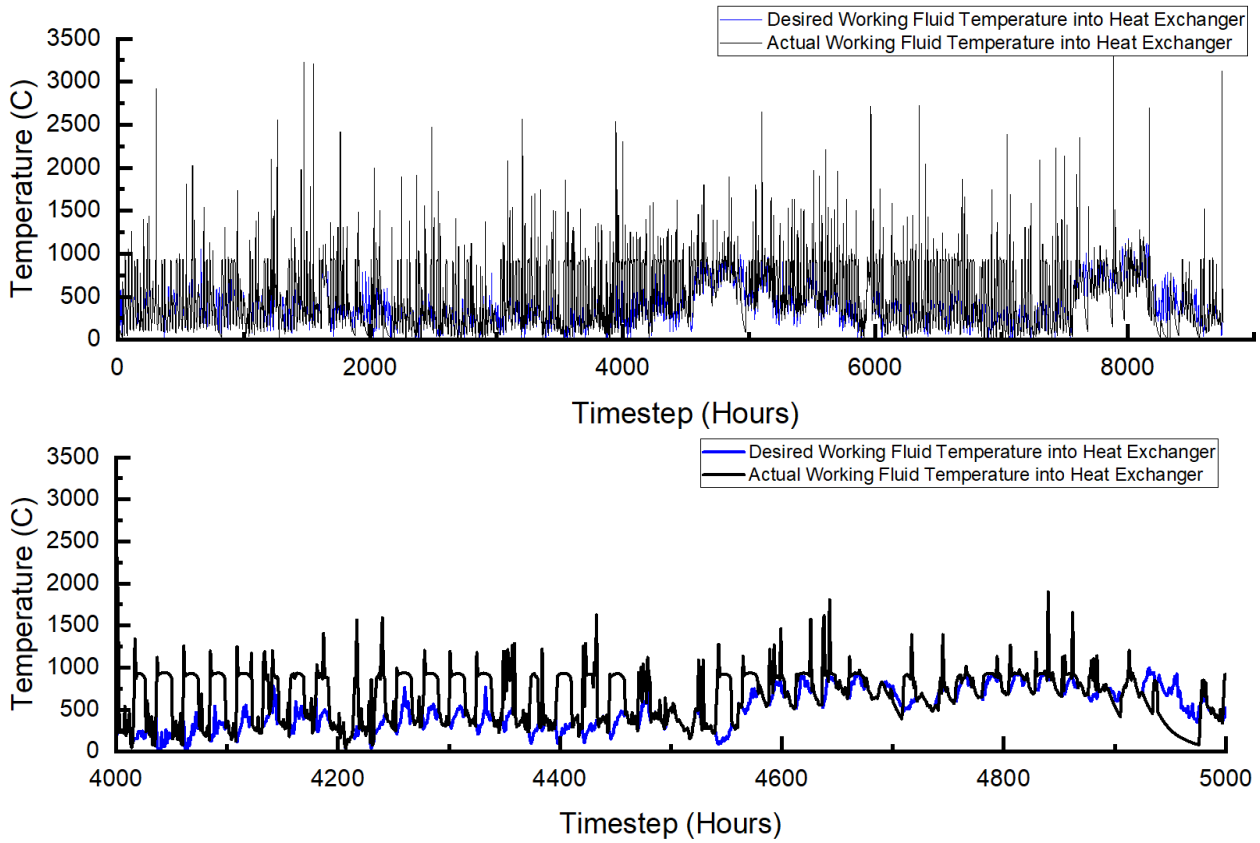

Figure 45: Working Fluid Temperature into Heat Exchanger – 100,000 Pa

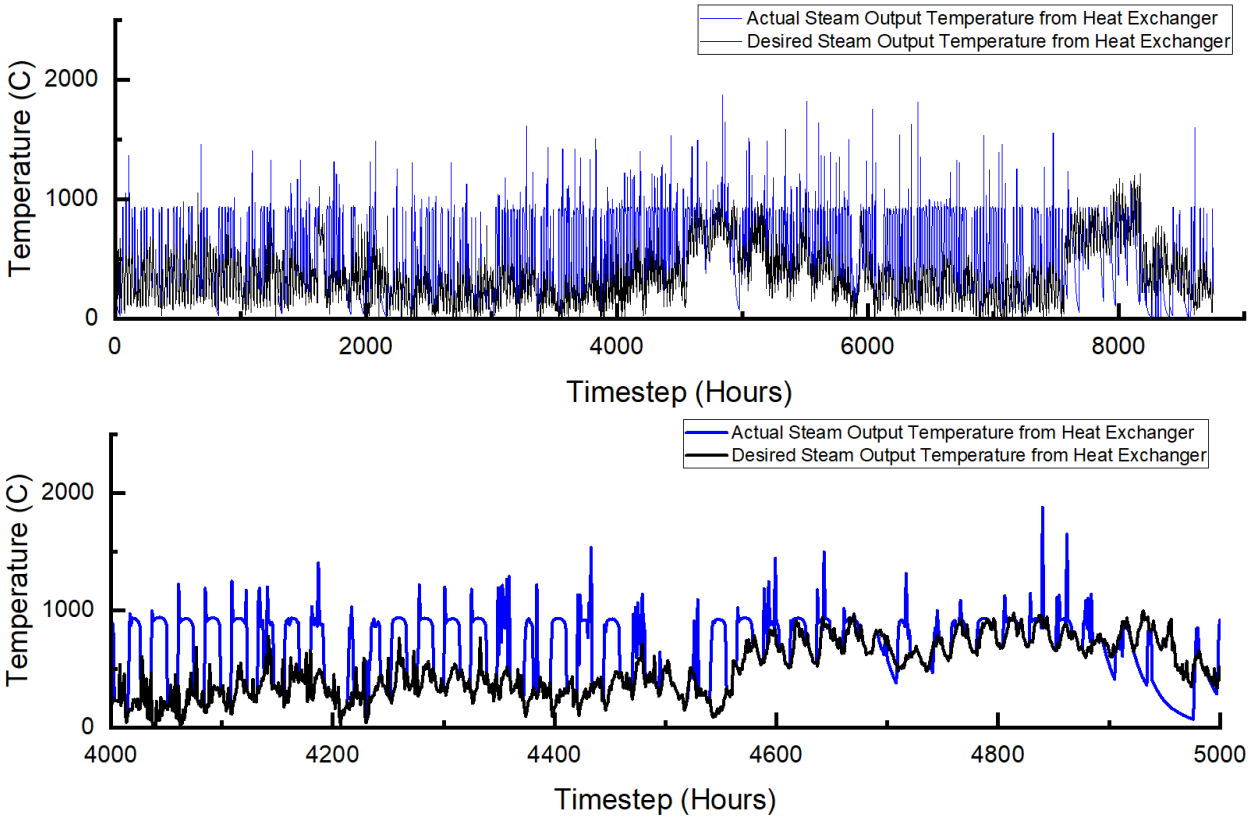

Figure 46: Steam Output Temperature from Heat Exchanger – 10 Pa

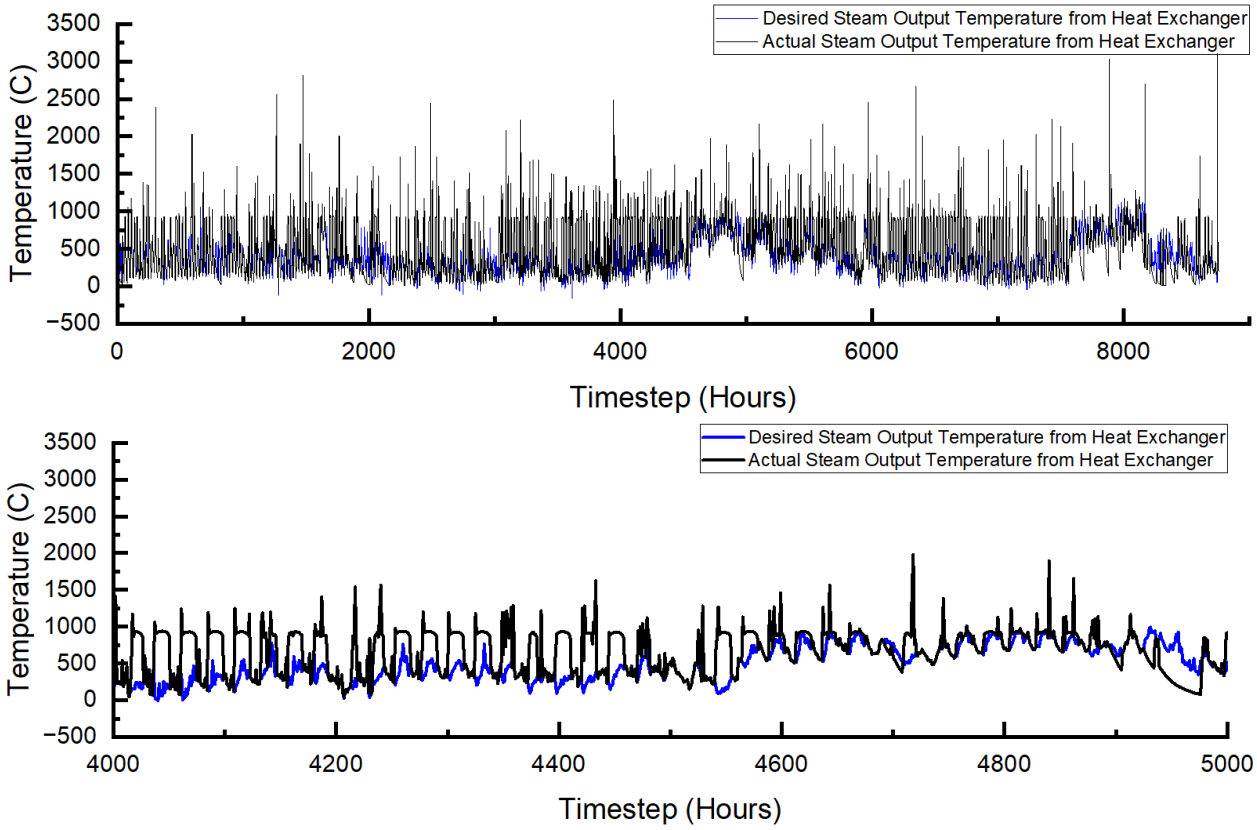

Figure 47: Steam Output Temperature from Heat Exchanger – 1000 Pa

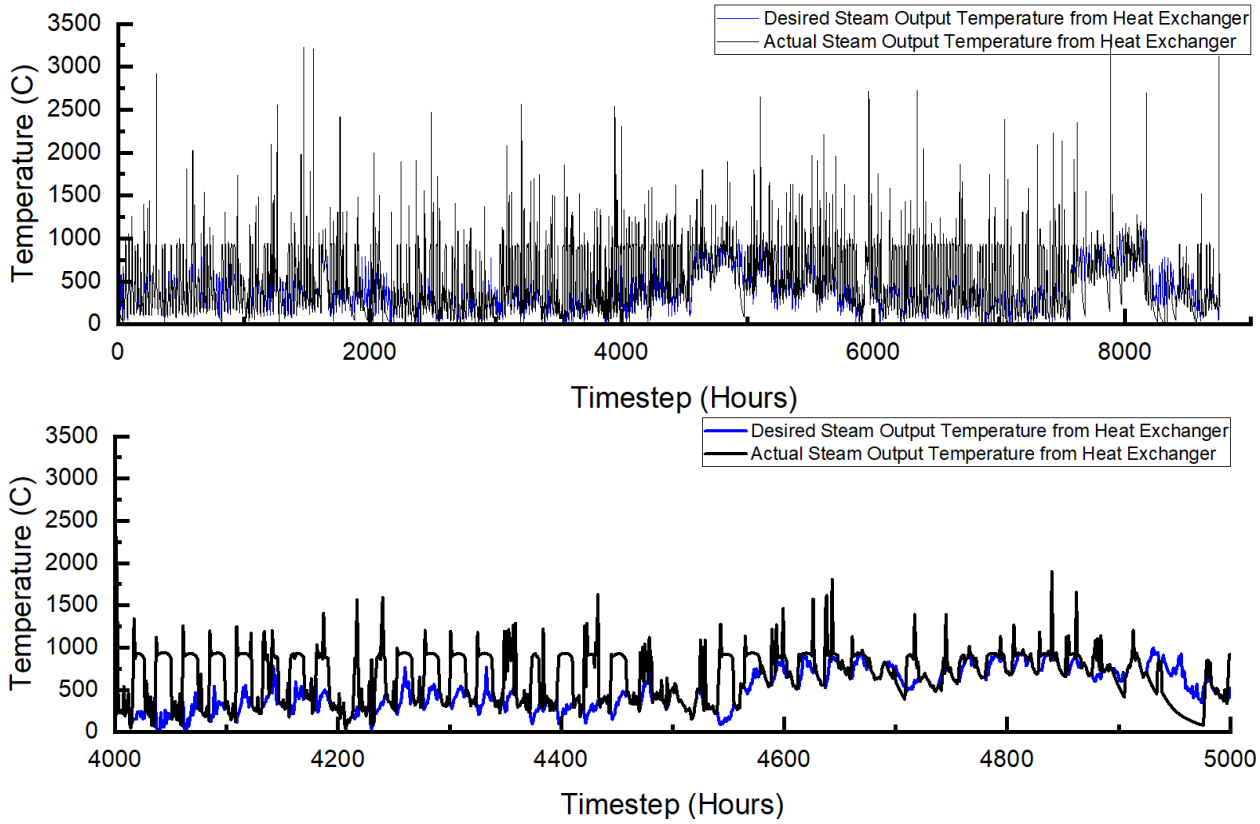

Figure 48: Steam Output Temperature from Heat Exchanger – 100,000 Pa

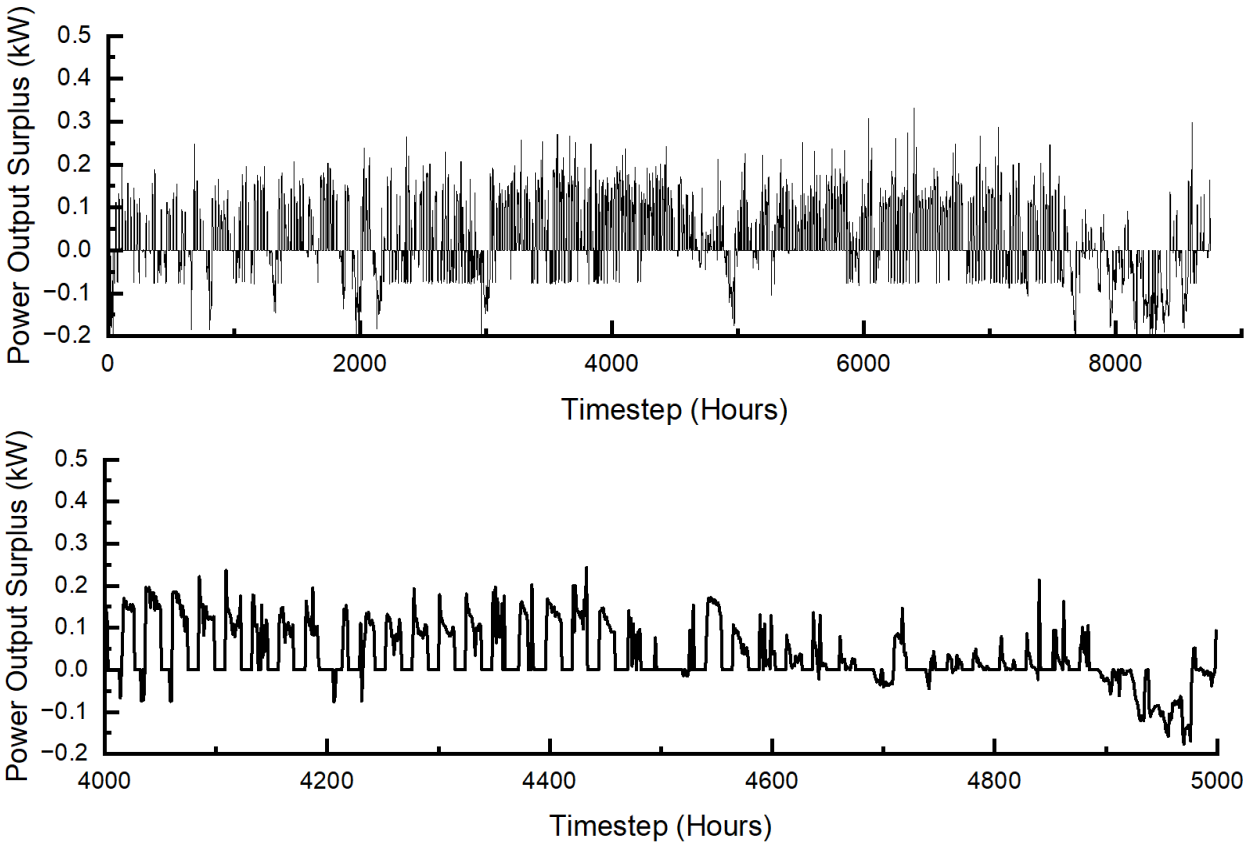

Figure 49: CSP System Power Output Surplus – 10 Pa

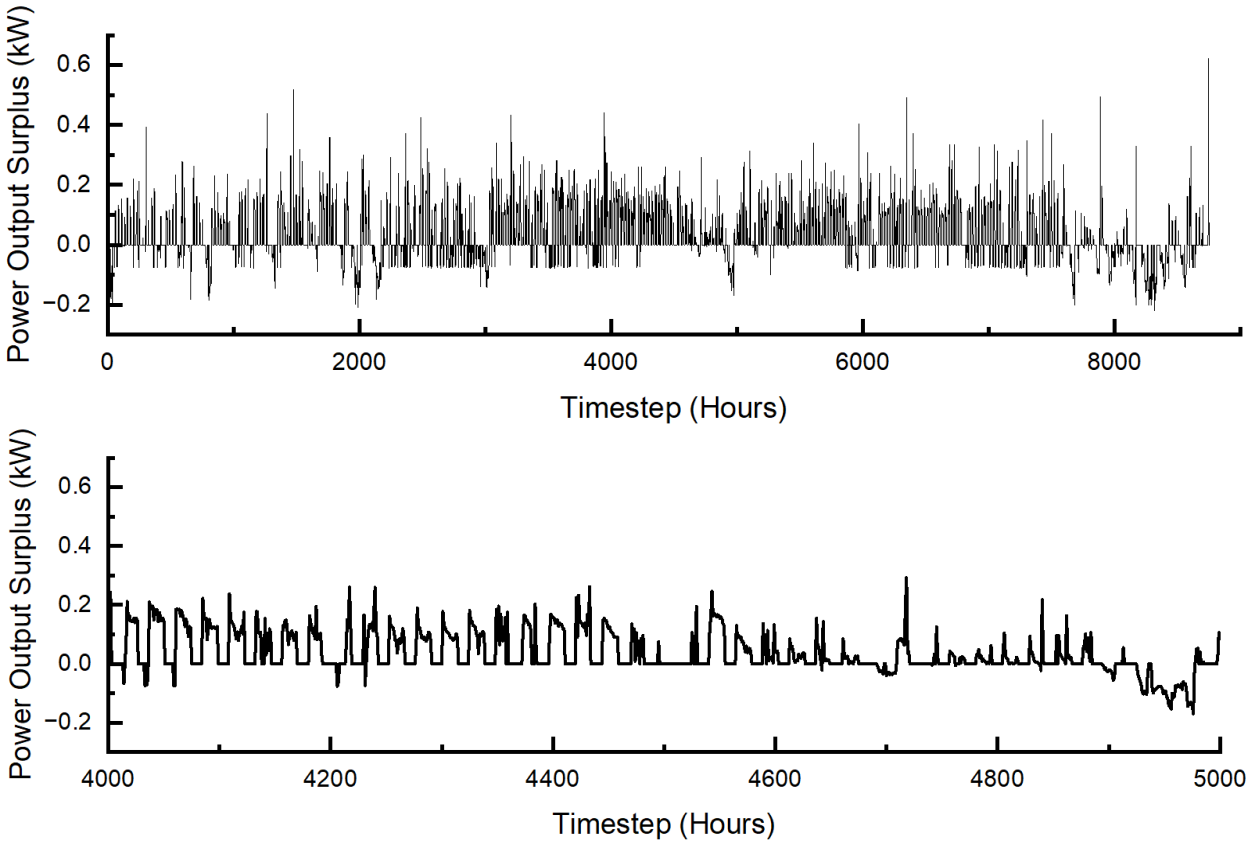

Figure 50: CSP System Power Output Surplus – 1000 Pa

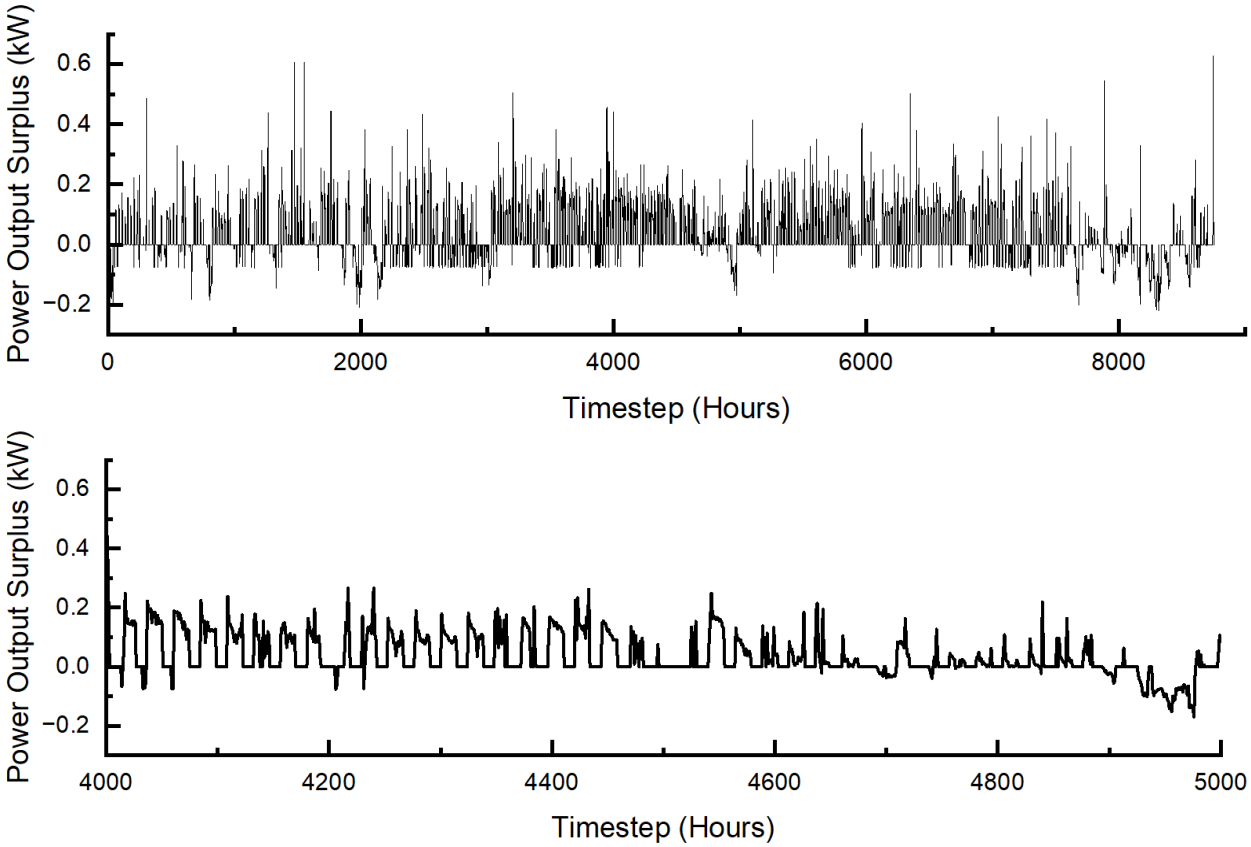

Figure 51: CSP System Power Output Surplus – 100,000 Pa